NOTE TO USERS

This reproduction is the best copy available.

ULTRAFAST PHOTOPHYSICS OF π-CONJUGATED POLYMERS AND POLYTHIOPHENE/FULLERENE BLENDS FOR ORGANIC PHOTOVOLTAIC APPLICATIONS

by

Sanjeev Singh

A dissertation submitted to the faculty of
The University of Utah
in partial fulfillment of the requirements for the degree of

Doctor of Philosophy

Department of Physics and Astronomy

The University of Utah

May 2010

THE UNIVERSITY OF UTAH GRADUATE SCHOOL

SUPERVISORY COMMITTEE APPROVAL

of a dissertation submitted by

Sanjeev Singh

This dissertation has been read by each member of the following supervisory committee and by majority vote has been found to be satisfactory.

2/23/2010 [redacted]

Chair: Zeev Valy Vardeny

2/23/2010 [redacted]

Oleg Starykh

2/23/2010 [redacted]

John Lupton

2/23/2010 [redacted]

Michael Morse

3/8/2010 [redacted]

Ajay Nahata

THE UNIVERSITY OF UTAH GRADUATE SCHOOL

FINAL READING APPROVAL

To the Graduate Council of the University of Utah:

I have read the dissertation of Sanjeev Singh in its final form and have found that (1) its format, citations and bibliographic style are consistent and acceptable; (2) its illustrative materials inclusing figures, tables, and charts are in place; and (3) the final manuscript is satisfactory to the Supervisory Committee and is ready for submission to The Graduate School.

[redacted]

03/08/2010
Date

Zeev Valy Vardeny
Chair, Supervisory Committee

Approved for the Major Department

[redacted]

David B. Kieda
Chair / Dean

Approved for the Graduate Council

[redacted]

Charles A. Wight
Dean of the Graduate School

ABSTRACT

The present work reports studies of the ultrafast photoexcitations in various pristine π-conjugated polymers as well as compounds of polythiophene/fullerene blends, which act as the active layer of donor/acceptor in organic photovoltaic applications. The main technique used is the ultrafast (~150 fs) transient photomodulation (PM) spectroscopy in the range of 0.25 to 2.5 eV using two different laser systems. In addition, two-photon-absorption and electroabsorption have also been complementary used.

In organic photovoltaic studies, two different donor polymers namely, Regio-Regular-poly(3-hexylthiophene) (RR-P3HT) that forms lamellae, and Regio-Random-poly(3-hexylthiophene) (RRa-P3HT) that forms lamellae with lesser extent have been compared. The transient PM measurement of the most efficient RR-P3HT/fullerene blend shows that the decay of exciton does not result in the generation of polarons in the donor and acceptor materials, as assumed by the present model of charge dissociation in photovoltaic devices. On the contrary, the decay of exciton fits very well to the build-up of charge-transfer (CT) state in the fullerene phase, which indicates the migration of the photoexcited exciton in the polymer phase to the fullerene nano-domains. The transient PM measurement of RRa-P3HT/fullerene blend, which does not form phase-separated nano-domains, shows the formation of a CT state at the interface following by ultrafast geminate recombination.

The transient PM measurement of poly(phenylene-vinylene) (PPV) derivatives show that in 2-methoxy-5-(2'-ethylhexyloxy) PPV (MEH-PPV) film there are two kinds of primary photoexcitations, namely, intrachain exciton and excimer, but only intra-chain exciton in other PPV derivative polymers. Furthermore the high-pressure study of MEH-PPV film shows two kinds of polymer chain orders: isolated-chains and closely packed-chains. The high pressure mainly affects photoexcited excimers in the closely packed-chains. In contrast there is no pressure effect on the photogenerated intrachain excitons in the isolated-chains.

The other π-conjugated polymers investigated in this dissertation are platinum(Pt)-containing conjugated polymers. The different parity excited states of these Pt-polymers are studied by electroabsorption and two-photon-absorption spectroscopies. These results show that, even after the incorporation of Pt atoms into the backbone of conjugated polymer, the behavior of the excited states is similar to regular π-conjugated polymers.

To my parents and my wife

CONTENTS

ABSTRACT iv

LIST OF FIGURES x

LIST OF TABLES xv

ACKNOWLEDGEMENTS xvi

CHAPTERS

1. INTRODUCTION 1

1.1 π-conjugated polymers 1
1.2 Symmetry and ordering of the excited state 4
1.3 Excitation models for π-conjugated polymers 6
1.4 Photoexcitations in π-conjugated polymers 9
1.4.1 Charge photoexcitations in the NDGS polymers 10
1.4.1.1 The polaron excitation 10
1.4.1.2 The bipolaron excitation 11
1.4.2 Neutral photoexcitations in the NDGS polymers 11
1.4.2.1 The singlet exciton 11
1.4.2.2 The triplet exciton 16
1.4.2.3 The polaron pair excitation 17
1.4.3 Excimer, pi-dimer and exciplex species 18

2. EXPERIMENTAL TECHNIQUES 21

2.1 Ultrafast excitation sources 21
2.1.1 Femtosecond Ti:Sapphire setup 21
2.1.1.1 Autocorrelation 24
2.1.2 White light super-continuum generation 24
2.1.3 Low-energy high repetition-rate system 28
2.2 Transient pump-probe spectroscopy 28
2.3 Two-photon absorption 32
2.4 Electroabsorption spectroscopy 33

2.5 Fourier transform infrared spectroscopy 36
2.6 Photoluminescence quantum efficiency 38
2.7 High pressure measurements 40

3. ULTRAFAST PHOTOPHYSICS OF P3HT/FULLERENE DERIVATIVES 46

3.1 Materials 47
3.1.1 P3HT 47
3.1.2 PCBM 47
3.1.3 P3HT/Fullerene blend 51
3.2 Electroabsorption of P3HT/Fullerenes 52
3.3 Ultrafast measurements 55
3.3.1 Ultrafast photophysics of RR-P3HT polymer 55
3.3.2 Ultrafast photophysics of PCBM film and isolated molecules 57
3.3.3 Ultrafast photophysics of RR-P3HT/PCBM film 61
3.3.4 Ultrafast photophysics of RR-P3HT/PCBM blend in OPV device structure 65
3.3.5 Ultrafast photophysics of RR-P3HT/PCBM blend with below-gap excitation 67
3.3.6 Ultrafast photophysics of RR-P3HT/JAL and /HAB (1.2:1) blends 67
3.3.7 Effect of spin-1/2 radical on the ultrafast photophysics of RR-P3HT/PCBM blend 70
3.3.8 Ultrafast photophysics of RRa-P3HT polymer 77
3.3.9 Ultrafast photophysics of RRa-P3HT/PCBM (1.2:1) 77
3.3.9.1 Above-gap excitation 77
3.3.9.2 Below-gap excitation 79
3.4 Conclusions 82

4. DECAY SPECTROSCOPY OF PHOTOEXCITATIONS IN PPV-DERIVATIVE POLYMERS AT AMBIENT AND HIGH HYDROSTATIC PRESSURE 85

4.1 Materials 85
4.2 Polarization memory decay spectroscopy of photoexcitations in PPV-derivative polymers 86
4.2.1 Ultrafast measurement of DOO-PPV film 90
4.2.2 Ultrafast measurement of MEH-PPV solution 93
4.2.3 Ultrafast measurement of MEH-PPV film 95
4.2.4 Conclusions 99
4.3 High pressure study of MEH-PPV films 99

4.3.1 Introduction 100
4.3.2 Effect of pressure on the photoluminescence of MEH-PPV film 102
4.3.3 Ultrafast transient photomodulation measurements 104
4.3.4 Conclusions 109

5. PHOTOEXCITED STUDIES OF PLATINUM CONTAINING π–CONJUGATED POLYMERS 113

5.1 Introduction 113
5.1.1 Polymer materials 113
5.1.2 Quantum chemistry calculation of the excited states in Pt-polymers 114
5.2 Electroabsorption of Pt-3 polymer 116
5.3 Two-photon absorption of Pt-3 polymer film and solution 119
5.4 Electroabsorption of Pt-1 polymer 121
5.5 Two-photon absorption of Pt-1 solution 123
5.6 Ultrafast photomodulation of Pt-1 polymer 125
5.7 Conclusions 128

6. CONCLUSIONS 129

REFERENCES 133

LIST OF FIGURES

1.1 Chemical structure of trans-$(CH)_x$ 2

1.2 A different ordering of the first excited states gives rise to different optical properties. Upon absorption of a photon the polymer fluoresces if $1^1A_g < 1^1B_u < 2^1A_g$ 6

1.3 Effect of dimerization on the electronic properties of polyacetylene (a) The undimerized state of π-electrons that has the properties of a metal; (b) the dimerized state with properties of a semiconductor..... 8

1.4 Energy levels and associated optical transitions of (a) positive, and (b) negative polarons..... 12

1.5 Energy levels and associated optical transitions of (a) positive, and (b) negative bipolarons..... 12

1.6 Schematic energy diagram and optical transitions associated with (a) singlet, and (b) triplet excitons..... 17

1.7 Energy diagram and optical transitions associated with polaron-pairs..... 19

2.1 Schematic diagram of Ti:Sapphire regenerative amplifier laser system..... 22

2.2 Characterization of fundamental pulses at 800nm; (a) temporal profile measured by autocorrelation, and (b) spectral profile..... 25

2.3 Characterization of white light continuum (WLC) source; (a) Spectrum of WLC generated by 800 nm fundamental laser, and (b) chirp of WLC against wavelength fitted with second-order polynomial function 27

2.4 Schematic diagram of (a) ultrafast high intensity transient pump-probe set-up (b) broad probe range generated by both low and high intensity laser systems..... 30

2.5 Two-photon absorption in Pt-3 solution at 3.9 eV, measured with the pump-probe system, where the pump beam was fixed at 1.55 eV whereas the probe beam was at 2.35 eV..... 34

2.6 Experimental set-up for electroabsorption (EA) spectroscopy (a) sapphire substrate with interpenetrating finger electrodes used in EA measurement (b) experimental arrangements..... 35

2.7 Schematic illustration of Michelson interferometer. I_0 is the initial beam and I_{out} is the measured beam after interference of the split beams..... 37

2.8 Experimental set-up for the measurement of photoluminescence quantum efficiency..... 39

2.9 Schematics and image of the diamond anvil cell (DAC) (a) typical structure of DAC assembly [55] (b) image and (c) schematic of Merrill Bassett type DAC [56]..... 41

2.10 Transmission spectrum of diamond anvil cell (DAC) assembly used in the Near-ir/visible pump-probe measurement..... 42

2.11 Pressure calibration measurement for MEH-PPV film. (a) shift of Ruby fluorescence line at different applied pressure (b) shift of MEH-PPV infra-red absorption line at the same pressures as used for Ruby fluorescence..... 45

3.1 Chemical structure of (a) RegioRegular-poly(3-hexylthiophene)(RR-P3HT) (b). RegioRandom-poly(3-hexylthiophene)(RRa-P3HT); (c) schematic diagram of lamella folding and ordering on a substrate Adapted from Ref.[69]; (d) chemical structure of [6,6]-phenyl C61butyric acid methyl ester (PCBM) 48

3.2 Optical properties for a 12% PCBM:88% PS blend (gray line) and pristine PCBM film (black line); (a) absorption spectra (b) PL spectra. Adapted from Ref. [70]..... 50

3.3 Transmission electron microscope images of (a) RR-P3HT/PCBM (1.2:1) (b) RRa-P3HT/PCBM (1.2:1)..... 53

3.4 Electroabsorption spectra of (a) RR-P3HT/PCBM [Adapted from Ref. [82]](b) RR-P3HT/JAL (c) RR-P3HT/HAB. For clarity, the magnified nearir spectra are plotted together with EA spectra..... 54

3.5 Transient photomodulation (PM) measurement of RR-P3HT film. (a) Transient PM spectrum at t = 0 ps. (b) Transient normalized decays of their respective bands P1, P2, PA1 and PB..... 56

3.6 Transient PM measurement of PCBM film. (a) Transient spectra at t = 0 ps and 100 ps showing two bands, Ex and CT (b) the time decay of these bands and their fitted parameters are given in inset..... 58

3.7 Transient PM spectra of (a) PCBM, JAL and HAB films at t = 0 ps (b) PCBM molecule (1% by weight) in the polystyrene matrix at t = 0 ps and 100 ps..... 60

3.8 Transient PM measurement of RR-P3HT/PCBM film. (a) Transient PM spectra at t = 0 ps, 50 ps & 300 ps showing different bands of P1, P2, PA1. PA' and PB and (b) the transient normalized decays of different bands P1, P2, PA1 PA' and PB. 62

3.9 The transient decay of bands PA1, [-PA'] and PB of the RR-P3HT/PCBM film are compared..... 63

3.10 Transient PM measurement of RR-P3HT/PCBM film in the device structure of *Glass/ITO/PEDOT/RR-P3HT+PCBM (1.2:1)/Al.* (a) Transient spectra at t = 0 ps and 100 ps showing PA' and PB bands, and (b) the transient decay of PA'..... 66

3.11 Transient PM measurement of RR-P3HT/PCBM film. (a) Transient spectra at t = 0 ps and 100 ps, when excited at 1.55 eV, showing different bands of P1, P2 and PB and (b) the transient decay at 1.77 eV when excited AG (3.1 eV) and BG (1.55 eV)..... 68

3.12 Transient PM spectra of (a) RR-P3HT/PCBM (1.2:1) film (b) RR-P3HT/JAL (1.2:1) film (c) RR-P3HT/HAB (1.2:1) film at different times. 69

3.13 The transient decay of RR-P3HT/(PCBM or JAL or HAB) (1.2:1) film at (a) 1.3 eV, (b) 2.26 eV, and (c) 1.77 eV..... 71

3.14 The transient decays in RR-P3HT / PCBM (1.2 : 1) films mixed with 0, 3 and 10% of Galvinoxyl impurities measured at (a) 2.26 eV (PB), and (b) 1.3 eV (P2). The inset to (a) shows the chemical structure of Galvinoxyl radical impurity..... 74

3.15 Schematic diagram of our assumed model for spin-spin scattering due to spin-1/2 radical, Galvinoxyl, with singlet exciton at the interface of P3HT/PCBM..... 76

3.16 Transient PM measurement of RRa-P3HT film. (a) Transient spectra at t = 1 ps and 200 ps, showing two bands PA1 and SE (b) the decay dynamics of these bands. Inset of (b) shows the fitting parameters..... 78

3.17 Transient PM measurement of RRa-P3HT/PCBM (1.2:1) film. (a) Transient spectrum at t = 0 ps showing different bands of CT1, CT2 and (b) the transient normalized decays of these bands..... 80

3.18 Comparison of above gap (3.1 eV) and below gap (1.55 eV) excitation of RRa-P3HT/PCBM (1.2:1) film (a) PM spectra at t = 10 ps; (b) transient decay dynamics at 1.7 eV; and (c) at 1.25 eV..... 81

3.19 Schematic diagram of model for the photophysics of P3HT/Fullerenes.... 83

4.1 Chemical structures of DOO-PPV and MEH-PPV polymers..... 86

4.2 Transient PM measurement of DOO-PPV film. (a) Transient PM spectrum at t = 0 ps (right axis); various bands such as PA_1, SE and PB are assigned. The cw PL with 0-0 and 0-1 phonon replica, and absorption spectra are also shown (left axis). (b) PMD, and (c) PA kinetics at probe energies of 1.35 (PA_1) (green, diamonds), 1.6 (zero-crossing) (blue, squares) and 2.0 eV (SE) (red, circles). The continuous lines are a guide to the eye, and for ease of comparison the various decays are shifted vertically along with their zero value. Adapted from Ref.[85]..... 91

4.3 Same as in Figure 4.2, but for MEH-PPV solution..... 94

4.4 Same as in Figure 4.2 and 4.3, but for MEH-PPV film at t = 0 and 60 ps, respectively. In (a) the new PA_{ex} is assigned; and in (b) [(c)]the PMD [PA] kinetics is plotted in logarithmical time scale..... 97

4.5 Photoluminescence (PL) spectra of MEH-PPV film at different pressures at 300K. Inset shows the pressure dependence of PL peak positions along with quadratic ($E_{PL} = -10P + 0.11 P^2$) and linear ($E_{PL} = -2.76P$) fits, where E_{PL} is in meV and P is in kbar. (Adapted from Ref. [123])..... 103

4.6 Transient photomodulation spectra of MEH-PPV film at two different pressures of 0 and 77 kbar at t = 0 ps. Various bands such as PA', PA'', PA_1, PA''' and SE are assigned. The blue-shifts of PA' and PA'' are shown by arrows..... 105

4.7 Transient photomodulation (PM) spectra of MEH-PPV film at three different pressures of 0 67 and 103 kbar at t = 5 ps. Various bands such as PA'', PA''' and SE are assigned. Inset shows the CW PM spectra of MEH-PPV film at the pressure of 77 kbar..... 107

4.8 Photomodulation decay kinetics of MEH-PPV film at different indicated pressures and at different probe energies of (a) 2.0 eV, (b) 1.29 eV and (c) 1.63 eV..... 108

4.9 Polarized PM decay kinetics and their ratio (parallel/perpendicular) of MEH-PPV film at ambient pressure at the PM spectrum bands (a) PA1 (0.95 eV) and (b) PA' (0.33 eV)..... 111

5.1 Chemical structures of (a) Pt-1 spacer, (b) Pt-3 spacer, and (c) the generalized form of Pt-polymers..... 115

5.2 Schematic energy levels of the singlet and triplet manifolds in Pt-1 showing that the singlet MLCT lie below the π–electron state. Calculations were done by Dr. Tretiak at Los Alamos National Lab (2007)..... 116

5.3 Electroabsorption (EA) measurement of Pt-3 film. (a) EA spectrum with linear absorption. The essential states $1B_u$, mA_g, $m'A_g$ and nB_u are assigned. (b) Polarized EA spectrum of Pt-3 film with light polarization parallel (red, empty circle) and perpendicular (blue, empty square) to the applied electric field vector..... 118

5.4 The two-photon absorption (TPA) measurement of Pt-3 polymer. (a) TPA spectrum compared to the linear absorption spectrum.(b) TPA spectra with pump and probe polarizations either parallel (red, empty circle) or perpendicular (blue, empty square) to each other..... 120

5.5 The two-photon absorption (TPA) measurement of Pt-3 polymer in solution. (a) TPA spectrum compared to the linear absorption spectrum.(b) TPA spectra with pump and probe polarizations either parallel (red, empty circle) or perpendicular (blue, empty square) to each other..... 122

5.6 Electroabsorption (EA) measurement of Pt-1 polymer film. (a) EA spectrum with linear absorption. The essential states $1B_u$, mA_g, and nB_u are assigned. (b) Polarized EA spectrum with light polarization parallel (red, empty circle) and perpendicular (blue, empty square) to the applied electric field vector..... 124

5.7 The two-photon absorption (TPA) measurement of Pt-1 polymer in solution. (a) TPA spectrum compared to the linear absorption spectrum.(b) TPA spectra with pump and probe polarizations either parallel (red, empty circle) or perpendicular (blue, empty square) to each other..... 126

5.8 Transient photomodulation (PM) measurement of Pt-1 polymer. (a) The transient PM spectra using excitation of 3.1 eV at t = 0 ps, 0.5 ps and 1 ps, showing different bands PA_1, PA_2 and PA_3. (b) The decay dynamics of these bands in the spectrum. These measurements were done by Drs Tong and Gambetta in our group..... 127

LIST OF TABLES

3.1 The transient decay parameters (lifetimes and relative weight contributions) of the PA and PB bands in the PM spectrum of RR-P3HT film..... 57

3.2 The transient decay parameters (lifetimes and relative contributions) of different bands of RR-P3HT/PCBM film..... 63

3.3 The transient decay parameters (lifetime and relative contribution) and photovoltaic device parameters of annealed RR-P3HT/PCBM (1.2 : 1) films with different % of Galvinoxyl radical impurities..... 73

4.1 The photophysics parameters of DOO-PPV and MEH-PPV solutions and films. The measured and calculated steady state PL QE; and the PM and PMD lifetimes, τ at various probe frequencies in the transient PM spectra. P(0) is the PM value at t = 0. The short component lifetime is given as needed for a few samples and photon frequencies..... 92

4.2 Photomodulation decay fitting parameters with their relative contributions of MEH-PPV film at different pressures and at the probe energies of 1.29 and 1.63 eV..... 110

ACKNOWLEDGEMENTS

I would like to express my deepest and sincere gratitude to my advisor Prof. Z. Valy Vardeny for his constant support, guidance and encouragement through all the years of my Ph.D. His scientific passion and intuition, and discussion through "Monday-group-meeting" have been an invaluable experience to me. I also express my sincere gratitude to my supervisory committee members: Professors John Lupton, Oleg Starykh, Michael Morse and Ajay Nahata for their encouraging discussions and suggestions. I also thank Prof. Sumit Mazumdar from University of Arizona, for his theoretical insights.

A Ph.D.degree in experimental physics needs a lot of technical assistance, and this was available to me through the help of Dr. Randy Poslon, Mr. Leonard Wojcik, Dr. Mathew Delong and Wayne Wingert. I am grateful for their help. I would like to thank my former group members, Dr. Minghong Tong, for introducing me to the ultrafast measurements, Drs. ChuanXiang Sheng, Josh Holt, Tomer Drori, Valentina Morandi, and Alessio Gambetta for their valuable support and collaborations.

My sincere gratitude is extended to my current group members, Golda Hukic, Ye Zhang, Ella Olejnik, Bill Pandit, Dr. Tho Nguyen, Joshua Kennedy, Maria Navas, Bhoj Gautam, Tek Prasad Basel and Ruiyao Wang for their collaboration, support and friendly suggestions.

Last but not least, I thank my wife, Asha, and my family in India for their endless support, love and encouragement through all these years of my Ph.D.

CHAPTER 1

INTRODUCTION

1.1 π-conjugated polymers

π-conjugated polymers (PCPs) were discovered about 30 years ago. Since their discovery, they have been widely used for the fabrication of electronic and optoelectronic devices [1, 2] such as organic light emitting diodes (OLEDs) [3, 4], thin film transistors (TFTs) [5-7], photovoltaic cells [8, 9], optical switches and modulators. The PCPs, also called conducting polymers, owe their name to the delocalized π-electrons along the polymer backbone. The simplest PCP, namely polyacetylene, $(CH)_x$ consists of carbon atoms in its backbone chain (see Figure 1.1), which has six electrons, the $1S_2 2S_2 2P_2$. In the case of $(CH)_x$, and also in most other conjugated polymers, the carbon 2S orbital mixes with $2P_x$ and $2P_y$ orbitals to form three energy equivalent sp^2 orbitals; this is dubbed sp^2 hybridization. The sp^2 hybridized electrons are responsible for the so-called 'σ- bonding' to the three in-plane neighbors in polyacetylene, namely, two with the nearest neighbor carbons forming the polymer chain backbone, and the other bond with an adjacent hydrogen atom. The $2P_z$ orbitals of all carbon atoms are linearly combined to form what is called "π molecular orbital" which is delocalized electrons along the

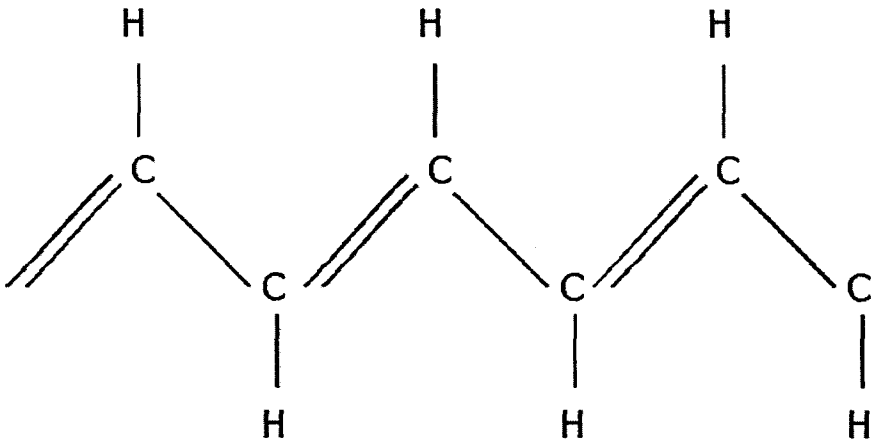

Figure 1.1: Chemical structure of trans-$(CH)_x$

polymer chain, and perpendicular to the σ bonding plane.

Because of the Peierls distortion [10], in principle the pristine one-dimensional (1D) $(CH)_x$ is an insulator. The adjacent CH groups move towards each other, forming alternating single and double bonds that have different bond lengths and thus creating an energy gap of about 1.5 eV between the highest occupied molecular orbital (HOMO) and the lowest unoccupied molecular orbital (LUMO). This process is called "dimerizaiton" [10, 11].

Trans-$(CH)_x$ is the simplest but special polymer, since it has twofold degenerate ground state (DGS) [12]; the other polymers that will be discussed in this dissertation, are nondegenerate ground state (NDGS) PCPs [11, 12], e.g., 2,5-dioctyloxy poly-(phenylene vinylene) (DOO-PPV), and poly[2-methoxy-5-(2'-ethylhexyloxy)-p-phenylene vinylene] (MEH-PPV). Despite the apparent differences in their chemical structures, the common feature among the various PCPs is the delocalized π-electrons along the chain, which are manifested in the single-double bond alteration.

In 1973, H. Shirakawa et al. [13] first synthesized a polyacetylene film from powder. It was nonconducting because the bandgap was too large for thermal excitations of electrons from HOMO to LUMO. This polymer was found to be susceptible to chemical doping, reaching a metallic state [14, 15]; this was a milestone that began the extensive research and applications of the PCPs, now called conducting polymers. In subsequent developments, the first PCPs field-effect transistor (FET) was made in 1986 using polythiophene [16]. A big breakthrough in FET research came from the use of Regio-regular polythiophene (RR-P3HT) in 1996 [17], which reached electron mobility of ~0.045 $cm^2(Volt\ sec)^{-1}$ in comparison with 10^{-5} $cm^2(Volt\ sec)^{-1}$ that had being reported before in Ref. [15]; in 2004, the carriers mobility was improved to reach 0.7 $cm^2(Volt\ sec)^{-1}$ in RR-P3HT FET device [18].

The first polymer light-emitting diode (PLED) [3] was demonstrated by R. Friend and coworkers, where the generation of light was achieved by radiative recombination of electrons and holes injected into the active layer of PPV polymer film from the opposite electrodes using different metals. The reverse process, namely, photovoltaic effect, was also inspired using the device based on a mixture of PPV-derivative and buckminsterfullerene (C60) [8, 9].

Optically driven laser action was discovered in the PCP [19-21]. This is a prerequisite for electrically driven polymer lasers. The realization of such a goal still remains a big challenge. Also, random laser was discovered in conducting polymer [22]; it adds a new twist to the physics of light propagation in multiple scattering media.

1.2 Symmetry and ordering of the excited state

The optical properties of π-conjugated polymers such as linear absorption, two-photon-absorption, fluorescence, phosphorescence etc., are governed by the symmetry of the molecular wave functions of the polymer. To illustrate this point, let us consider the simple example of polyenes [23].

Polyenes ($C_{2n}H_{2n+2}$) are linear chains of CH units with sp^2 hybridization of p_z atomic orbitals. The symmetry of such a polymer is described by the point group symmetry, C_{2h} [24], and thus the electronic wave functions are classified according to their inversion and rotation properties. If the orbitals change (do not change) sign under inversion at the symmetry center they are dubbed as u (g); they are denoted with b (a) if they change (do not change) sign under 180° rotation around the symmetry axis. The atomic 2p-orbitals change sign under reflection in the symmetry plane, so p-electron orbitals are only a_u or b_g.

The wave function describing the electronic states along the polymer chain is still distinguished by its g or u character, but now the inversion properties are denoted with capital letters A or B. The π-electron states in polymers can then have either A_g or B_u symmetry according to:

$$a_u \otimes a_u = b_g \otimes b_g = A_g \tag{1.1}$$

$$a_u \otimes b_g = b_g \otimes a_u = B_u \tag{1.2}$$

All the π orbitals in the HOMO in the PCPs are doubly occupied; hence the ground state of PCPs has A_g character. The next excited state, in most PCPs, has B_u

character, the next excited state will be again A_g, and so on. It is useful to label the PCP excited states as n^pX, where n is the overall quantum number, p is the spin degeneracy of the quantum state; 1 stands for singlet, and 3 for triplet; and X is its electronic wave function symmetry, such as A_g or B_u.

The luminescent properties of the PCP class of materials depend on the ordering of their excited states. When the electron-electron interactions can be neglected, then the excited states order is:

$$1^1A_g < 1^1B_u < 2^1A_g \tag{1.3}$$

The energies of these configurations can be regarded as approximately equal to the sum of the orbital energies. However, when including the electron-electron interaction then the energetic ordering of the first excited states may be reversed:

$$1^1A_g < 2^1A_g < 1^1B_u \tag{1.4}$$

The ordering of the first excited states affects the optical properties of the material. When the $1B_u$ excited stated has lower energy than the $2A_g$ excited state (Figure 1.2(a)), the material is expected to show strong fluorescence, since the $B_u \rightarrow A_g$ transition is dipole allowed. This is the case of polythiophene and poly (p-phenylenevenylene)s, among other PCPs. Instead, if the $1B_u$ excited stated has higher energy than the $2A_g$ excited state as shown in Figure 1.2(b), then the first excited state decays nonradiatively to the ground state, due to the dipole forbidden $A_g \rightarrow A_g$ transition, and very little

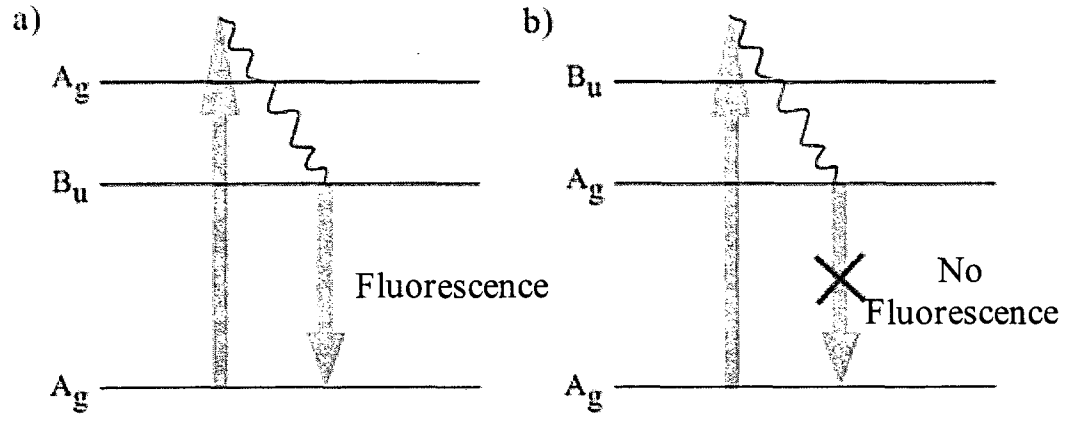

Figure 1.2: A different ordering of the first excited states gives rise to different optical properties. Upon absorption of a photon the polymer fluoresces if $1^1A_g < 1^1B_u < 2^1A_g$.

fluorescence occurs, mainly during the thermalization process (~1ps or less). This happens, for instance, in the case of trans-polyacetylene and polydiacetylenes. A complete discussion about the interplay of electron-electron and electron-phonon coupling on state ordering is given in reference [25].

1.3 Excitation models for π-conjugated polymers

Su, Schriefer and Heeger proposed a model (SSH) based on tight binding approximation calculations taking into account only the electron-phonon interaction, thus ignoring the electron-electron interaction [26]. They applied a semiclassical Huckel Hamiltonian that contains two components: the lattice kinetic energy, which is treated classically, and the electron-phonon interaction, which is treated quantum mechanically, as expressed in the following Hamiltonian:

$$H_{SSH} = \frac{K}{2}\sum_{n}(u_n - u_{n-1})^2 + \frac{M}{2}\sum_{n}\left(\frac{du_n}{dt}\right)^2 - \sum_{n,s}(t_0 + \alpha(u_{n+1} - u_n))(C^{+}_{n+1,s}\,C_{n,s}$$

$$+C^{+}_{n,s}C_{n+1,s}) \qquad (1.5)$$

where t_o is the hopping integral between the nearest neighbors for an undistorted chain, α is the electron lattice coupling constant, $C^{+}_{n,s}$ and $C_{n,s}$ are the creation and annihilation operators of an electron on site n with spin s, K is the spring constant due to the π-electrons and u_n is the deviation of the n-th site from the equilibrium position in an undistorted chain with equal distance between sites.

The SSH model predicts that dimerization caused by strong electron-phonon interaction lowers the system energy, and opens an energy gap $\Delta = 4\alpha u$. Thus the occupied electronic states in equilibrium are lowered, causing this configuration to be more stable (Figure 1.3(b)). In this way the system no longer acts as a one-dimensional metal, but instead it has the properties of a semiconductor.

Models including electron-electron interaction and 3D interchain coupling are based on Hubbard type Hamiltonians, where the Hubbard contribution to the Hamiltonian is:

$$H_{Hub} = U\sum_i n_{i,\uparrow}n_{i,\downarrow} \qquad (1.6)$$

where U is the Coulomb repulsion between two electrons on the same site, $n_{i,\uparrow}$ and $n_{i,\downarrow}$ describe the density operators for electrons with spin up and spin down, respectively.

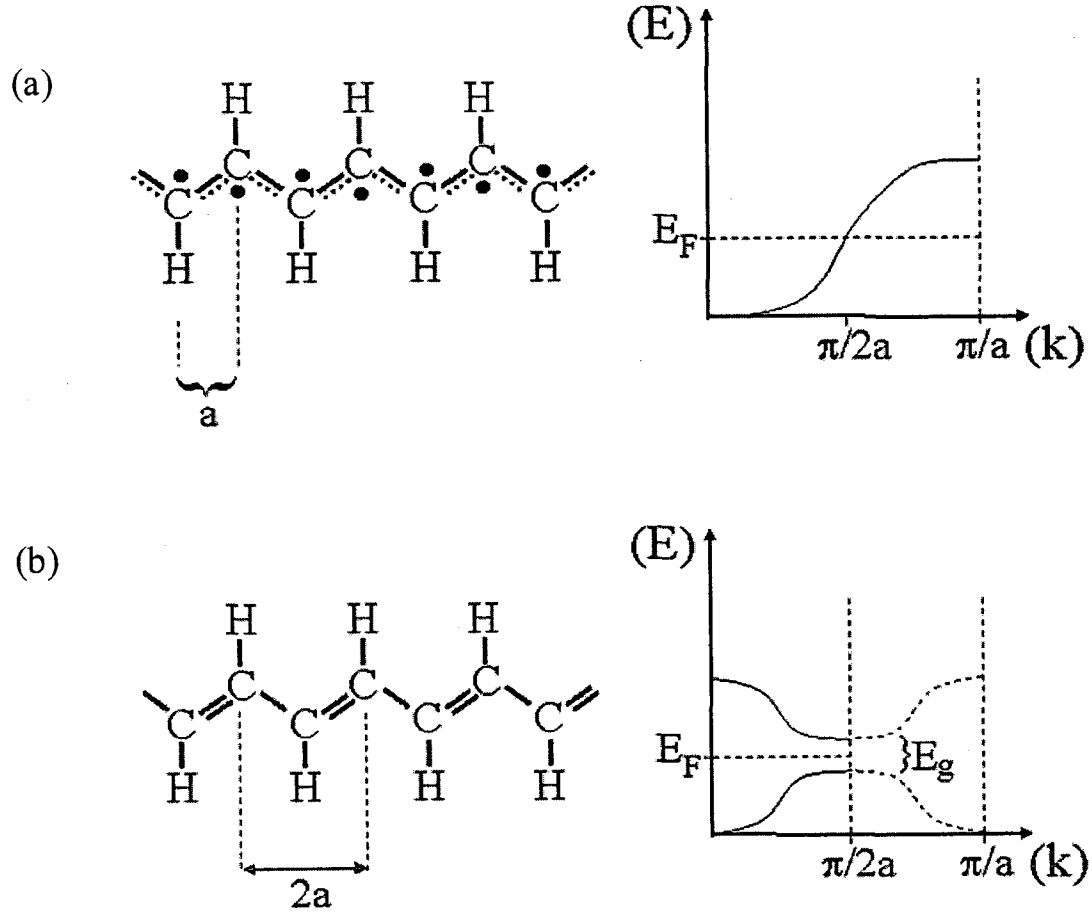

Figure 1.3: Effect of dimerization on the electronic properties of polyacetylene (a) The undimerized state of π-electrons that has the properties of a metal; (b) the dimerized state with properties of a semiconductor.

However, since the Hubbard model disregards electron-phonon interaction, which is quite strong in the polymer system, a combination of both SSH model and Hubbard model is more realistic, as has been used by Mazumdar and Dixit [27, 28] to explain the energy levels of excitations in the class of π-conjugated polymers. Since electron-electron interaction is so strong in one-dimensional polymers, the lowest optical transition is not a transition from the valence band into the conduction band, like in usual semiconductors, but instead an excitonic transition, where intrachain exciton binding energies as large as 0.4 to 0.8 eV have been inferred.

1.4 Photoexcitations in π-conjugated polymers

When the π-conjugated polymer is excited with above-gap photon energy, both short- and long-lived photoexcitations are created. These photoexcitations can be detected and characterized by transient and CW photomodulation (PM) techniques, where a pump beam generates the photoexcitations, and subsequently the induced optical absorption spectrum due to the presence of photoexcited species is monitored with the probe beam in a broad spectral range from mid-IR to visible using different probe sources. The PM spectrum essentially measures difference spectra, i.e., the difference in the optical absorption ($\Delta\alpha$) of the polymer when it contains a nonequilibrium carrier concentration and that in the equilibrium ground state. Therefore the optical transitions of the various photoexcitations are of fundamental importance.

1.4.1 Charge photoexcitations in the NDGS polymers

The charge excitations in the NDGS class of polymers can be in the form of polaron ($P^{\pm}$) with spin quantum number, s = 1/2 or bipolaron ($BP^{2\pm}$) with s = 0. In addition there is a third possibility of interchain bipolaron or π-dimer. Generally, these charge excitations are long-lived (nano-second to milli-second) in the polymer; but they may be photogenerated in very short time, and this enriches the photophysics in the pico-second time domain.

1.4.1.1 The polaron excitation

A polaron is a charged excitation that lowers its energy compared to a bare electron (or hole) due to a distortion of the lattice structure (electron-phonon relaxation). The polaron species carries spin 1/2 and a unit charge, e. The energy diagram and associated optical transitions for a polaron excitation ($P^{\pm}$) are shown in Figure 1.4. The positive polaron energy states in the gap are SOMO (single occupied molecular orbital) and LUMO, respectively, separated by $2\omega_0(P)$. There are three possible optical transitions P_1, P_2, P_3. In oligomers, the parity of the HOMO, SOMO, LUMO and LUMO+1 levels alternate; they have symmetry of g, u, g, and u, respectively. Therefore, polaron has two allowed optical transitions P_1 and P_2, whereas the third possible transition P_3 is dipole forbidden. Polarons can be created by doping, charge injection from metallic electrodes, or photogeneration. When polarons are created, then their absorption spectrum contains two absorption bands, which upon photogeneration are dubbed photoinduced absorption (PA). For PPV type polymers, the two PA bands are in the near IR (1.4 eV) and mid IR

(0.35eV) spectral range, respectively [29]. The theory of polaron transitions has so far not been proposed for a long correlated polymer chain.

1.4.1.2 The bipolaron excitation

When two "same charge" polarons come together on the same chain of a nondegenerate ground state conjugated polymer, they tend to reduce their elastic energy by forming a bipolaron ($BP^{2\pm}$), which is a more stable excitation species. The energy diagram and the possible optical transitions for bipolaron ($BP^{2\pm}$) are given in Figure 1.5. For positive bipolaron there are two unoccupied energy states separated by $2\omega_0$ (BP): the LUMO and LUMO+1, which are deeper in the gap than corresponding states for P^+. Two optical transitions are then possible: BP_1 and BP_2. In short oligomers, however, the parity of HOMO, LUMO and LUMO+1 alternate (g, u, and g, respectively). Therefore BP_1 transition is allowed and BP_2 transition is dipole forbidden. Electron correlation and disorder-induced relaxation of the optical selection rules however may cause the BP_2 transition to gain intensity, and therefore BPs with one strong transition at low energy and a second, weaker transition at higher energy might be observed in "real" films.

1.4.2 Neutral photoexcitations in the NDGS polymers

1.4.2.1 The singlet exciton

Excitons are neutral, Coulombically bound electron hole pairs. When an exciton is optically created, it is initially in a spinless singlet configuration. In terms of the "four essential states" model [30] there are four essential excitonic states: the ground state $1A_g$

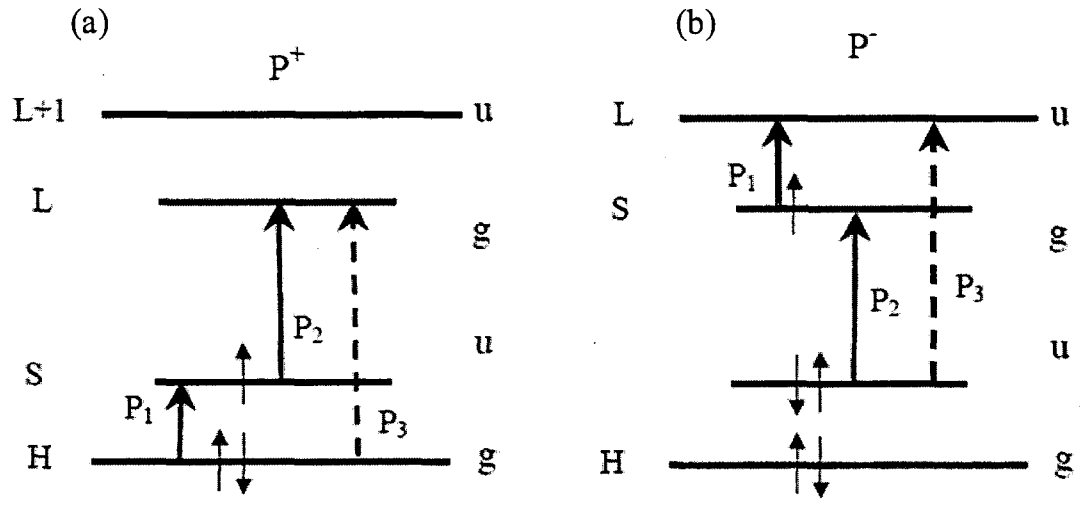

Figure 1.4: Energy levels and associated optical transitions of (a) positive, and (b) negative polarons.

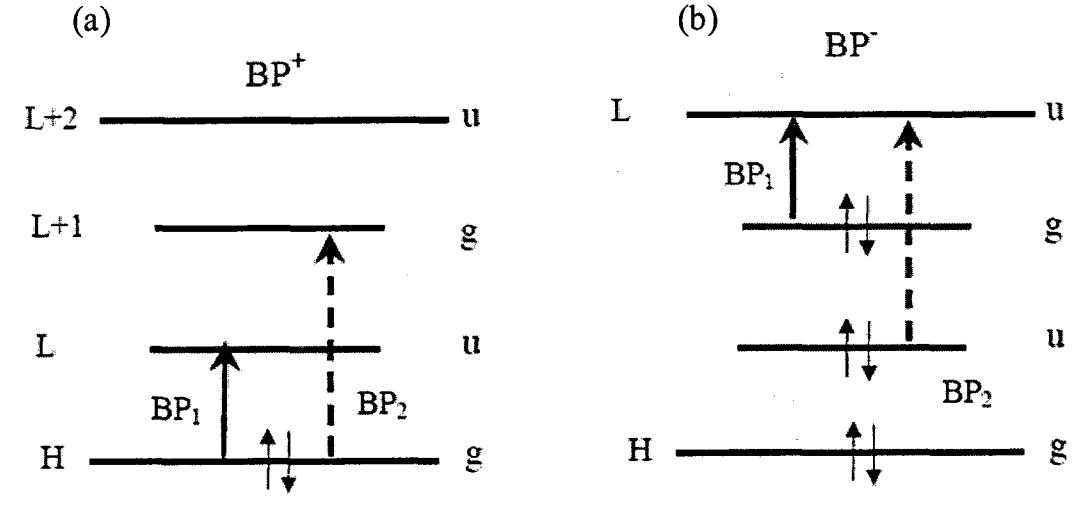

Figure 1.5: Energy levels and associated optical transitions of (a) positive, and (b) negative bipolarons.

and three singlet excited exciton levels: $1B_u$, mA_g and kA_g, which predict most nonlinear optical (NLO) properties of π-conjugated polymers. The energy diagram of the four essential states is shown in Figure 1.6(a). The mA_g is an excited state above the $1B_u$ level, whereas the kA_g excited state may be due to a biexciton state, i.e., a bound state of two $1B_u$ excitons. The mA_g and kA_g levels are known to have strong dipole moment coupling to $1B_u$, as deduced from the various optical nonlinear spectra of π-conjugated polymers. Therefore two strong optical transitions were expected to form following the $1B_u$ photogeneration: PA_1 and PA_2, as shown in Figure 1.6(a). Due to exciton self-trapping, however, we do not know whether PA_1 would maintain its strength, since the relaxed $1B_u$ state may no longer overlap well with the mA_g state. PA_2, on the other hand, will be always relatively strong regardless of the $1B_u$ relaxation, since there is always room for a second exciton photogeneration on a chain following the photogeneration of the first exciton. For PPV type conjugated polymer the PA_1 band is usually around 1 eV, and PA_2 is in the visible/near IR range.

Following photogeneration the exciton may relax nonradiatively to the lowest excited state within sub-picosecond time interval. This relaxation is due to either vibrational cooling within the vibronic sidebands of the same electronic state, or phonon assisted transitions between two different electronic states. In molecular spectroscopy the latter is called internal conversion. Internal conversion is usually the fastest nonradiative relaxation channel in electronic states with the same spin configuration. In π-conjugated polymers the internal conversion is very effective due to the strong interaction of excitons

with optical phonons. As a result Vavilov-Kasha's rule [31] is also viable in luminescent conjugated polymers, which states that the main fluorescence occurs from the lowest excited electronic state, and its quantum efficiency is independent of the excitation energy. However in polymers there are other processes that may interfere and compete with the internal conversion. For example there are singlet exciton fission, which creates two triplet excitons with opposite spins, and exciton disassociation, which generates charge carriers (polarons) albeit in the spin singlet configuration.

π-conjugated polymers are generally characterized by significant inhomogeneous broadening, which manifests itself in a featureless absorption spectrum. The broad distribution of conjugation length leads to a broad distribution of energy levels. Excitons may migrate to the bottom of the inhomogeneously broadened density of states, i.e., to the energetically favorable states with the longest conjugation length, via the incoherent intermolecular energy transfer, dubbed Förster energy transfer. Thus the inhomogeneous broadening opens an additional relaxation pathway for the excited states. This effect is absent in solution, since the average interchain distance is relatively large. Förster energy transfer within the excitons density of states in films gives rise to transient PL red shift on ps time scale. For studying this process in detail, polarization memory dynamics is usually measured.

Typical lifetime of the lowest singlet exciton in luminescent π-conjugated polymers is of the order of 100 ps. Two processes contribute to the exciton lifetime: radiative and nonradiative recombination processes. Exciton radiative lifetime in π-conjugated polymers was determined to be about 1 ns; it actually fits well with the exciton size in the dipole approximation. The temporal evolution of excitons can be

detected using transient pump-probe spectroscopy and PL up-conversion based on NLO processes. Transient pump-probe is a powerful tool to study not only the optical transitions of excitons but also other secondary photoexcitations such as polarons. Large binding energy of excitons is expected in low-dimensional systems with strong electron correlation effects [32, 33]. The binding energy of intrachain excitons in π-conjugated polymers is still debated, but a consensus seems to put it at about 0.5 eV. This value is in agreement with the exciton binding energy in polydiacetylene, which is universally accepted [34]. With such large binding energy solutions of the Coulomb interaction Hamiltonian in one dimension (1D) obtained by Loudon several decades back show that the exciton state 'grabs' most of the oscillator strength from interband transition [35]. As a result the interband transition strength is weak, and because of inhomogeneity is in fact invisible in linear absorption, unless sophisticated modulation techniques are employed.

In the "band model" that describes excitations in polymers in terms of free electrons and holes, photon absorption by the photogenerated carrier in the continuum band (i.e., valence or conduction bands) is forbidden due to two particle energy quasi-momentum conservation rules; it can be assisted however by phonons and/or impurities. Furthermore photogenerated carriers in more common semiconductors do not show structured PA bands; instead, their PA is in the form of a structureless Drude free carrier absorption that peaks at low energies. On the contrary, in the "exciton model" for describing the photoexcitations in polymers, photon absorption by a low-lying exciton that results in the creation of higher energy exciton is, in fact an allowed two-particle process and the PA bands have clear structure due to large bonding energy.

1.4.2.2 The triplet exciton

Triplet excitons can be generated from singlet excitons through intersystem crossing, which is more efficient when the energy difference between the singlet and triplet states is small. The most important electronic states in the triplet manifold are shown in Figure 1.6(b). The lowest triplet level is 1^3B_u, which is lower than the corresponding singlet level ($1B_u$) by the singlet-triplet energy splitting Δ_{ST}. In principle, 1^3B_u can directly recombine radiatively to the ground state by emitting photons (leading to phosphorescence, PH) or nonradiatively by emitting phonons. However the optical transition is spin-forbidden and therefore extremely weak, which leads to the well-known long triplet lifetime. The other two levels shown in Figure 1.6(b) are the m^3A_g level, which is equivalent to mA_g in the singlet manifold, and the k^3A_g level, which is a complex composed of a triplet exciton and a singlet exciton bound together.

As in the case of singlet excitons, for triplet excitons there are two strong transitions T_1 and T_2. T_1 is a transition from 1^3B_u to m^3A_g level; T_2 is transition from 1^3B_u to k^3A_g level (has never been identified, though). Since the m^3A_g and mA_g levels should not be far from each other, it is possible to estimate Δ_{ST} from the relation:

$$\Delta_{ST} = T_1\text{-}PA_1 \tag{1.7}$$

Δ_{ST} has been recently been directly measured in π-conjugated polymers from phosphorescence emission involving heavy atoms and other techniques [36], and

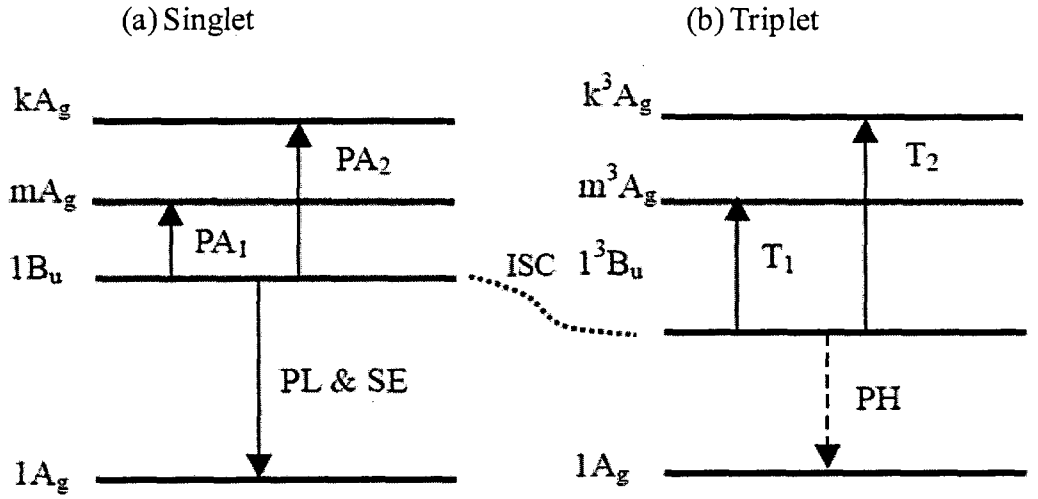

Figure 1.6: Schematic energy diagram and optical transitions associated with (a) singlet, and (b) triplet excitons.

Equation 1.7 has actually been confirmed. Unfortunately we do not know whether T_1 is indeed strong, since as for singlet excitons the relaxed triplet exciton may not well overlap with the m^3A_g state, leading to a decrease in T_1 intensity. In contrast, it is quite certain that transition T_2 into the k^3A_g level is strong, because it is always possible to photogenerate a second (singlet) exciton close to a previously formed triplet exciton. However, this transition has not yet been identified in π-conjugated polymers.

1.4.2.3 The polaron pair excitation

A polaron pair (PP) species is a bound pair of two oppositely charged polarons, P^+ and P^-, formed on two neighboring chains. The binding energy is mainly Coulombic in nature, and is normally weaker than that of the intrachain exciton. Due to the interaction

between the polarons, the energy levels of the polaron pair are shifted with respect to the energy levels of a single polaron, as shown in Figure 1.7. There are three strong transitions, PP_1-PP_3. For loosely bound PP excitations these transitions are not far from transitions P_1-P_3 of polarons. However for a tightly bound PP excitations a single transition, PP_2 will dominate the spectrum, as PP_1 is considered to be intraband with traditional low intensity and PP_3 is close to the fundamental transition and therefore difficult to observe.

We note that the PP_2 transition is close in spirit to transition PA_2 discussed above for excitons, as a second electron is also promoted to the excited level in the case of PP. Then from the experimental point of view, it is not easy to identify and separate in the PM spectra the PA2 transition due to exciton from those of a tightly bound PP. They may differ, however, in their PADMR spectra.

1.4.3 Excimer, pi-dimer and exciplex species

A variety of interchain species may be introduced when two adjacent chains interact with each other.

Excimers and pi-dimers only exist in the excited state. They are formed when two neighboring polymers share their π-electrons in the excited state but not in the ground state [37-39]. These emissive excited state complexes have a dissociative ground state, that is, the ground state of the dimer spontaneously dissociates into two ground-state molecules. Furthermore, the excimer cannot be directly excited optically. Instead, an

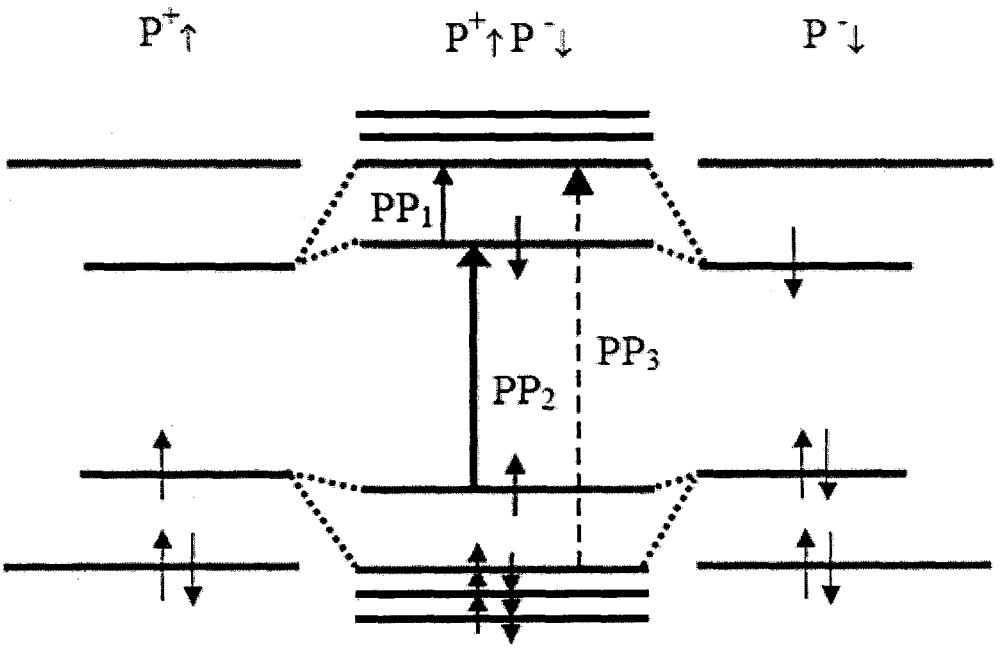

Figure 1.7: Energy diagram and optical transitions associated with polaron-pairs.

intramolecular singlet exciton is photoexcited that at a later time delocalizes over two molecules, forming the excimer. Excimer formation is accompanied by a strong geometric distortion along the intermolecular axis that, when combined with the dissociative nature of the ground state, leads to featureless, strongly Stokes-shifted emission of films in comparison to dilute solution. Excimer formation was observed in PPV-based films [40], leading to quenching of luminescence due to their large nonradiative decay in this polymer.

An interchain excited state, called an exciplex, can also be formed when an *unequal* sharing of π-electron density between chains or a partial degree of charge transfer occur [37, 39].

While excimers exist only in the excited state, interchain interaction may also lead to ground-state interactions, with formation of aggregate states [23, 38]. Upon aggregation, both the ground- and excited-state wave functions are delocalized over several polymer chains. The aggregate is therefore directly accessible by spectroscopic means. The existence of these species was suggested in ladder-type polymers [41] (and later conclusively disproved [42]) and poly-pyridine films [43], where it appears to quench PL efficiencies in film samples compared to solution.

CHAPTER 2

EXPERIMENTAL TECHNIQUES

The present chapter discusses the experimental techniques used for characterizing the polymer thin film, solution, or blend films of polymer with fullerene. Polymer thin films have been deposited on glass or quartz substrates by either drop casting or spin casting the solution. To avoid oxygen contamination all the handling steps of polymer films were done inside the inert (N_2) atmosphere of a glove box with oxygen level less than 0.5 ppm.

2.1 Ultrafast excitation sources

2.1.1 Femtosecond Ti:Sapphire setup

Our low repetition rate Ti:Sapphire laser system consists of a home-made Ti:Sapphire oscillator and Ti:Sapphire amplifier. Its schematic diagram is shown in Figure 2.1. The oscillator is passively mode-locked, and was assembled at the university of Utah laser institute based on "Kapteyn-Murnane 11 fs scheme" [44]. It yields a pulse laser output of ~350 mW at 800 nm, with pulse duration of less than 100 fs and a repetition rate of 76 MHz. The oscillator is pumped by a cw 5W diode laser (532 nm) *Millenia Pro (Spectra Physics),* and its cavity contains two fused silica prisms to

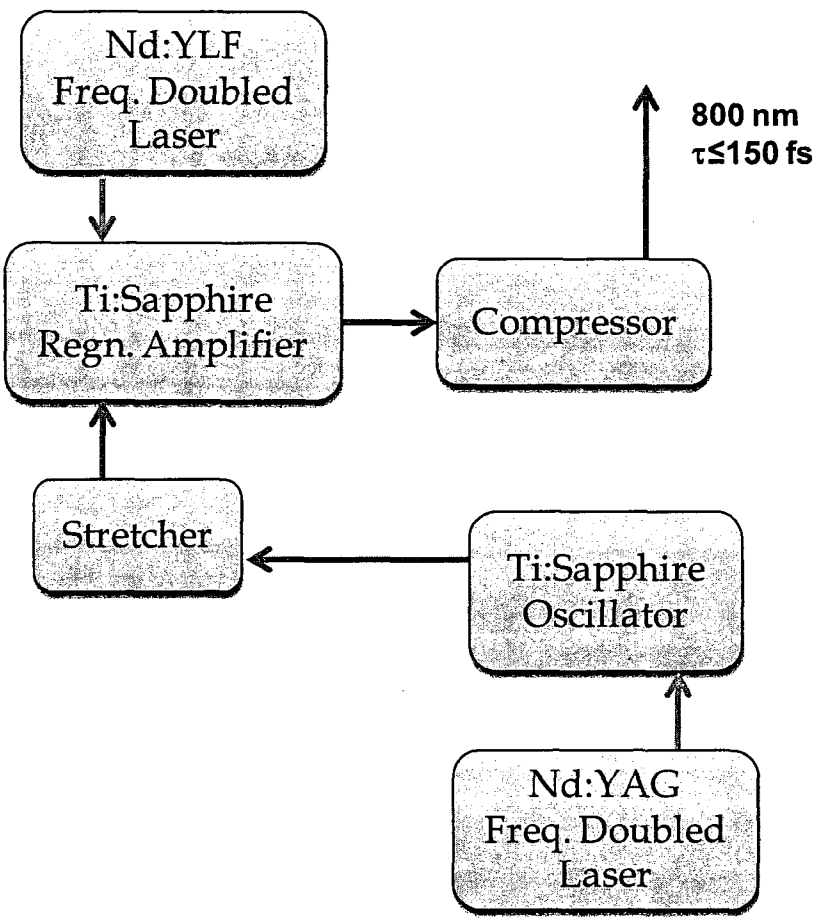

Figure 2.1: Schematic diagram of Ti:Sapphire regenerative amplifier laser system.

compensate the dispersion caused by the 4.75 mm long Ti:sapphire crystal. The oscillator can run either in cw mode or in mode-locked pulse mode. The mode locking is achieved by fine adjustment of one of prism in the cavity. The output stability of this oscillator is crucial to the stable performance of the amplifier. Usually the fluctuations in the output power of the oscillator are <1%. The output power of the oscillator is monitored by a fast-scan autocorrelator that measures the pulse duration of the pulse train. The output beam of the oscillator is fed into a regenerative amplifier cavity.

Our Ti:sapphire regenerative amplifier, which is home-made, was built based on the configuration provided by Positive Light Inc. [45]. It is pumped by *Coherent Evolution-15* ~200 nanosecond Q-switched Nd:YLF laser at 527 nm at a repetition rate of 1 kHz. The output of the amplifier is 1 kHz repetition rate 800 nm wavelength pulses of ~150 fs. The pulse energy at the output beam is five orders of magnitude higher compared to that from the oscillator, due to the lower repetition rate and amplification that occurs in the system. There are three major parts of the Ti:Sapphire regenerative amplifier setup; these are: 'stretcher', 'amplifier' and 'compressor'. The 'stretcher' role is to stretch the ultrashort pulses into long pulses by delaying different frequency components of the pulse with respect to each other using group velocity dispersion. This is done to avoid damaging the optical components inside the cavity due to the high peak power. The stretched pulses enter into the 'amplifier' cavity, where they are amplified by 5-6 orders of magnitude. The pulses are finally recompressed by the 'compressor', which works in a way just the opposite to that of 'stretcher' part.

2.1.1.1 Autocorrelation

The output pulses from the oscillator and amplifier are characterized by the autocorrelation technique [46, 47]. In this technique a beam is split (50/50) into two almost equally optical paths that go through different delay stages; and they meet again on a nonlinear BBO crystal. The generated sum-frequency signal from the crystal is monitored by a detector (PMT or CCD arrays). Figure 2.2(a) shows the temporal profile of the pulses from the amplifier. Their spectral profiles are also shown in Figure 2.2(b). These pulses are not 'transform-limited' because the time-bandwidth product ($\Delta E \times t_p$) for the pulses is 1.08. The time-bandwidth product for a transform-limited Gaussian pulse is 0.44.

2.1.2 White light supercontinuum generation

White light supercontinuum acts as a femtosecond probe source in ultrafast pump-probe measurements. It is generated by focusing the amplified pulses onto a transparent substance where the output pulses are substantially spectral broadened. White light supercontinuum has been observed in many different materials including solids, liquids and gases. There are many nonlinear processes responsible for white light supercontinuum generation such as self-phase-modulation, four-wave-mixing, Raman scattering, self-focusing, etc. But in case of femtosecond pulses self-phase-modulation due to the nonlinear refractive index of the transparent medium is the dominant mechanism [48].

In our laboratory we create white light supercontinuum by focusing <10 mW of the fundamental 800 nm light onto a 1 mm thick sapphire plate. This yields an output

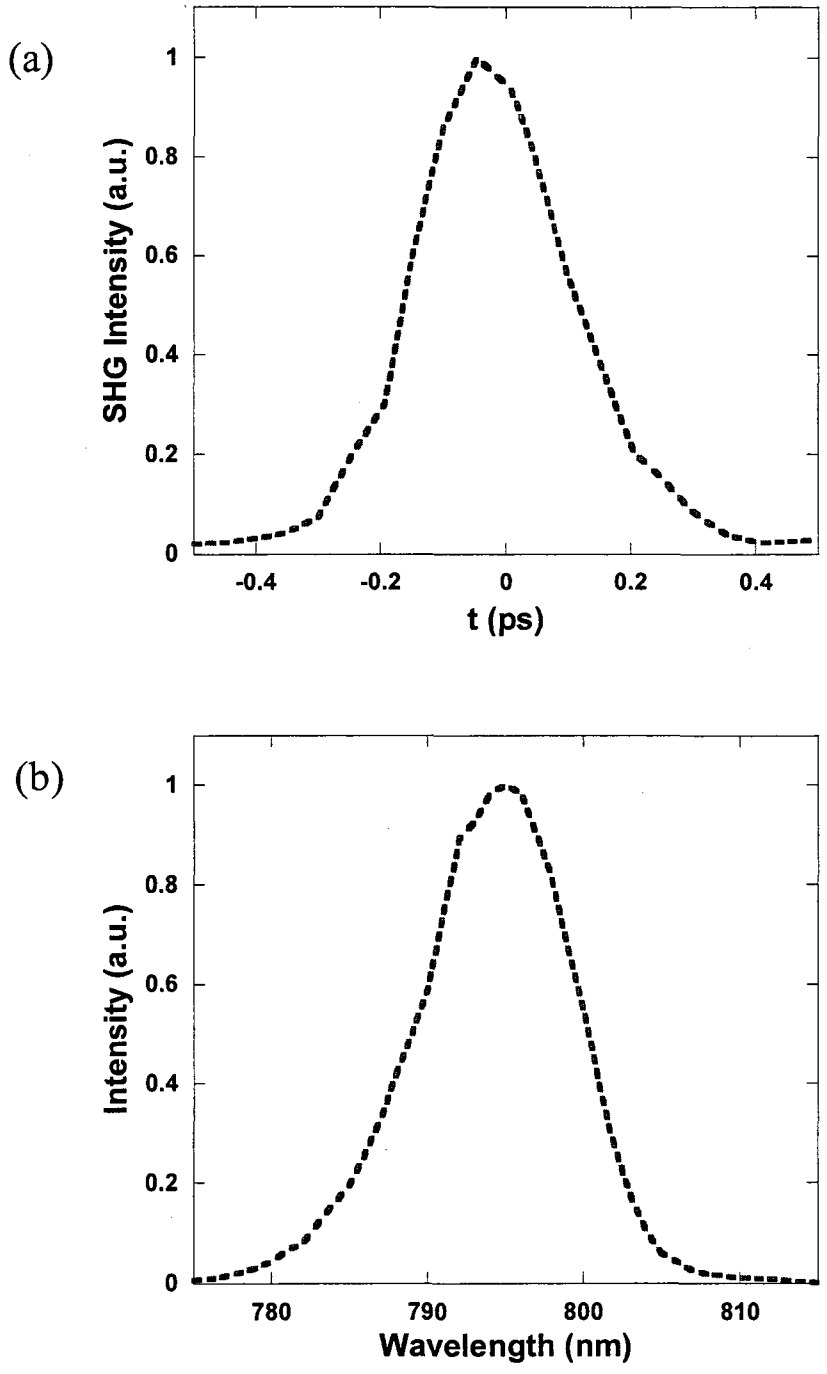

Figure 2.2: Characterization of fundamental pulses at 800nm; (a) temporal profile measured by autocorrelation, and (b) spectral profile.

pulse train of a broad spectrum from 450 nm to 1000 nm; but the spectrum is not uniform as shown in Figure 2.3(a). We also use a notch filter after the sapphire plate to remove the residual 800 nm fundamental laser from the white light supercontinuum probe pulses. Otherwise the high intensity at 800 nm would saturate the monitoring photodiode, and this creates an artifact.

Generating a stable white light supercontinuum out of the 800 nm amplified laser pulses train is a bit 'tricky', and requires the attainment of the following conditions: (1) minimum fluctuations; (2) maximum compression (this leads to shortest possible pulses); and (3) minimum intensity of the fundamental 800 nm beam. This intensity is controlled by a neutral density filter and an aperture, making the fundamental beam perfectly circular by blocking the unwanted peripheral beam. After the iris, the light beam is focused onto the transparent sapphire plate by a lens, and the generated white light supercontinuum is then collimated by another lens. The white light supercontinuum contains chirp pulses due to group velocity dispersion present at different frequency part of their spectrum. Due to this chirp, the redder part of the supercontinuum spectrum is delayed compared to the bluer part, and this has to be compensated while taking the transmission spectrum at a fixed time delay in the pump-probe correlation measurements.

The way to compensate for this chirp is by making two-photon-absorption (TPA) measurements which gives the 'zero-time' position at each wavelength of the pulse spectrum. These 'zero-time' positions are plotted against the respective wavelengths as shown in Figure 2.3(b); we fit it using a second-order polynomial function, as shown in the inset table with different coefficients. Finally, this calibration is used in a computer

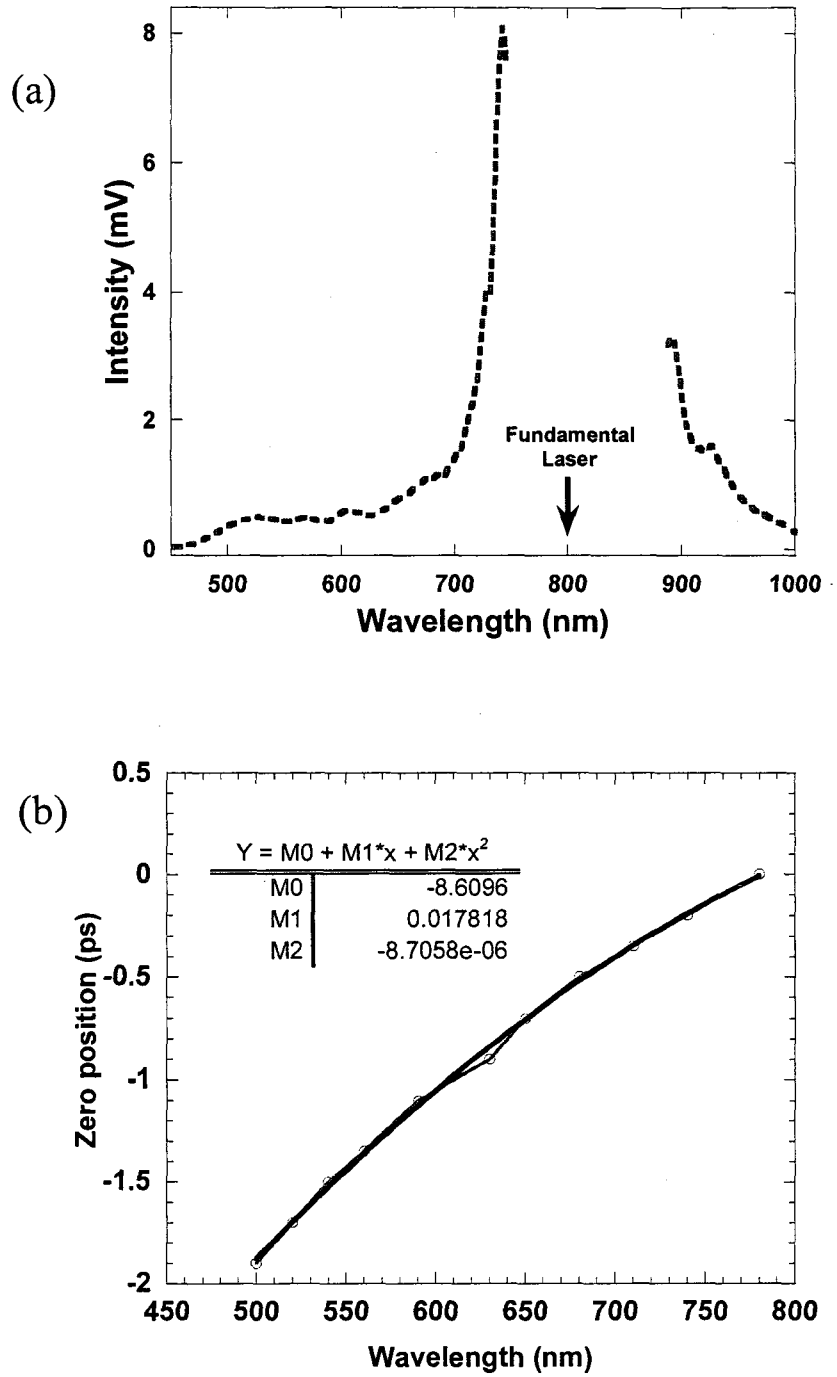

Figure 2.3: Characterization of white light continuum (WLC) source; (a) Spectrum of WLC generated by 800 nm fundamental laser, and (b) chirp of WLC against wavelength fitted with second-order polynomial function

controlled stage program to move the translation stage during the time of the measurements when ΔT spectrum is obtained.

2.1.3 Low-energy high repetition-rate system

In addition to the high-energy low repetition-rate ultrafast laser system, we also used a low-energy high repetition-rate ultrafast system based on an optical parametric oscillator (OPO) *(OPAL, Spectra-Physics)* which covers the mid-infrared range, namely 0.1–1.1 eV. A 10 Watt, 532 nm CW solid-state laser *(Millennia Xs, Spectra-Physics)* pumps a 100 fs Ti:Sapphire pulsed laser with a repetition rate of 80 MHz *(Tsunami, Spectra-Physics)*, which, in turn pumps the OPO system. This set-up was earlier operated by Dr. Josh Holt, and is now run by Mr. Bill Pandit.

2.2 Transient pump-probe spectroscopy

Two ultrashort pulses are utilized for measuring transient PM spectra using pump-probe spectroscopy. The first pulse (pump) is a high intensity pulse that excites the sample at time t = 0, and the second pulse (probe) is a low intensity pulse that crosses the excited sample at a later time by a controlled translation stage delay line. The change in the transmitted intensity of the probe pulse, which is induced by the pump pulse, is monitored with the help of a detector.

In the transient photomodulation (PM) measurement two quantities are usually obtained. The first is the transmission T of the probe beam when the pump beam is

blocked; and the second is the change in transmission ΔT of the probe when the pump beam is on. For small ΔT we can write

$$\frac{\Delta T}{T}(t) \cong -\Delta\alpha(t)d = -\Delta N(t)\sigma d \qquad (2.1)$$

where $\Delta\alpha$ is the change in the absorption coefficient, d is the thickness of the film, σ is the absorption cross-section of the photogenerated species, and N is the excited state population at time t. In this way, measuring $\frac{\Delta T}{T}(t)$ provides direct information on the density of the excited species as a function of time, assuming σ does not change with time.

The schematic of the experimental arrangement for the pump-probe measurement is shown in Figure 2.4(a). The output from the Ti:Sapphire amplifier is a pulse train at 1 kHz repetition rate with pulses 150 fs in duration at 800 nm; it is divided by a 90/10 beam splitter into two beams, namely pump and probe. The delayed pump beam (90% of the power) is frequency doubled to 400 nm (~3.1 eV) using a nonlinear BBO crystal. The probe beam (10% remaining power) is used to create broadband 1.24–2.76 eV white light supercontinuum in a 1 mm thick sapphire plate. The broad probe spectral range 0.12-2.76 eV used in our measurement is obtained by combining the low-intensity and high-intensity laser systems as shown in Figure 2.4(b).

The time resolution in our pump-probe set-up over the entire spectral probe range is ~150 fs, as confirmed by cross-correlation, or two photon absorption measurement. The delay of pump beam with respect to probe beam is determined by computer controlled translation stage with an accuracy of 0.1 μm (or 0.03 fs). Spectral resolution of

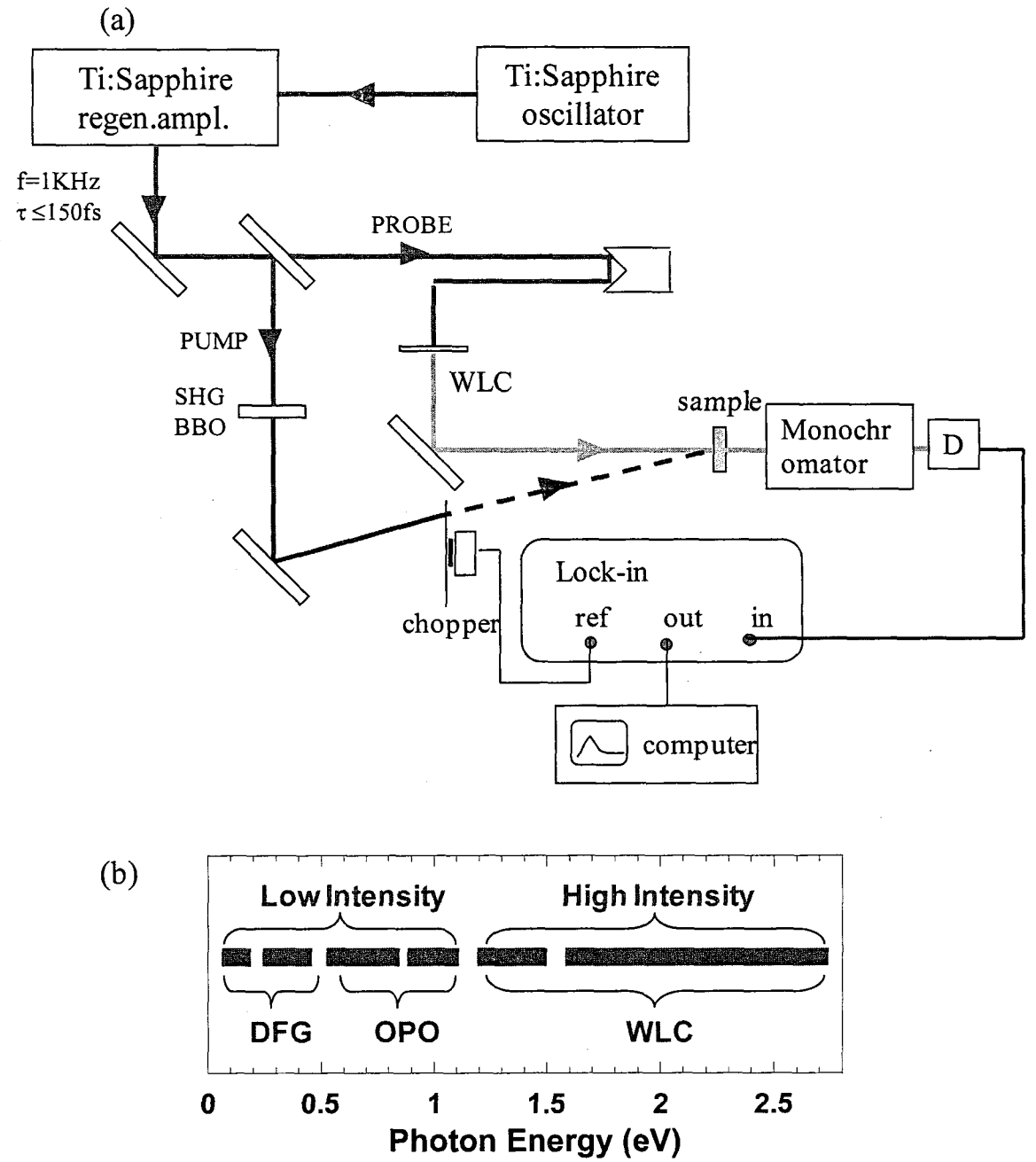

Figure 2.4: Schematic diagram of (a) ultrafast high intensity transient pump-probe set-up (b) broad probe range generated by both low and high intensity laser systems.

about 4 nm is achieved by CM-110 Digikröm monochromator with 0.6 mm entrance and exit slits. The pump beam is modulated by a mechanical chopper at exactly half the frequency of Ti:Sapphire laser system, and the change in transmission of probe, ΔT, is monitored by Si photodiode with a phase sensitive technique provided by a lock-in amplifier. Using this technique, a sensitivity of $\frac{\Delta T}{T} \approx 10^{-4}$ is easily achieved across all the probe range. Transient pump-probe measurements are done in two modes: (a) as a function of time at fixed wavelength; and (b) as a function of wavelength at a fixed time delay. In the second type of measurement, the chirp of white light supercontinuum has to be taken into account. Calibration of the white light supercontinuum chirp is done by a cross-correlation or two photon absorption measurement on a known material. Finally, while taking the transient PM spectrum, a chirp-free program is used that moves the translation stage according to the calibration of white light supercontinuum at different wavelengths.

The thin film polymer samples were always put in a dynamic vacuum of ~150 μtorr to prevent degradation and oxidation in the presence of intense laser light. Also the pump intensity in the pump-probe measurement was usually kept lower than the 0.3 mJ/cm^2 that ensures linearity of the response. The probe intensity should be much lower than the pump intensity to avoid any excitation of the sample (by TPA for example). The pump and probe beams were focused onto the sample film in order to overlap with each other concentrically; their diameters were set to be 500 μm (pump) and 100 μm (probe), respectively. Their alignment was done by a dedicated telescopic microscope.

The pump-probe signal, $\frac{\Delta T}{T}$, can either be positive or negative. In case of photoinduced absorption, it will be negative because of decrease in the probe transmittance due to absorption of the pump. Stimulated emission (SE) and photobleaching (PB) of the ground state result in a positive signal, since the transmittance increases for both processes. The SE spectrum can be easily separated from the PB spectrum because it resembles the PL spectrum of the sample under investigation.

2.3 Two-photon absorption

Most of the conjugated polymers belong to the C_{2h} symmetry group, which has four irreducible representations, namely A and B with even (g) and odd (u) parity: these are: A_g, B_u, B_g and A_u. The ground state is an A_g character. Linear or one photon absorption occurs between states of opposite parity, and therefore only higher B_u states may be tracked by the absorption spectrum. On the other hand, two-photon absorption (TPA) occurs between same parity states, so complementary higher lying A_g states can also be tracked by this NLO process [49-51]. Therefore TPA spectroscopy is a complementary method to linear absorption in the conjugated polymers.

The two-photon absorption coefficient is proportional to the imaginary part of the third order nonlinear susceptibility $\chi^{(3)}$ [52, 53]. It is relatively weak compared to linear absorption, and therefore very high peak power of ultrashort pulses is required to detect TPA. Here we use an efficient technique based on ultrafast nondegenerate pump probe spectroscopy. We note that there are other techniques used to observe TPA, such as Z-scan and two-photon luminescence.

The two-photon absorption spectrum is measured with the help of pump-probe correlation technique at time delay t = 0. The pump beam is set at 1.55 eV and the probe has the WLC spectrum which ranges from 1.2-2.9 eV. This measurement is different from the normal photoinduced absorption (PA) measurement because in TPA the pump is set at 1.55 eV, which is below the polymer optical gap, so that there is no real intermediate electronic level involved in the TPA, and this makes the transition to be instantaneous. Figure 2.5 shows TPA time resolved response at 3.9 eV in Pt-3 solution using 1.55 eV pump and 2.35 eV probe beams. The PA signal reaches maximum at t = 0 when the pump and probe pulses overlap in space and time, and follows the cross-correlation response of the pump and probe pulses.

2.4 Electroabsorption spectroscopy

In electroabsorption (EA) technique we measure changes in the absorption spectrum of the sample with the application of an electric field. Electroabsorption has been a very important method to characterize the optical properties of π-conjugated polymers. It can give information for both even and odd parity of states. The signal is proportional to the imaginary part of the third order nonlinear susceptibility $\chi^{(3)}$.

$$\frac{\Delta T}{T} \cong -\Delta\alpha d = \frac{4\pi\omega}{nc} Im[\chi^3(-\omega;\omega,0,0)F^2 d \qquad (2.2)$$

In the above relation, F is the applied electric field, d and n are film thickness and refractive index, respectively [54]. The modulation frequency of the electric field, f ~300 Hz, so that f << ω, and thus can be considered zero with respect to the optical frequency of electromagnetic wave used in the measurement.

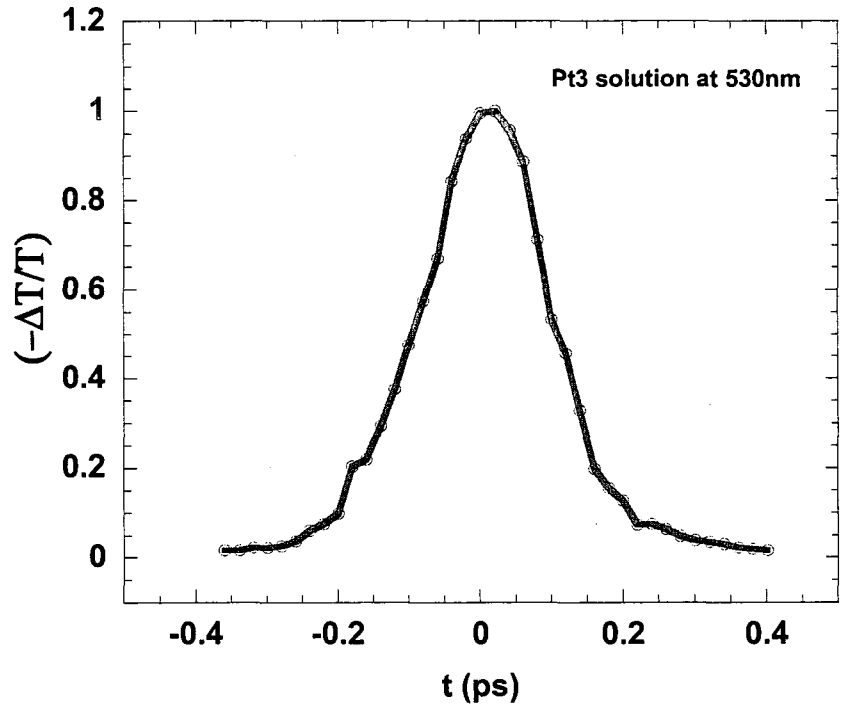

Figure 2.5: Two-photon absorption in Pt-3 solution at 3.9 eV, measured with the pump-probe system, where the pump beam was fixed at 1.55 eV whereas the probe beam was at 2.35 eV.

The EA measurement needs a special device structure that is in the form of interdigitated electrode array, as shown in Figure 2.6(a). The substrate is a 1 inch diameter, 2 mm thick sapphire plate. A 50 nm titanium film is sputtered on the substrate which is followed by 150 nm of gold deposition. Finally, the interdigitated electrodes are patterned using photo-lithography with 40 micron gap between the adjacent electrodes. Our sample is deposited on such a substrate with optical density of 0.2-0.4 to allow substantial EA signal even for photon energy above the polymer optical gap.

The experimental set-up for the EA measurement is shown in Figure 2.6(b). A xenon or tungsten light source is used as a probe. The probe light is dispersed via the

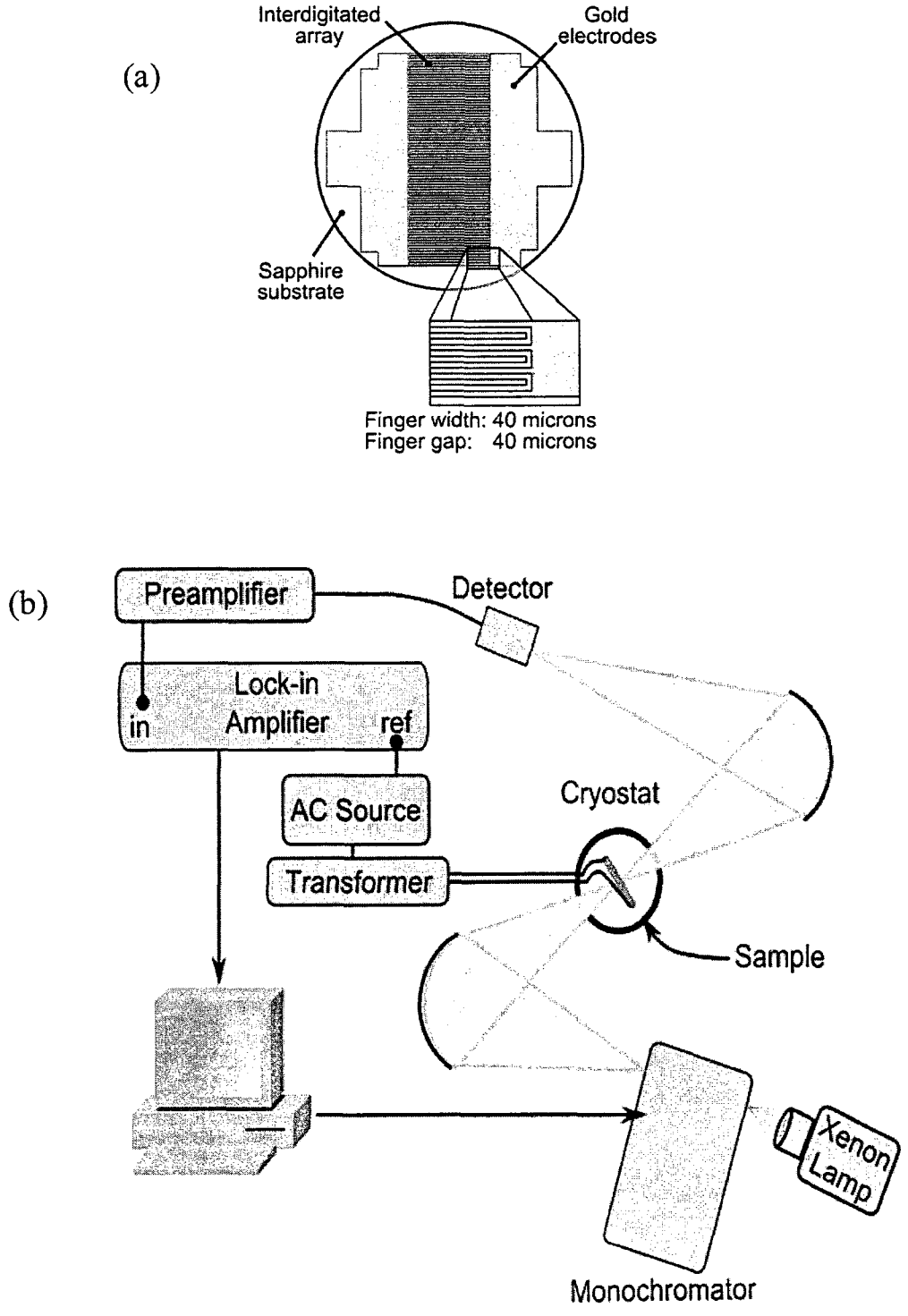

Figure 2.6: Experimental set-up for electroabsorption (EA) spectroscopy (a) sapphire substrate with interpenetrating finger electrodes used in EA measurement (b) experimental arrangements

grating monochromator, guided through the sample and focused onto a UV enhanced Silicon detector by a couple of curved mirrors. The sample is kept in a cold finger cryostat under dynamic vacuum of 150 μtorr. A high AC voltage of 200-300V is applied to the electrodes using a function generator and step-up transformer. A very high electric field of ~ 10^5 V/cm may easily be achieved between the electrodes, because of their small spacing of ~40 μm gap. The electric field is modulated at 520 Hz, and the EA signal (namely changes in the probe transmission) is detected at 2f, using phase-sensitive lock-in amplifier technique.

2.5 Fourier transform infrared spectroscopy

A Fourier transform infrared (FTIR) spectrometer was used for measuring absorption spectra in the Mid to Far-IR range. The FTIR is based on a Michelson Interferometer, where a beam, I_0 is split by a beam splitter into two beams, I_1 and I_2 as shown in Figure 2.7. These beams are subsequently reflected from a moving and stationary mirror, respectively, which changes the optical path by x. The two reflected beams are passed through the sample and generate an interferogram spectrum. The interference spectrum can be described as:

$$I_{out}(x) = \frac{1}{4}\int_{-\infty}^{+\infty} I_0(\bar{\nu})\,(1+\cos(2\pi\bar{\nu}x))d\bar{\nu} = const. + \frac{1}{4}\int_{-\infty}^{+\infty} I_0(\bar{\nu})\cos(2\pi\bar{\nu}x)\,d\bar{\nu} \quad (2.3)$$

where $I_{out}(x)$ is the interferogram spectrum as a function of displacement x. The inverse Fourier transform of the second part of the above equation describes the interference spectrum $\bar{\nu}$ as follows:

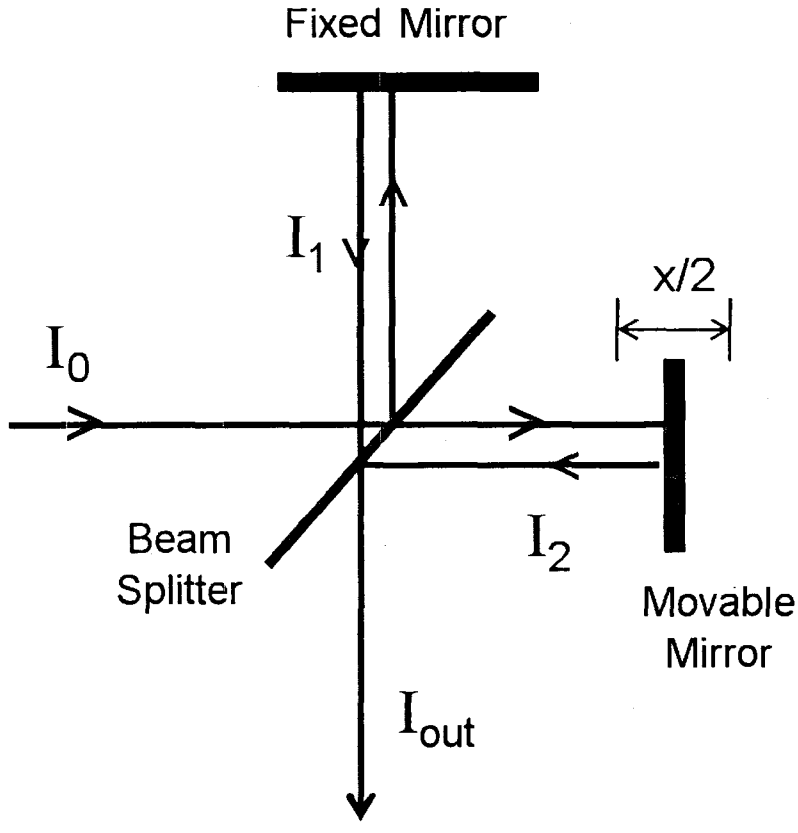

Figure 2.7: Schematic illustration of Michelson interferometer. I_0 is the initial beam and I_{out} is the measured beam after interference of the split beams.

$$I_0(\bar{\nu}) = \frac{2}{\pi}\int_{-\infty}^{+\infty} I_{out}(x)\cos(2\pi\bar{\nu}x)\,dx \tag{2.4}$$

The Glow-bar lamp is used as an infrared (IR) light source, and the beam is split by a KBr beam splitter. After passing through the sample the light intensity is measured by a liquid nitrogen cooled MCT detector (400-7500 cm^{-1}).

2.6 Photoluminescence quantum efficiency

The photoluminescence (PL) quantum efficiency (PLQE) of luminescent materials is defined as the ratio of number of emitted photons/ absorbed photons. It yields information about radiative versus nonradiative channels. The experimental set-up for measuring the PLQE is shown in Figure 2.8. A laser beam enters into the integrating sphere (IS) that distributes and reflects light homogeneously. The sample is placed in the path of the light inside the IS, and the emission is collected by a solid state detector. The excitation laser light is modulated by a mechanical chopper, and the detector is locked at the chopping frequency and measures the light intensity via a lock-in amplifier. The PLQE can be then calculated using the following equation:

$$PLQE = \frac{I_{PL}-(R+T)I_{PL,corr}}{(1-R-T)I_L}\frac{D_L}{D_{PL}}\frac{S_L}{S_{PL}}\frac{E_L}{E_{PL}}\frac{1}{T_F(PL)} \tag{2.5}$$

Three different intensities need be measured; these are: I_L, the reflected laser intensity without the sample inside the IS; I_{PL}, the reflected, uncorrected PL intensity when the sample is in the path of the excitation laser; and a correction term $I_{PL,corr}$, the reflected PL intensity when the sample is inside IS but not in the path of laser.

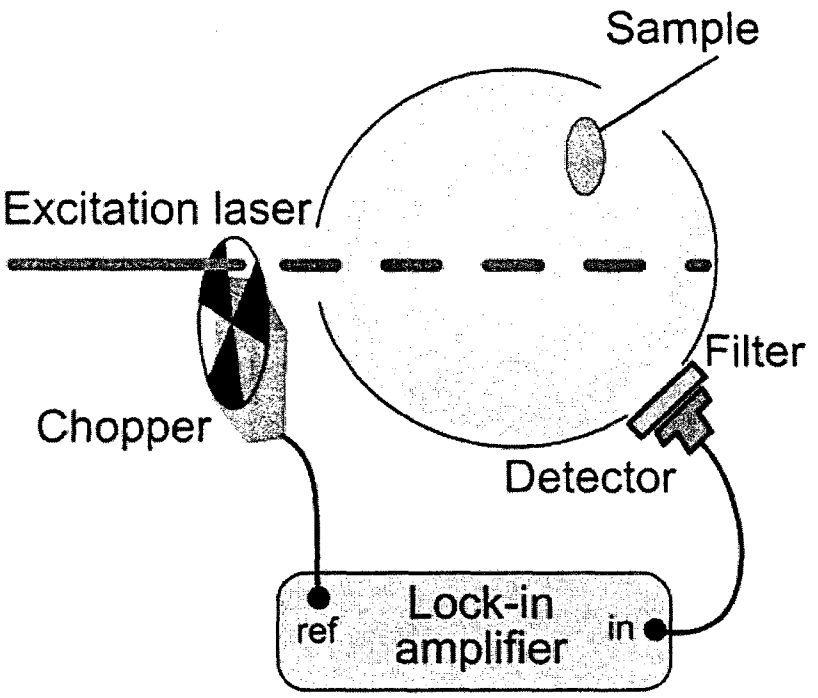

Figure 2.8: Experimental set-up for the measurement of photoluminescence quantum efficiency

The correction term is measured in order to eliminate the collected light emission of PL that is contributed by indirectly hitting photons (reflected by IS walls). I_{PL} and $I_{PL,corr}$ are measured with the help of an optical long-pass filter placed in front of the detector for blocking the excitation laser light. R and T are, respectively, the reflection and transmission coefficients of the sample at the laser wavelength; D_L and D_{PL} are the photodetector sensitivities at the laser and PL wavelengths, respectively; S_L and S_{PL} are the respective IS sensitivities at the laser and PL wavelengths; E_L and E_{PL} are the respective photon energies at the laser and PL wavelengths; and $T_F(PL)$ is the transmission of the optical long pass filter employed in the measurement at the PL

wavelength. The recommended thickness of the film should be between optical densities 1-2.

2.7 High pressure measurements

The high pressure measurements are done in a diamond anvil cell (DAC). A sample is placed between the parallel opposite faces of diamond anvils, and the anvils are then pressed together. Pressure generated is force divided by area, so even a modest force can produce a very high pressure between the small faces of the diamonds. Figure 2.9(a) shows a typical structure of the DAC used by us. The two opposed diamonds are separated by a metal gasket with a hole for accommodating the sample and pressure transmitting medium [55].

There are many different kinds of DACs used for high pressure scientific measurements. We used a Merrill-Bassett DAC type cell for our measurements [56, 57]; and its image and schematic are shown in Figure 2.9(b) and (c), respectively. In this structure the diamond anvils are embedded into two parallel Be-Cu plates. Pressure is applied by tightening the three set screws located at the apexes of the upper plate. The Be support is suitably shaped to provide wide-angle access to the incoming beam.

Due to its hardness and optical transparency in the visible and infrared range, diamond is the ideal material for high pressure cell measurements. Figure 2.10 shows the near-ir/visible range transmission spectrum of DAC used in our measurements. Diamonds used in DACs are selected from brilliant-cut gem stones, and are classified as type I and type II according to their purity. Type II diamonds are used for optical

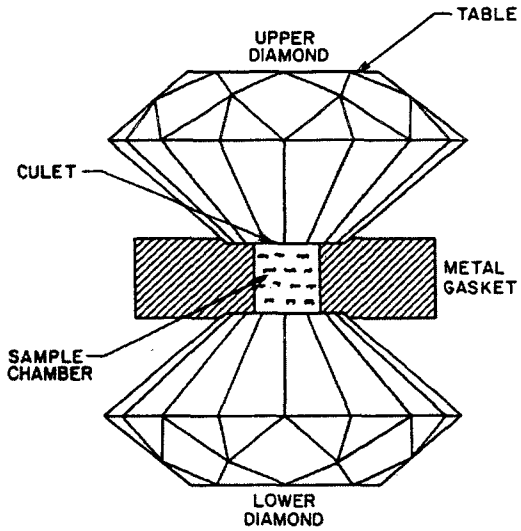

(a)

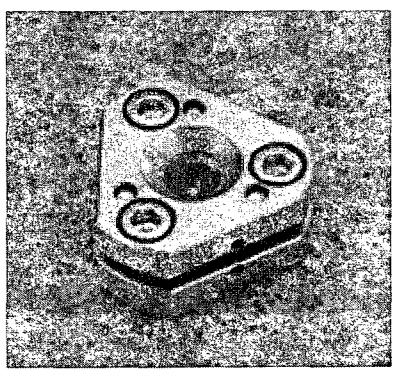

(b)

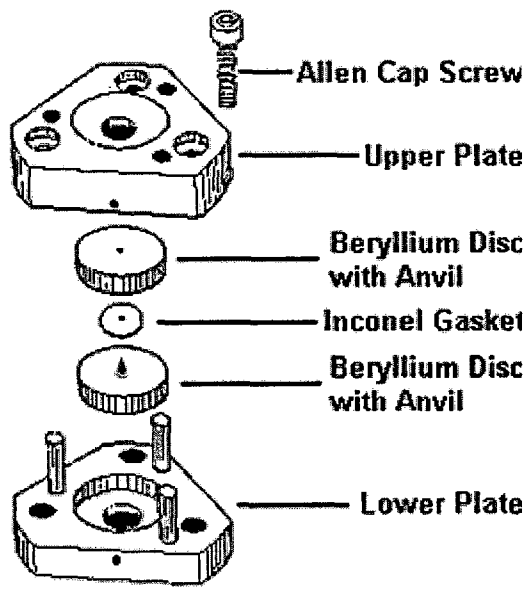

(c)

Figure 2.9: Schematics and image of the diamond anvil cell (DAC) (a) typical structure of DAC assembly [55] (b) image and (c) schematic of Merrill Bassett type DAC [57]

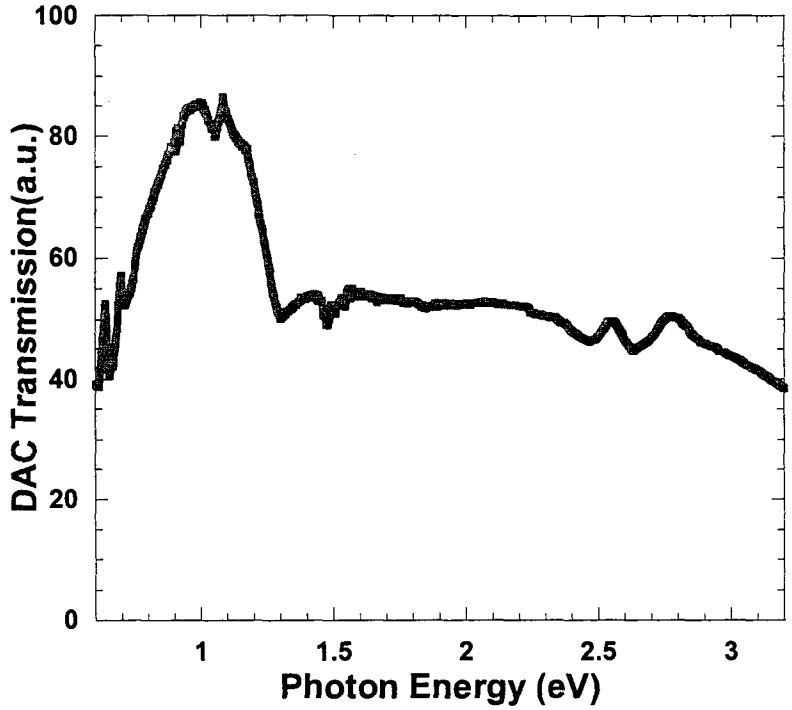

Figure 2.10: Transmission spectrum of diamond anvil cell (DAC) assembly used in the Near-ir/visible pump-probe measurement.

applications because they have smooth absorption spectrum that does not change much under applied uniaxial stress. A detailed classification divides diamonds into type Ia (large aggregates of nitrogen impurities), type Ib (single nitrogen dopant), type IIa (considered pure) and type IIb (including boron impurities). Among them, type IIa used for optical investigations.

The size of the diamond used for DAC may vary from 1/8 to 1/2 carat. The anvil flat (culet) is usually set parallel to the (100) or (110) plane of the diamond and ranges from 0.3 to 0.7 mm. The octagonal surface opposite to the anvil flat is called table and its size varies from about 2 mm in 1/8 carat diamonds to 3.5-4.5 mm in larger diamonds. The gaskets we used were purchased commercially. They are made of Inconel or

tempered stainless steel. The diameter of the gasket should be half the size of the culet. For alignment purpose, gasket should be placed at lower diamond flat and its center of the hole should match with the center of diamond. The centering of gasket is followed by filling the hole with sample and pressure transmitting medium and sealing it with upper anvil of the gasket.

Before the introduction of the ruby florescence method, calibration of pressure inside DACs was a big challenge. Forman et al. first showed that the R lines of Cr-doped Al_2O_3 (ruby) shift linearly with hydrostatic pressure in the range of 1-22 kbar [58]. Further work by Piermarini et al. showed that ruby florescence technique can be used as rapid and convenient in-situ method to measure the pressure [59]. For calibration, a tiny chip of ruby crystal is placed in the pressure transmitting medium with the sample, and its fluorescence is observed after excitation by an Ar+ laser (488 nm). The R ruby lines are intense, and their wavelengths are 692.7 nm and 694.2 nm at ambient conditions. Upon application of high pressure, these lines shift to higher wavelength with accuracy of 0.3 kbar in pressure determination. In another work, Piermarini and Block showed that this linearity holds up to 300 kbar [60]. Upon the application of nonhydrostatic pressure, these R florescence lines broaden.

The pressure medium transforms the uniaxial compression of diamonds into hydrostatic pressure inside the sample chamber. Sometimes a 4:1 methanol-ethanol mixture is preferred as pressure medium. The main advantage of liquid pressure medium is the ease of loading the cell, but one of the disadvantages is liquid sample interaction.

Solid media such as CsI, NaCl and KBr are good pressure transmitting media also, providing a hydrostatic pressure of 10-15 GPa. In this work we used liquid

perfluorotributylamine (PFTBA) as a pressure transmitting medium, because it does not react or dissolve with MEH-PPV and is transparent in the spectral range of interest, namely mid-IR to visible ranges.

Usually the pressure is determined in-situ by the ruby florescence. However, the small ruby chip cannot be taken into the DAC sample chamber together with the MEH-PPV film in the pump-probe measurements, because the ruby florescence would interfere with the probe signal range. We may avoid this problem by taking ruby chip and MEH-PPV sample together in the pressure medium *before* the pump-probe measurement, and calibrating the shift of the ir-active vibrations of the MEH-PPV against the ruby florescence shift upon pressure. The pressure is determined by following formula for the spectral shift of the ruby R1 line:

$$P(GPa) = \frac{1904}{b}\left[\left(1 + \frac{\delta\lambda}{\lambda_0}\right)^b - 1\right] \tag{2.6}$$

where $\delta\lambda$ and λ_0 are the R1 wavelength shift (in nm) under pressure and the wavelength at ambient pressure, respectively, and b is a parameter, either 5 or 7.665 depending on nonhydrostatic or hydrostatic pressure, respectively. Figure 2.11(a). shows the ruby PL spectra at different pressures and Figure 2.11(b) shows MEH-PPV FTIR absorption spectra at the same pressures. Consequently a linear relationship may be established between the ir-active vibration peaks and the applied pressure. This relation is used during the pump-probe measurement for the pressure determination.

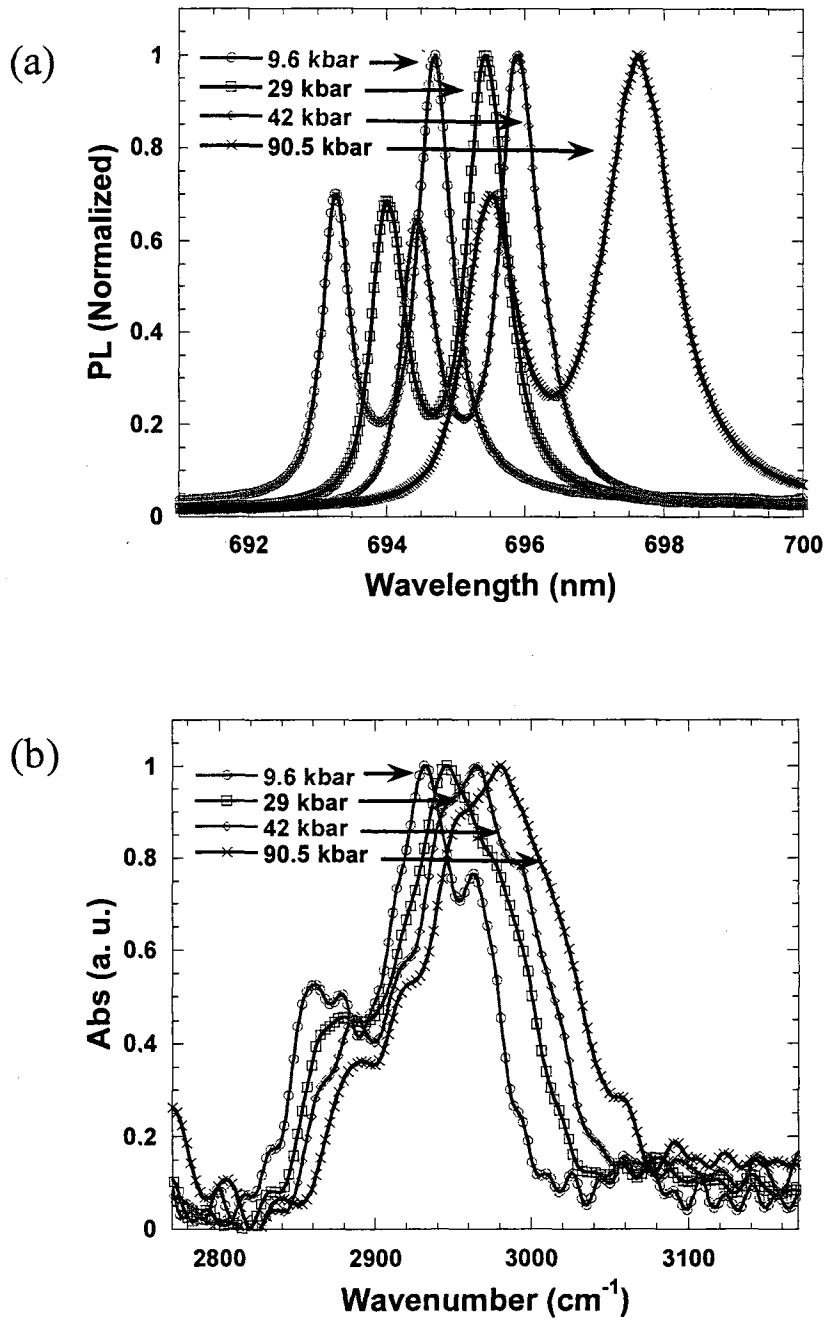

Figure 2.11: Pressure calibration measurement for MEH-PPV film. (a) shift of Ruby fluorescence line at different applied pressure (b) shift of MEH-PPV infrared absorption line at the same pressures as used for Ruby fluorescence

CHAPTER 3

ULTRAFAST PHOTOPHYSICS OF P3HT / FULLERENE DERIVATIVES

The present chapter discusses detailed ultrafast photophysics of different donor/acceptor based organic photovoltaic blend systems. The donor materials are thiophene based polymers, namely RegioRegular-poly(3-hexylthiophene) (RR-P3HT) and RegioRandum-poly(3-hexylthiophene) (RRa-P3HT), and the acceptors are [6,6]-phenyl C61butyric acid methyl ester (PCBM) and different derivatives of PCBM, namely Jalapeno (Jal) and Habanero (Hab) (*these are commercial name given by Plextronix Inc. to their PCBM derivatives).* These composites serve as an active layer in organic photovoltaic devices with high power conversion quantum yield (~ 6 %)[61-64], due to the existence of a photoinduced charge transfer (PCT) reaction between the polymer and the fullerene molecules and the donor and acceptor phase separation. The transient photomodulation (PM) spectrum spans a broad energy range from 0.1-2.4 eV, and this allows us to monitor the transient behavior of the various photoinduced absorption (PA) bands of polarons and excitons in the PM spectrum, as well as photobleaching (PB) of the ground state population.

3.1 Materials

3.1.1 P3HT

The chemical structure of poly 3-hexyl thiophene (P3HT) is shown in Figure 3.1((a) & (b)). The polymer shows two different types of arrangements of hexyl side group attached to the main chain. The polymer can be either regioregular (RR), where the side group is attached in a regular fashion (head to tail), or regiorandom (RRa), where the side group is in random order (head to head or tail to tail; no specific order) [65-68]. The interesting property of RR-P3HT is its self-organizing ability in the solid state that results in two-dimensional microcrystalline domains in the film, as shown in Figure 3.1(c). In these domains, the polymer chains are arranged in a planar structure called "lamellae" that are perpendicular to the substrate by stacking on one another, and these planar structures are closed packed so that interplanar interaction is large.

3.1.2 PCBM

The chemical structure of PCBM molecule is shown in Figure 3.1(d). It is a derivative of C60 or fullerene molecule with one side group attached. Fullerenes are well known for their electron accepting properties because of high electron negativity (affinity), and this makes them suitable candidates for acceptor materials in organic photovoltaic systems. The presence of a side group renders PCBM more soluble in organic solvent compared to C60, and therefore this derivative is preferable for solution-processible organic photovoltaic.

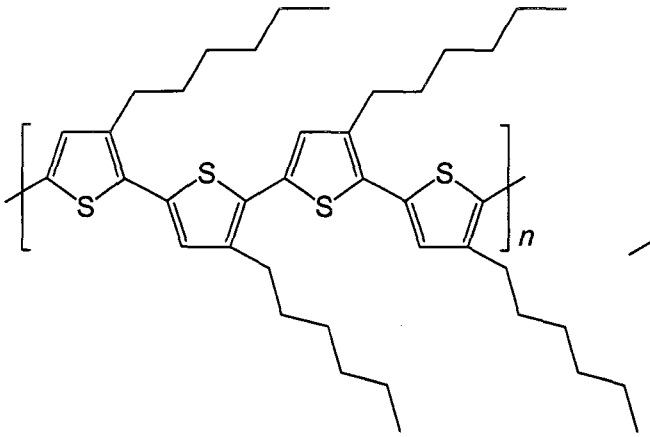

(a)
RegioRegular-poly(3-hexylthiophene)
RR-P3HT

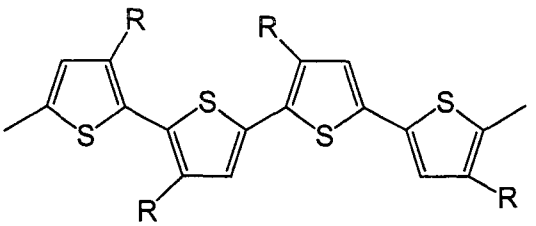

(b)
RegioRandom-poly(3-hexylthiophene)
RRa-P3HT

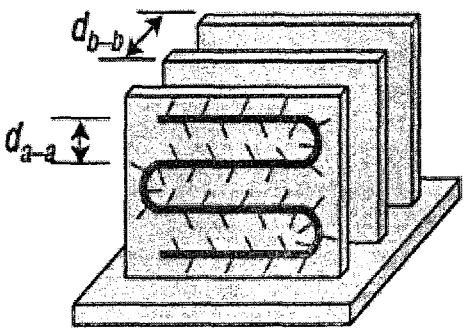

(c)
Lamella Structure

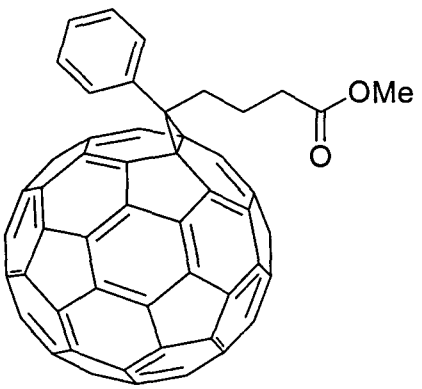

(d)
[6,6]-phenyl C61butyric acid methyl ester
PCBM

Figure 3.1: Chemical structure of (a) RegioRegular-poly(3-hexylthiophene)(RR-P3HT) (b). RegioRandom-poly(3-hexylthiophene)(RRa-P3HT); (c) schematic diagram of lamella folding and ordering on a substrate Adapted from Ref.[69]; (d) chemical structure of [6,6]-phenyl C61butyric acid methyl ester (PCBM)

The optical properties of PCBM in solid film are quite different than in solution because of large intermolecular interaction in the former form. For example many optically forbidden transitions in isolated molecules become weakly allowed in the film. Cook et al. reported that PCBM isolated molecules show absorption mainly below 450 nm wavelength, but in contrast PCBM film shows weak absorption tail down to 700 nm, as shown in Figure 3.2(a) [70]. Similarly, the emission spectrum of film shows two bands at ~700 nm and ~500 nm, respectively, as shown in Figure 3.2(b), whereas PCBM isolated molecules show only the ~700 nm emission band. These results were interpreted by postulating the existence of charge transfer state in the film (namely between the fullerene molecules), which arises due to intermolecular interaction.

Dick et al. reported the photophysics of C60 film by photoinduced absorption from picosecond to millisecond range, and also using absorption detected magnetic resonance (ADMR). In addition to the presence of Frenkel type excitons in the ps-ns time domain with their characteristic PA bands, they found in cw photomodulation (PM) spectrum three PA bands at ~0.8 eV , ~2.0 eV and ~2.4 eV that are due to charge species. The PA band at ~2.4 eV also appears in electroabsorption measurement, and therefore it was interpreted as due to charge transfer state in the film [71]. Since the P3HT/PCBM blend contains separated phases of polymer chain and fullerene molecule, it is interesting to see the influence of the polymers and fullerene photophysics on the PCT process in the blend. This chapter elucidates this relation.

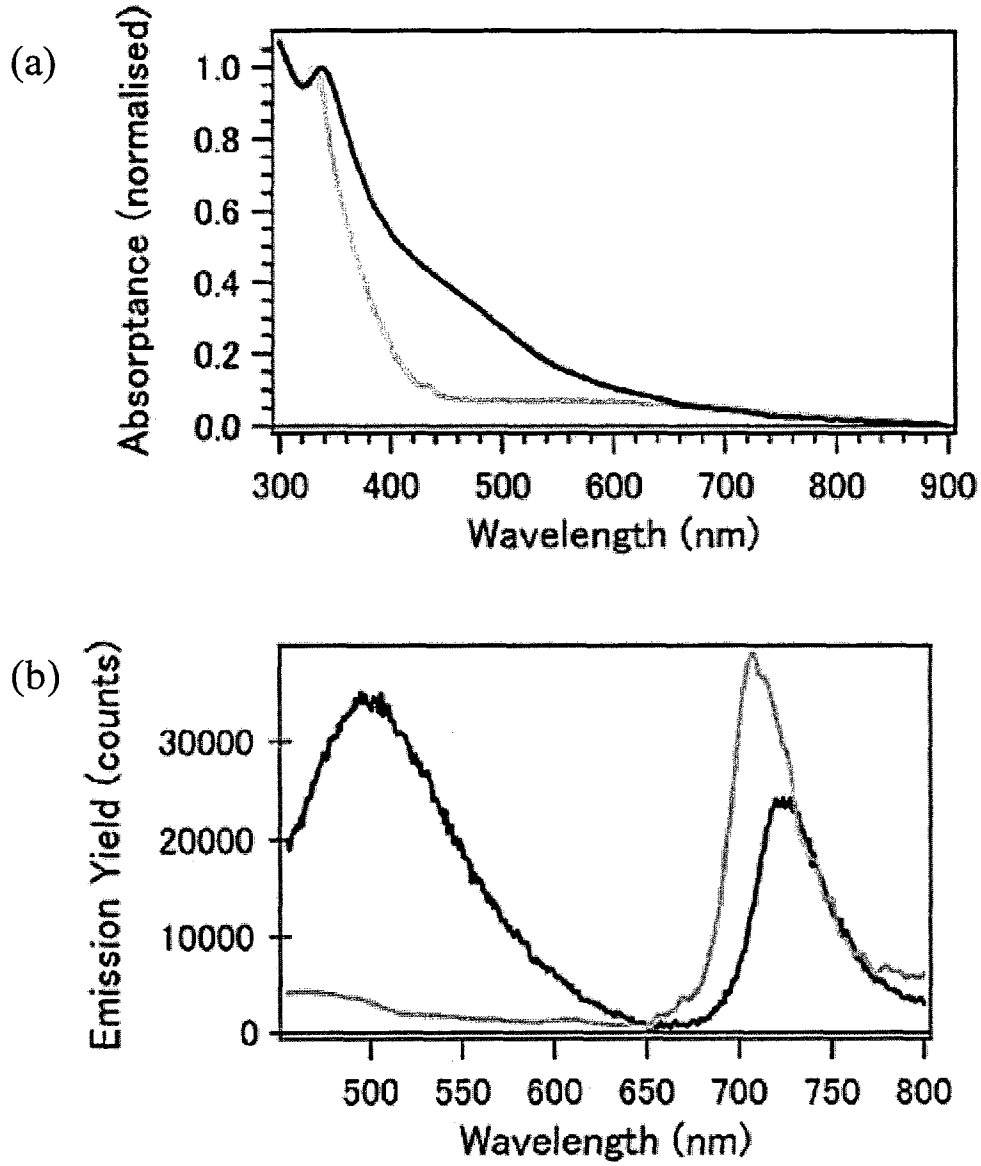

Figure 3.2: Optical properties for a 12% PCBM:88% PS blend (gray line) and pristine PCBM film (black line); (a) absorption spectra (b) PL spectra. Adapted from Ref. [70]

3.1.3 P3HT/Fullerene blend

If P3HT is blended with fullerene derivatives, then they act as donor/acceptor (D/A) organic semiconductors for bulk heterojunction photovoltaic devices. The interface of D/A plays a critical role in the dissociation of photoexcited excitons. The generally accepted PCT mechanism is the following: Upon photon absorption in the donor polymer chain (and acceptor to a lesser degree because of its weak absorption cross section), singlet excitons (bound electron-hole pairs) are created on the chains which may diffuse to the D/A interface, and finally dissociate due to energy difference between the LUMOs of donor and acceptor materials.

Originally photoinduced charge transfer at the interface of D/A in organic semiconductors was considered as single step process [8, 72], but over the years it was realized that it is facilitated via a charge transfer (CT) state which lies at the interface of D/A materials [73-77]. The presence of this CT state has been observed by near-ir photoluminescence, near-ir electroluminescence, and electroabsorption spectroscopy. In addition, these low lying CT states at the interface of D/A can be directly excited by photon energy below the band-gap of donor or acceptor constituents [74, 75].

In the case of a bulk heterojunction type solar cell, the morphology of D/A blend film plays a decisive role on the ultimate power conversion efficiency of the cell. For instance, RR-P3HT/PCBM blend forms nanocrystalline domains [78-80] of donor and acceptor materials, and solar cell based on this structure shows improved power conversion efficiency of the order of 5-6%. On the other hand, RRa-P3HT/PCBM blend is mixed on the molecular level [81], and the solar cell based on this blend shows poor power conversion efficiency of <0.5%. Figure 3.3(a) shows the transmission electron

microscopy (TEM) images of RR-P3HT/PCBM (1.2:1) annealed film, which contains the nano-domains (~50 nm) of PCBM network. When this nano structure is compared with the TEM images of RRa-P3HT/PCBM (1.2:1) film, shown in Figure 3.3(b), it is clear that there is no phase separation of polymer and PCBM in RRa-P3HT/PCBM blend. In fact, RRa-P3HT polymer and PCBM are mixed uniformly.

3.2 Electroabsorption of P3HT/Fullerenes

Our aim of using the electroabsorption (EA) technique for the P3HT/Fullerene blend film is to explore the CT states lying at the interface of D/A, below the band-gap of the polymer and fullerene constituents. EA measurement can reveal 'buried' optical transitions that are coupled by a dipole transition. Here we discuss three different mixtures of RR-P3HT with PCBM, JAL and HAB. EA of RR-P3HT/PCBM was measured by Dr. Tomer Drori [82]. Figure 3.4(a) shows the EA of RR-P3HT/PCBM (1.2:1) that reveals a new CT state below the gap due to RR-P3HT and PCBM interaction in the D/A interface. A broad derivative-like feature can be seen in the spectral range from 1.2 to 1.8 eV, having three modulated peaks within the band. Figure 3.4(b) and Figure 3.4(c) show the EA spectra of RR-P3HT/JAL (1.2:1) and RR-P3HT/HAB (1.2:1), respectively. These EA spectra also show a similar derivative-like feature between 1.2 to 1.8 eV to that in the RR-P3HT/PCBM EA spectrum. Similar below-gap CT states have also been seen in various D/A mixtures [74, 75, 82, 83]. Hence these blends can be excited below the band gap of the polymer donors.

(a)

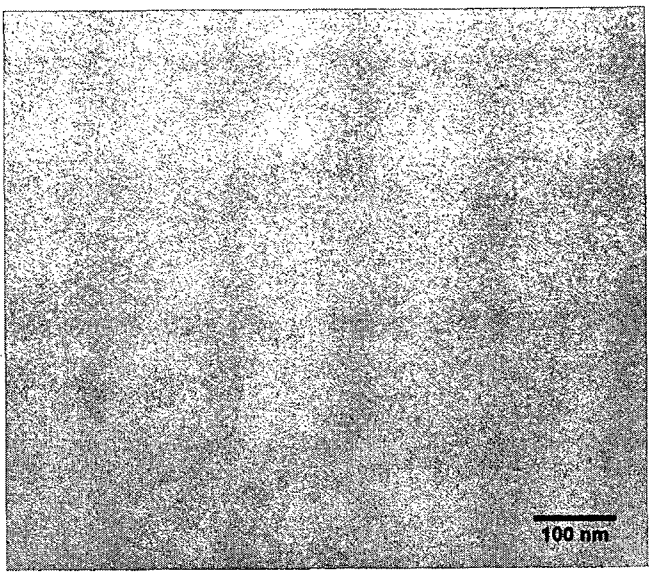

(b)

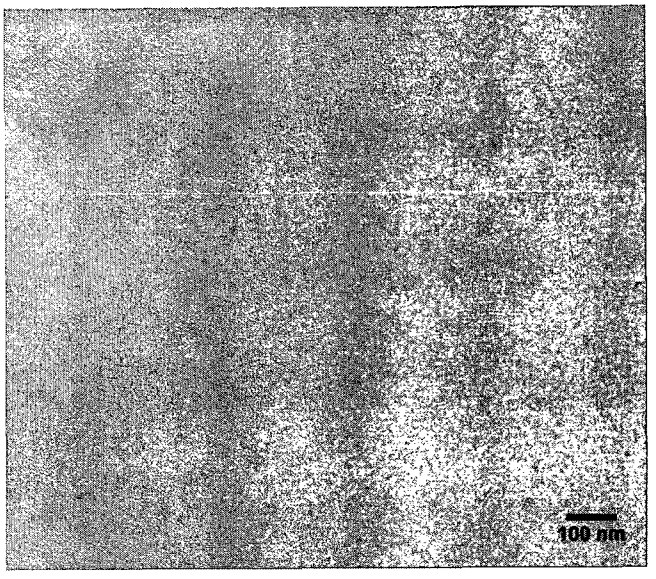

Figure 3.3: Transmission electron microscope images of (a) RR-P3HT/PCBM (1.2:1) (b) RRa-P3HT/PCBM (1.2:1)

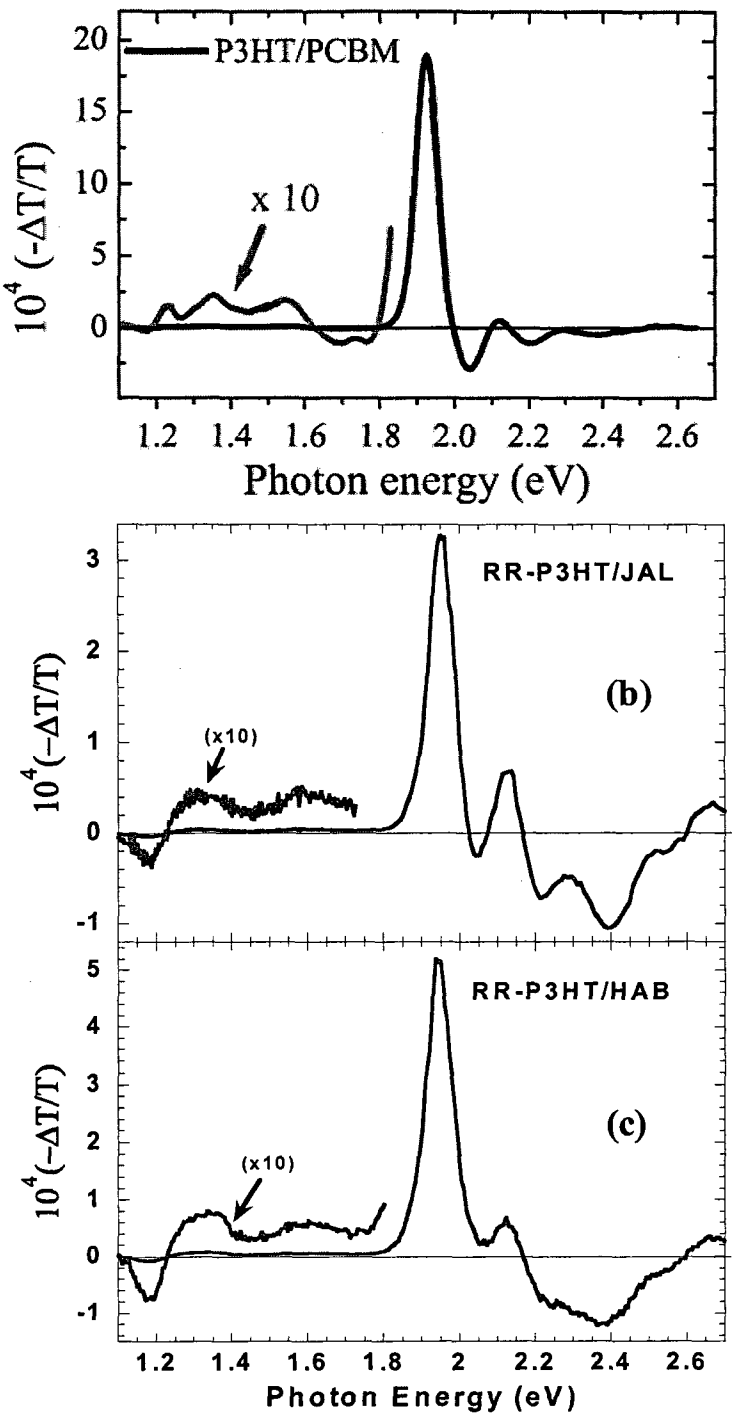

Figure 3.4: Electroabsorption (EA) spectra of (a) RR-P3HT/PCBM [Adapted from Ref. [82]](b) RR-P3HT/JAL (c) RR-P3HT/HAB blends. For clarity, the magnified nearir spectra are plotted together with EA spectra.

3.3 Ultrafast measurements

3.3.1 Ultrafast photophysics of RR-P3HT polymer

Figure 3.5(a) shows the ultrafast photomodulation (PM) spectrum of pristine RR-P3HT *film* in a broad probe spectral range of 0.2–2.5 eV upon excitation at 3.1 eV, above the polymer band gap The broad probe spectral range is covered using two different laser set-up (mentioned in experimental section): low intensity laser (0.2-1.1 eV) and high intensity laser (1.2-2.5 eV). Upon excitation of the polymer, two different kinds of species are created—charge polaron and neutral exciton. The PM spectrum contains various PA and PB bands: P1, P2, PA1, EA and PB. P1 and P2 are due to charge polarons, and PA1 is due to neutral singlet excitons; we note that the PM spectrum does not contain the stimulated emission band known to exist in PM spectra of other polymer films [84, 85]. PB is the ground state reduced absorption (by population reduction) that is also called photobleaching. The EA band looks like the lowest optical feature in the electroabsorption spectrum of this polymer film, and thus might be the result of photorefractive effect in the polymer [86]. In the present study, we will not thoroughly discuss this EA band.

Figure 3.5(b) shows the transient decay behavior of the bands P1, P2, PA1 and PB; their respective fitted time constants are reported in Table 3.1. P1 and P2 decay together, with a time constant of ~ 250 ps. In contrast PA1 decays faster with a shorter time constant of ~15 ps , whereas PB follows the same decay dynamics as PA1, i.e., singlet excitons. Therefore it is clear from the various decay dynamics that upon photoexcitation both charge and neutral species are created in the polymer

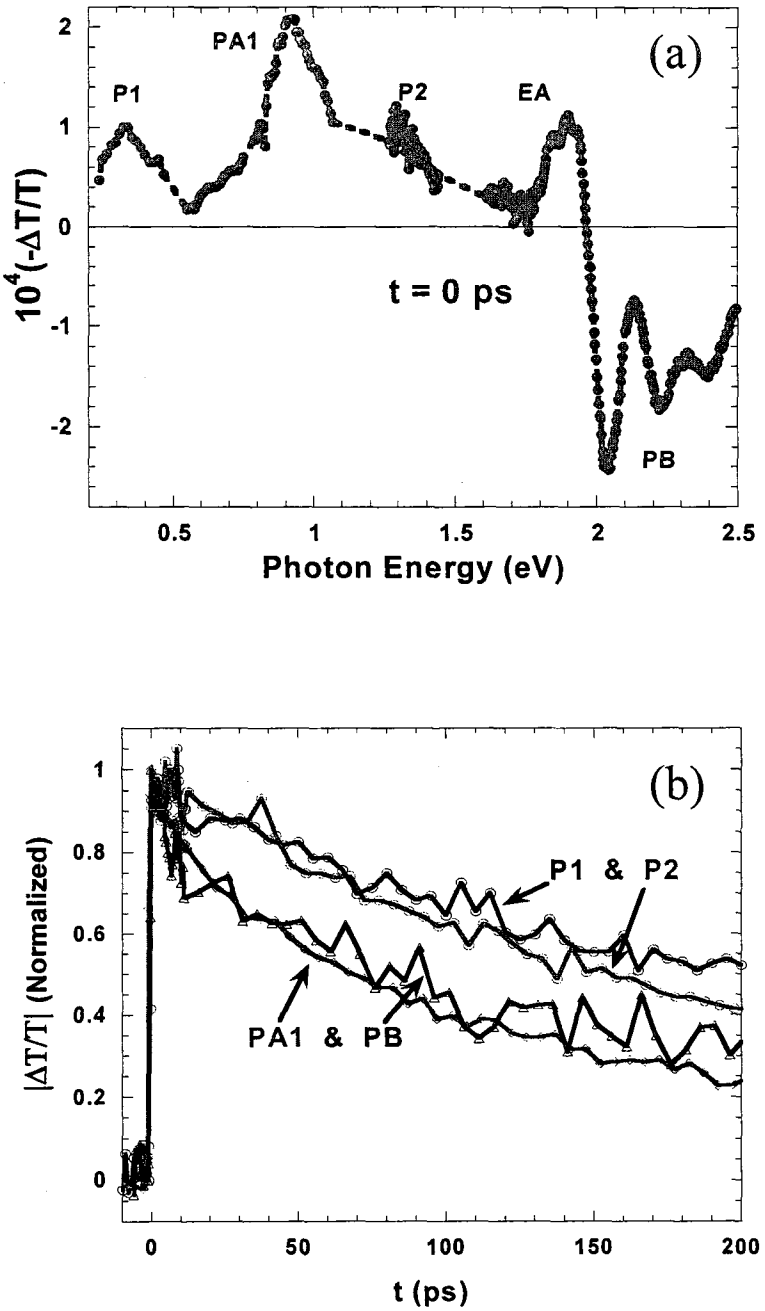

Figure 3.5: Transient photomodulation (PM) measurement of RR-P3HT film. (a) Transient PM spectrum at t = 0 ps. (b) Transient normalized decays of their respective bands P1, P2, PA1 and PB.

Table 3.1: The transient decay parameters (lifetimes and relative weight contributions) of the PA and PB bands in the PM spectrum of RR-P3HT film.

Band	Time Constants (τ)
P1	240 ps
P2	300 ps
PA1	15 ps (24%), 170 ps (76%)
PB	7 ps (24%), 230 ps (76%)

instantaneously, but the neutral species that are singlet excitons decay faster than the charge species or polarons.

3.3.2 Ultrafast photophysics of PCBM film and isolated molecules

Although the absorption of PCBM film at the excitation energy of 3.1 eV is weak compared to that in P3HT polymer, and thus may not contribute much to the blend photophysics. Nevertheless it would be worthwhile to look into the PM spectrum of pristine PCBM film before we discuss the PM spectrum of P3HT/PCBM blend. Figure 3.6(a) shows the ultrafast PM spectra of PCBM film at t = 0 ps and 100 ps in the visible/near-ir spectral range. Two PA bands appear in this spectral range: Ex at 2.25 eV and CT at 1.8 eV. Their different decay dynamics indicate that these PA bands belong to two different photoexcited species having different lifetimes. Figure 3.6(b) shows their

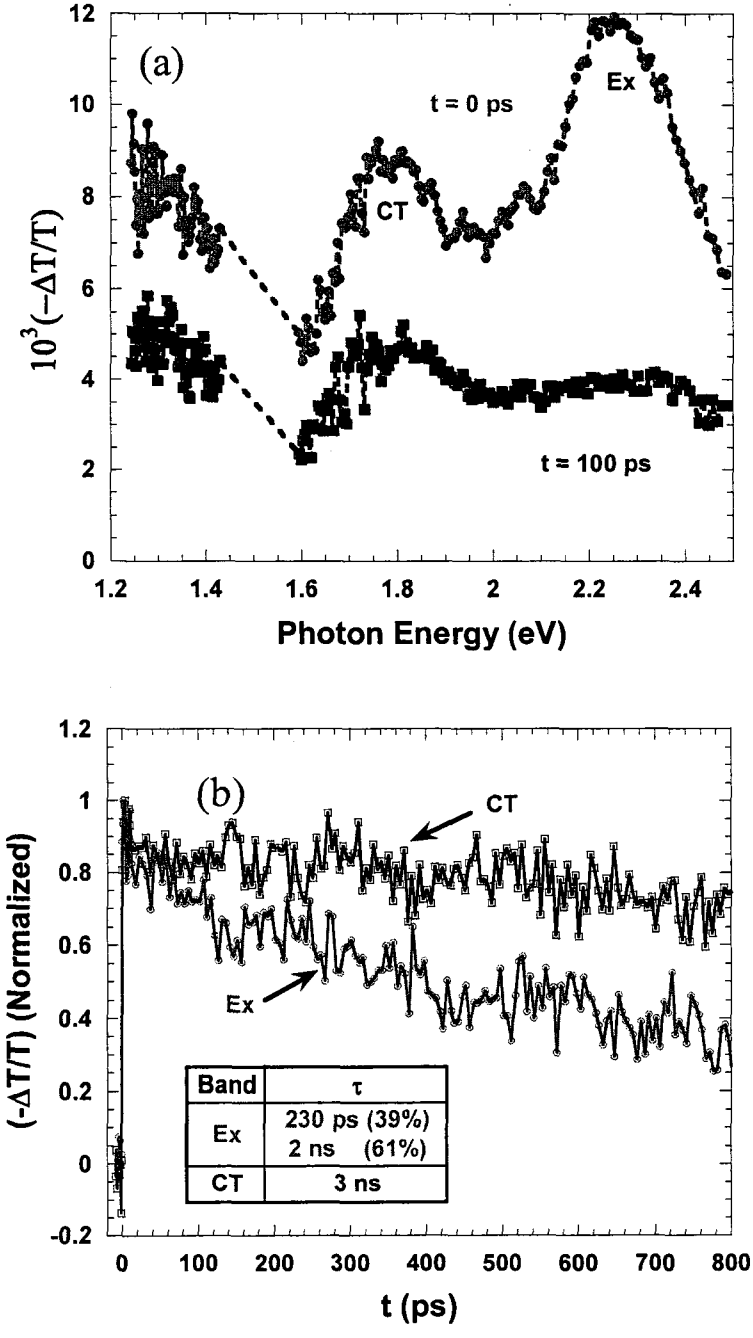

Figure 3.6: Transient PM measurement of PCBM film. (a) Transient spectra at t = 0 ps and 100 ps showing two bands, Ex and CT (b) the time decay of these bands and their fitted parameters are given in inset.

transient decay, having decay constants as given in the inset table. The CT PA band at ~1.8 eV decays much slower compared to the Ex PA band at ~2.26 eV. In order to find the origin of these different PA bands, the PM spectra of PCBM molecules were also studied.

Figure 3.7(a) shows the ultrafast spectra of PCBM, JAL and HAB films in the Vis/near-ir spectral range at t = 0 ps. The two PA bands, namely Ex and CT, also exist in the PM spectra of JAL and HAB films. This shows that JAL and HAB have similar photophysics to those of PCBM.

Figure 3.7(b) shows the PM spectra of PCBM molecules at t = 0 ps and 100 ps in the visible-near-ir range. The film was drop cast from a solution of polystyrene with 1% (by weight) PCBM addition. At such a low concentration of PCBM, we assume that most of the PCBM molecules are isolated in the polystyrene matrix. The PM spectra contain only the Ex PA band at ~2.4 eV, which decays much slower compared to that in the film. Since it is known that the primary excitations in the PCBM molecule are Frenkel type singlet exciton, therefore the Ex band in the film originates from singlet excitons. A similar argument, but the opposite conclusion follows the CT PA band – its absence in the PM spectrum of isolated PCBM molecules shows that this is due to charge transfer species in the film. The occurrence of CT excitons in the films but not in isolated fullerene molecules is justified, because neighboring fullerene molecule in the films may interact to create CT states, but this interaction is impossible for isolated molecules.

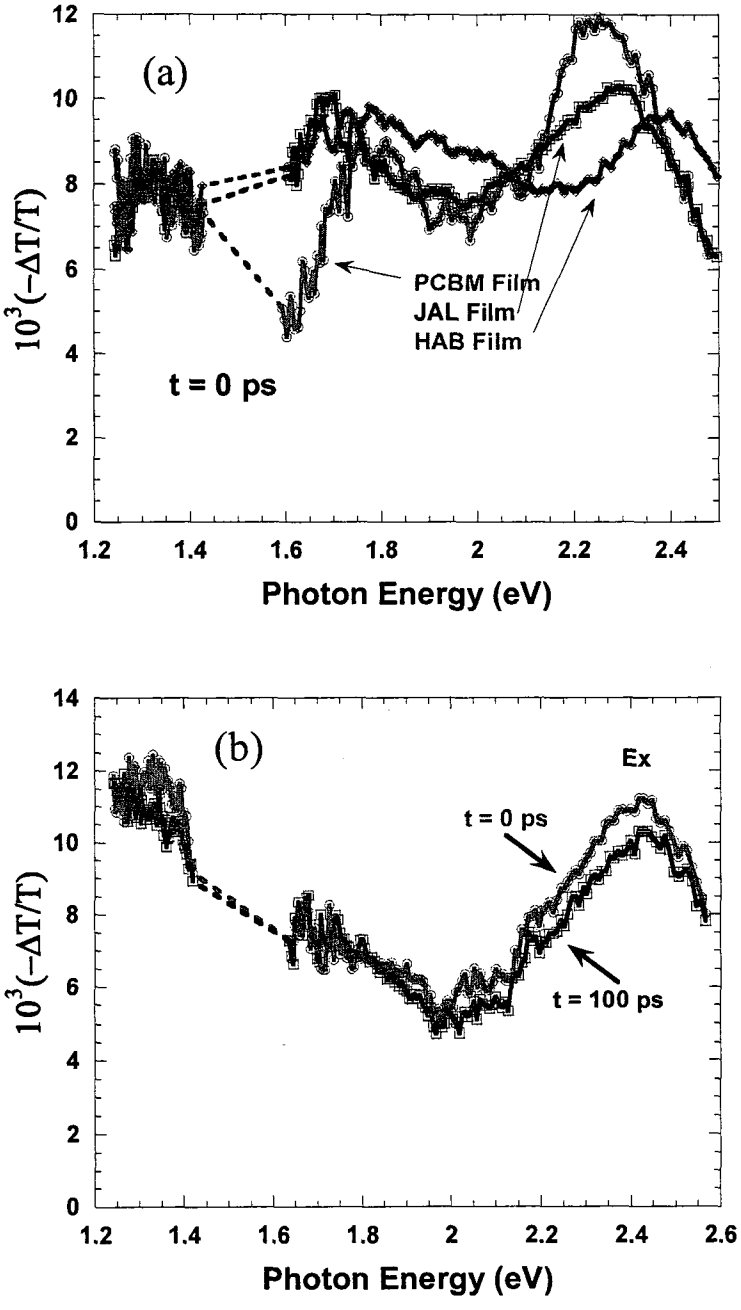

Figure 3.7: Transient PM spectra of (a) PCBM, JAL and HAB films at t = 0 ps (b) PCBM molecule (1% by weight) in the polystyrene matrix at t = 0 ps and 100 ps.

3.3.3 Ultrafast photophysics of RR-P3HT/PCBM film

The ultrafast PM spectra of RR-P3HT/PCBM (1.2:1) annealed sample is shown in Figure 3.8(a) upon excitation at 3.1 eV. The initial PM spectrum at t = 0 ps looks very similar to the spectrum of pristine RR-P3HT polymer film - we again observe P1, P2, PA1 and PB bands; this indicates that even in the blend system most of the absorption occurs in the polymer phase. However, the decay dynamics of these PA bands are different from those in the pristine polymer. The PM spectrum at t = 50 ps in the spectral range of 0.25-1.1 eV shows that PA1 disappears completely, whereas the band P1 decays much slower. We also note that P1, which is due to polarons, does not increase on the expense of PA1 decay. The PM spectrum at t = 300 ps in the range of 1.2–2.4 eV shows an appearance of a new band, dubbed PA' at ~1.75 eV. The transient decays of the various PA bands are shown in Figure 3.8(b); their corresponding time constants are given in Table 3.2. P1 and P2 polaronic bands in the blend decay slower than in the pristine film, and could be fit with a single exponential decay of ~520 ps. In contrast PA1 of singlet exciton in the blend decays faster than in the pristine film presumably due to dissociation of exciton at the donor/acceptor interface. It is fitted with double exponential decay of 6 ps (43%) and 43 ps (57%). The initial decay of PB (photobleaching) in fact follows the PA1 decay, indicating that it is dominated by excitons in the polymer phase. In addition, the new band PA' rise time exactly matches with the decay of PA1. For a better comparison the negative of PA' (-PA') decay is compared with that of PA1 band in Figure 3.9; it is clear that their dynamics exactly match.

We focus on two important things that need be mentioned in the ultrafast photophysics of the blend: (a) There is no build-up of polaron bands, P1 and P2, at the

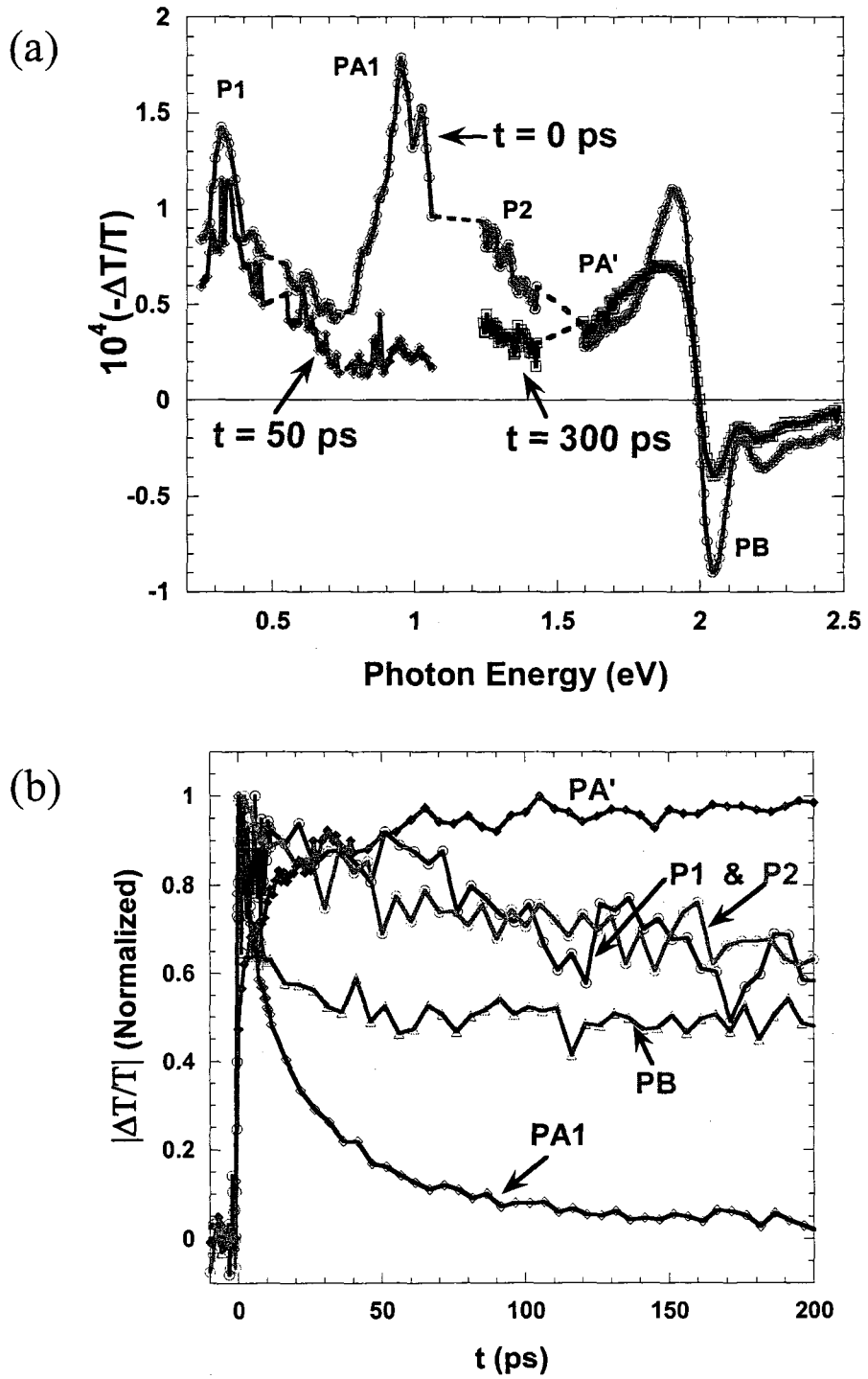

Figure 3.8: Transient PM measurement of RR-P3HT/PCBM film. (a) Transient PM spectra at t = 0 ps, 50 ps & 300 ps showing different bands of P1, P2, PA1. PA' and PB and (b) the transient normalized decays of different bands P1, P2, PA1 PA' and PB.

Table 3.2: The transient decay parameters (lifetimes and relative contributions) of different bands of RR-P3HT/PCBM film.

Band	Time Constants (τ)
P1	520 ps
P2	520 ps
PA1	6 ps (43%), 43 ps (57%)
PB	6 ps (43%), >1.5 ns (57%)
PA'(rise)	Same as PA1

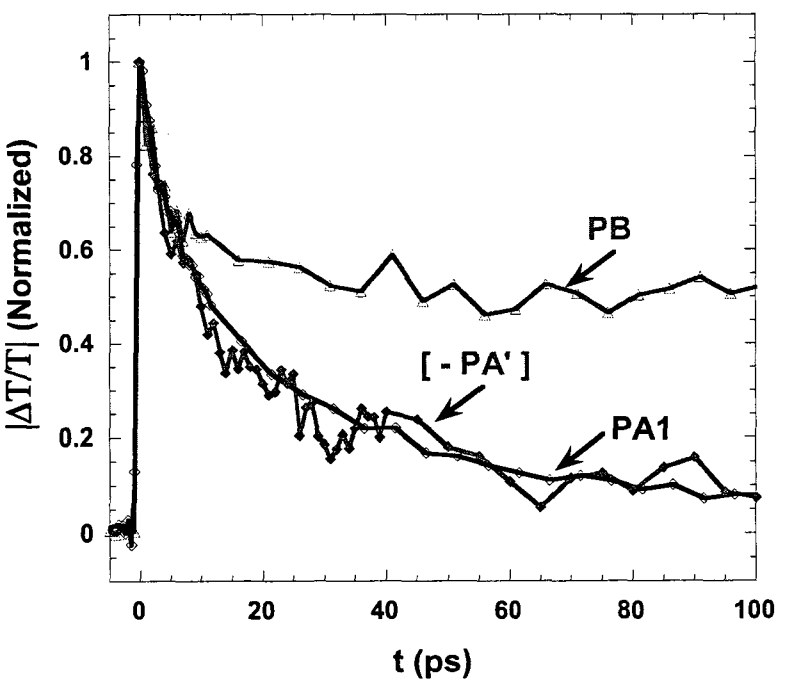

Figure 3.9: The transient decay of bands PA1, [-PA'] and PB of the RR-P3HT/PCBM film are compared.

expense of dissociation of exciton, PA1. According to the assumed photovoltaic model, the decay of exciton (i.e., their dissociation) should be mirrored by a build-up of polarons in the polymer. (b) The rise of PA' band exactly matches with the decay of the exciton band PA1, and we note that PA' does not belong to the polymer phase (as seen in the PM spectrum of the pristine polymer). These two arguments support the idea that PA' originates neither from the polymer domain nor from the interface of donor/acceptor. On the contrary it should be related with the PCBM phase. On closely observing the PM spectra of PCBM film, there is in fact a CT band at ~1.8 eV. Therefore, we believe that *the majority of photogenerated excitons in the polymer phase do not dissociate at the interface of D/A upon their arrival, but are transferred to the PCBM phase as charge transfer (CT) excitons*. The CT excitons in the PCBM phase may further dissociate, whereby electrons may remain in the fullerene phase and a hole may come back into the polymer phase as positive polarons in the chains.

Ultrafast photophysics of RR-P3HT/PCBM was also completed by Hwang et al.[87], in the probe range of 1.1-2.1 eV, but some of their interpretations are very different from ours, presumably due to the narrower spectral range that they used. They assumed a two- step process for the charge generation in the blend, where CT state at the interface plays an intermediate step. According to this model, the build-up PA' is due to release of bound polaron into mobile polaron in the polymer, and the rise time was measured to be ~4 ps, much faster than in our measurements. In addition their PM spectrum goes to zero at ~1.0-1.1 eV, which is the range of PA1 band. On the contrary, we found here that the PA1 band ~1 eV initially survives upon blending, while its decay exactly matches the rise of PA' band.

In order to study the effect of electric field due to the built-in voltage in a real photovoltaic device structure, the ultrafast photophysics of RR-P3HT/PCBM (1.2:1) blend was also studied, in the reflective mode in OPV device structures.

3.3.4 Ultrafast measurement of RR-P3HT/PCBM blend in OPV device structure

In the actual photovoltaic device structure *Glass/ITO/PEDOT/RR-P3HT+PCBM (1.2:1)/Al* an internal built-in electric field (E_b) is formed due to difference in the work functions of the electrodes. In order to study the effect of the electric field on the photophysics of the active layer, PM spectra of blend (in the given device structure) were measured in the Vis-NIR spectral range, but in reflective mode. Figure 3.10(a) shows the PM spectrum of the P3HT/PCBM blend in a *device structure*. The PM spectrum and its dynamics are in fact similar to those in blend *film*. In particular Figure 3.10(b) shows the rise of band PA' that also dominated the dynamics at 1.75 eV, also in the presence of E_b. We thus conclude that the exciton energy transfer from the polymer phase to the fullerene phase is generic; it definitely also occurs in real devices, and therefore needs be taken into account in discussing charge photogeneration in real OPV devices based on BHT mode of operation.

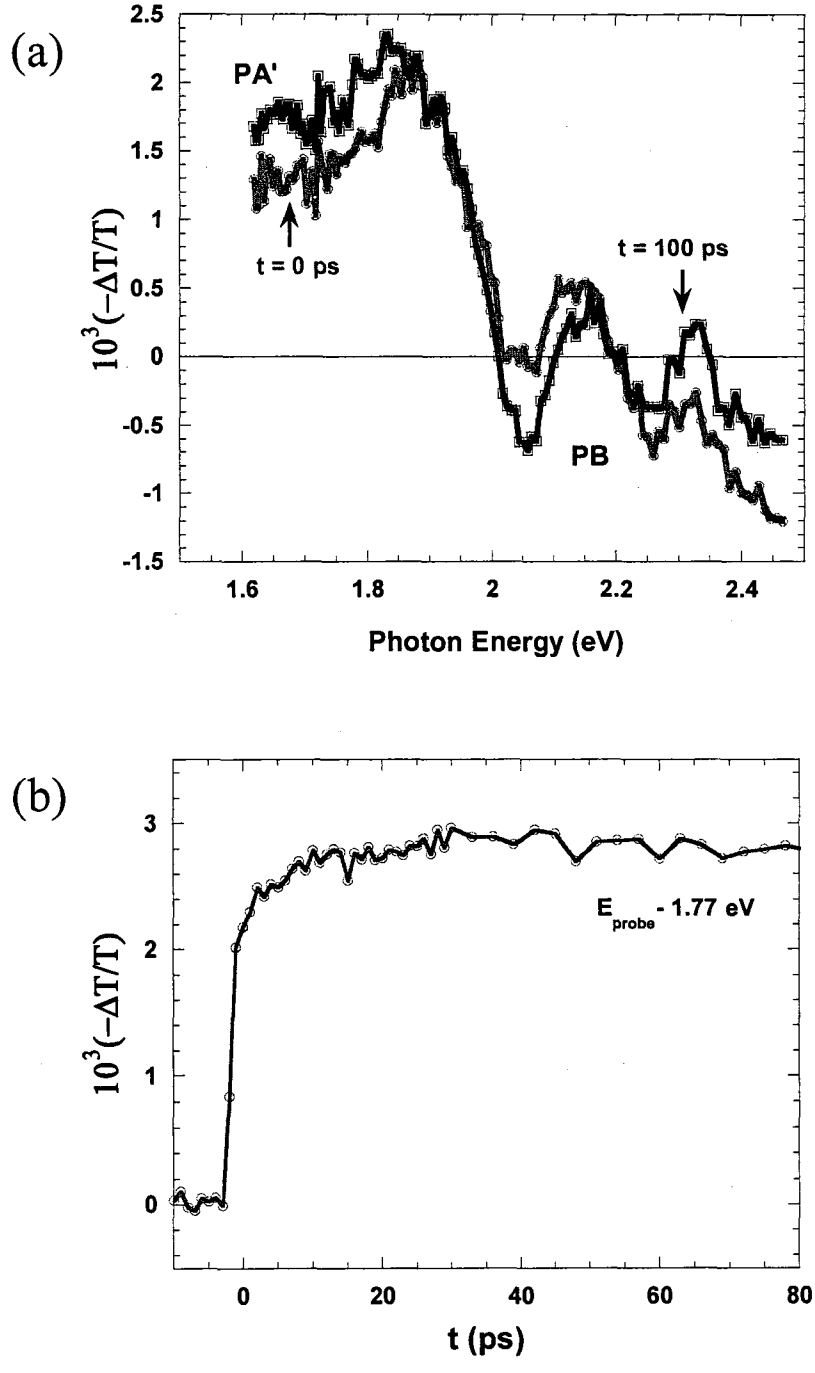

Figure 3.10: Transient PM measurement of RR-P3HT/PCBM film in the device structure of *Glass/ITO/PEDOT/RR-P3HT+PCBM (1.2:1)/Al.* (a) Transient spectra at t = 0 ps and 100 ps showing PA' and PB bands, and (b) the transient decay of PA'.

3.3.5 Ultrafast photophysics of RR-P3HT/PCBM (1.2:1) blend with below-gap excitation

The electroabsorption measurements discussed above have shown the presence of charge transfer state at the interface of D/A in the blend, below the band-gap of the polymer and fullerene constituents. Therefore, below-gap excitation is possible in the blend and in fact would resonantly excite the CT state at the interface. Moreover the ultrafast PM spectrum would preferentially show photoexcitations at the D/A interface. Figure 3.11(a) shows the PM spectra of RR-P3HT/PCBM (1.2:1) blend upon excitation at 1.55 eV. The spectrum contains polaronic bands, P1 & P2, and photobleaching, PB; ***but no excitonic PA bands***. The photogenerated polarons resides at the D/A interface of the RR-P3HT polymer/fullerene domains. Figure 3.11(b) shows the comparison of PA signal at ~1.8 eV upon excitation with above-gap and below-gap pump photon energy. It is clear that there is ***no PA' 'build-up'*** associated with the below-gap excitation case. This proves our statement that the build-up of PA' band (in above-gap excitation) is the result of singlet exciton decay in the polymer as reflected by the PA1 dynamics.

3.3.6 Ultrafast photophysics of RR-P3HT/JAL and /HAB (1.2:1) blends

The ultrafast photophysics of different blends (RR-P3HT with PCBM or JAL or HAB) are not very different from one another. Figure 3.12 shows the PM spectra of RR-P3HT/PCBM, RR-P3HT/JAL and RR-P3HT/HAB, respectively, in the Vis/near-ir probe spectral range. These PM spectra are similar to each other except that the geminate

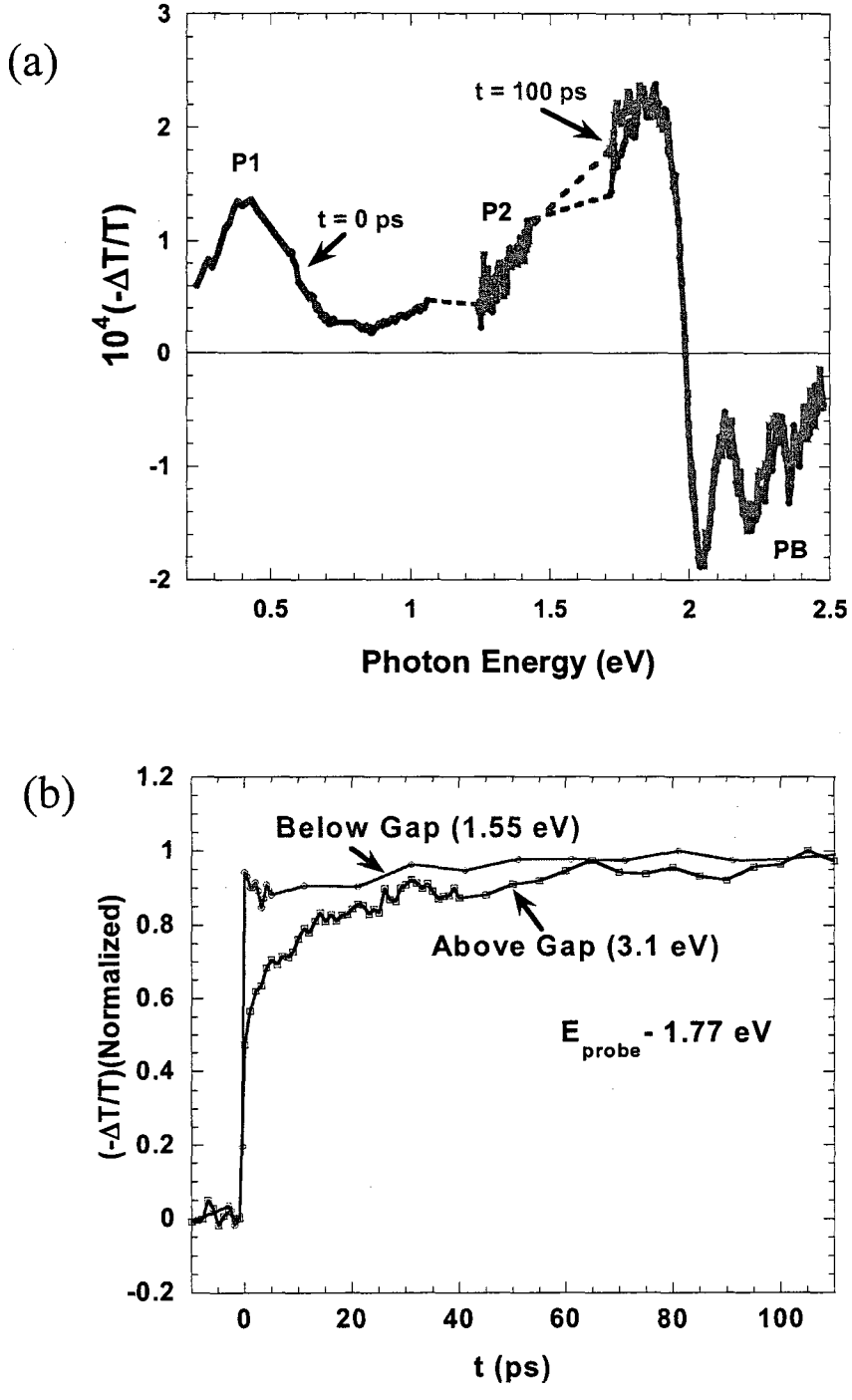

Figure 3.11: Transient PM measurement of RR-P3HT/PCBM film. (a) Transient spectra at t = 0 ps and 100 ps, when excited at 1.55 eV, showing different bands of P1, P2 and PB and (b) the transient decay at 1.77 eV when excited AG (3.1 eV) and BG (1.55 eV).

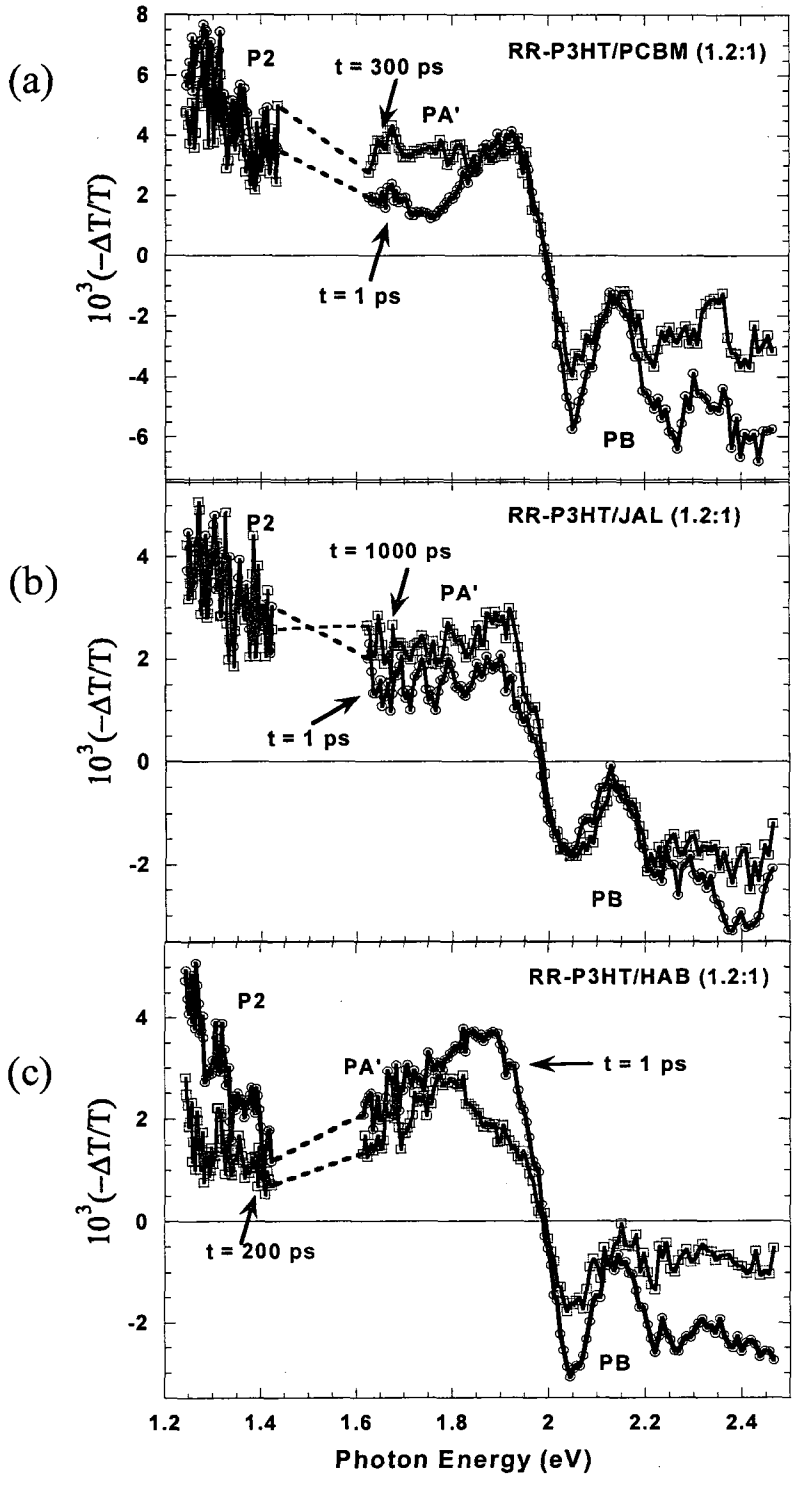

Figure 3.12: Transient PM spectra of (a) RR-P3HT/PCBM (1.2:1) film (b) RR-P3HT/JAL (1.2:1) film (c) RR-P3HT/HAB (1.2:1) film at different times

recombination (~1.3 eV, P2 band) is faster in the case of the P3HT/HAB blend. Figure 3.13 shows the comparative transient decays of different bands in these three blends. It is clear that the only difference in decays appear for P2 band (~1.3 eV), and their decay time constants are in the decreasing order of JAL > PCBM > HAB. The decay dynamics of other bands-PA1, PA' and PB- are approximately the same. We have found that the solar power conversion efficiency of photovoltaic devices made from these blends is also in the decreasing order of JAL > PCBM > HAB, which is consistent with the decay of P2 band. We thus conclude that ultrafast geminate recombination is an important factor that governs the OPV conversion efficiency. In fact by studying P2 decay in the blend, one may be able to investigayte this fast process and thereby improve the OPV cell operation.

3.3.7 Effect of spin-1/2 radical on the ultrafast photophysics of RR-P3HT/PCBM (1.2:1)

The success of bulk heterojunction photovoltaic devices compared to bilayer devices lies in the enhanced interfacial area of the donor-acceptor nano-sized domains, which is important for enhanced exciton dissociation. However the increased interface area between the donor and acceptor phases in the blends provides additional surface recombination channels (both geminate and nongeminate) of the loosely bound polaron-pairs [74, 88-90], and consequently limits the power conversion efficiency, η; this holds true even after taking into account the exciton dissociation into free electrons and holes that leads to photoluminescence quenching.

We found that the addition of few weight percentage of a spin ½ organic radical impurity, namely Galvinoxyl [91, 92], substantially reduces the geminate recombination

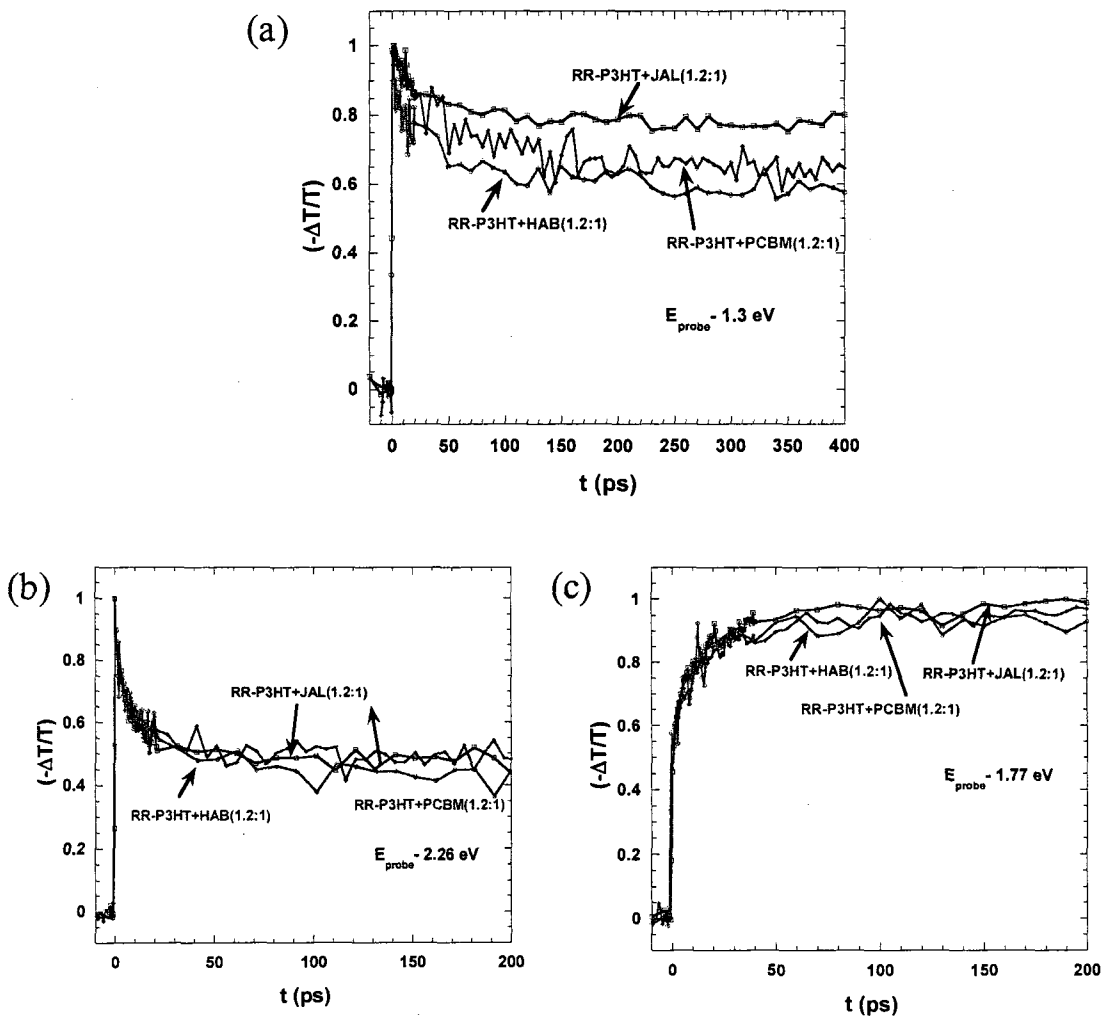

Figure 3.13: The transient decay of RR-P3HT/(PCBM or JAL or HAB) (1.2:1) film at (a) 1.3 eV, (b) 2.26 eV, and (c) 1.77 eV

process of photogenerated polaron-pairs in the blend system of RR-P3HT/PCBM (1.2:1). Consequently most of the typical parameters that characterize the photovoltaic (PV) solar cell made from this blend mixture as the active layer in fact improve, and consequently the power conversion efficiency of such cells dramatically increases by about 10% compared to the undoped blend reaching ~ 4.2 % (as shown in Table 3.3).

The transient PM spectrum of the RR-P3HT/PCBM blend film has already been discussed in section 3.3.3. We also note that the initial PM spectrum does not change much upon adding the radical impurities to the blend, and thus monitoring the transient decay at several wavelengths is sufficient to get information about the carrier dynamics in the radical-doped blends. We mainly focus on two distinct PM bands, namely, photobleaching (PB) in the range of 2.0-2.4 eV; and P_2 in the near-IR at ~ 1.3 eV [66, 67]. From the cw and optically-detected magnetic resonance studies in our group we identify P_2 as due to photogenerated hole-polarons in the P3HT polymer chains. In the present spin-1/2 radical study we focus on the PB and P_2 spectral features. These bands decay with time, and we analyze their transient dynamics in terms of ultrafast geminate recombination.

Figure 3.14(a) shows the PB decay at 2.26 eV for different radical-doped blend films at 0, 3 and 10 % radical impurities. The decay of PB at 2.26 eV is directly related to the ground state recovery of all excited species, including neutral excitons and charge polarons, in the *P3HT polymer*, since neither PCBM nor Galvinoxyl strongly absorb in this spectral range. Consequently the fast decay component of PB is related with decay of exciton in the P3HT polymer, but also hole polaron decay in the polymer contribute to it. We note that the contribution of fast polaron decay rate observed in pure P3HT decreases

Table 3.3: The transient decay parameters (lifetime and relative contribution) and photovoltaic device parameters of annealed RR-P3HT/PCBM (1.2 : 1) films with different % of Galvinoxyl radical impurities

Galvinoxyl (%)	*Transient Decay at 2.26eV*	*Transient Decay at 1.3eV*	J_{sc} *(mA/cm^2)*	V_{oc} *(V)*	*Fill-Factor (%)*	*Efficiency (%)*
0	7ps (47%) >5ns (53%)	62ps (32%) >5ns (68%)	11.3	0.57	55	3.5
3	8ps (33%) >5ns (67%)	73ps (16%) >5ns (84%)	12.7	0.58	60	4.2
10	7ps (28%) >5ns (72%)	63ps (10%) >5ns (90%)	11.2	0.61	53	3.6

upon adding the radical impurities to the blend. We fitted these decays using a double exponential decay function that contains a short (~7 ps) and long (> 5 ns) lifetime components. The best-fit lifetimes and relative weight contributions of the double exponentials are given in Table 3.3. PB decay indicates that the addition of radical impurities to the blend reduces the contribution of short time hole polaron recombination loss in the P3HT chains in the blend.

Figure 3.14(b) shows the decay of P_2 band at 1.3 eV for the various radical-doped blend films; similar to Figure 3.14(a). P_2 is associated with excited state absorption from the polaron species in the polymer chains [66, 67], and consequently its decay dynamics show the reduction in polaron density with time due to geminate (fast) recombination. From transient measurements of pure PCBM film we verified that polarons in PCBM film do not have strong PA in this spectral range. P_2 decay dynamics are again fitted with a double exponential function as given in Table 3.3. Similar to the PB band dynamics,

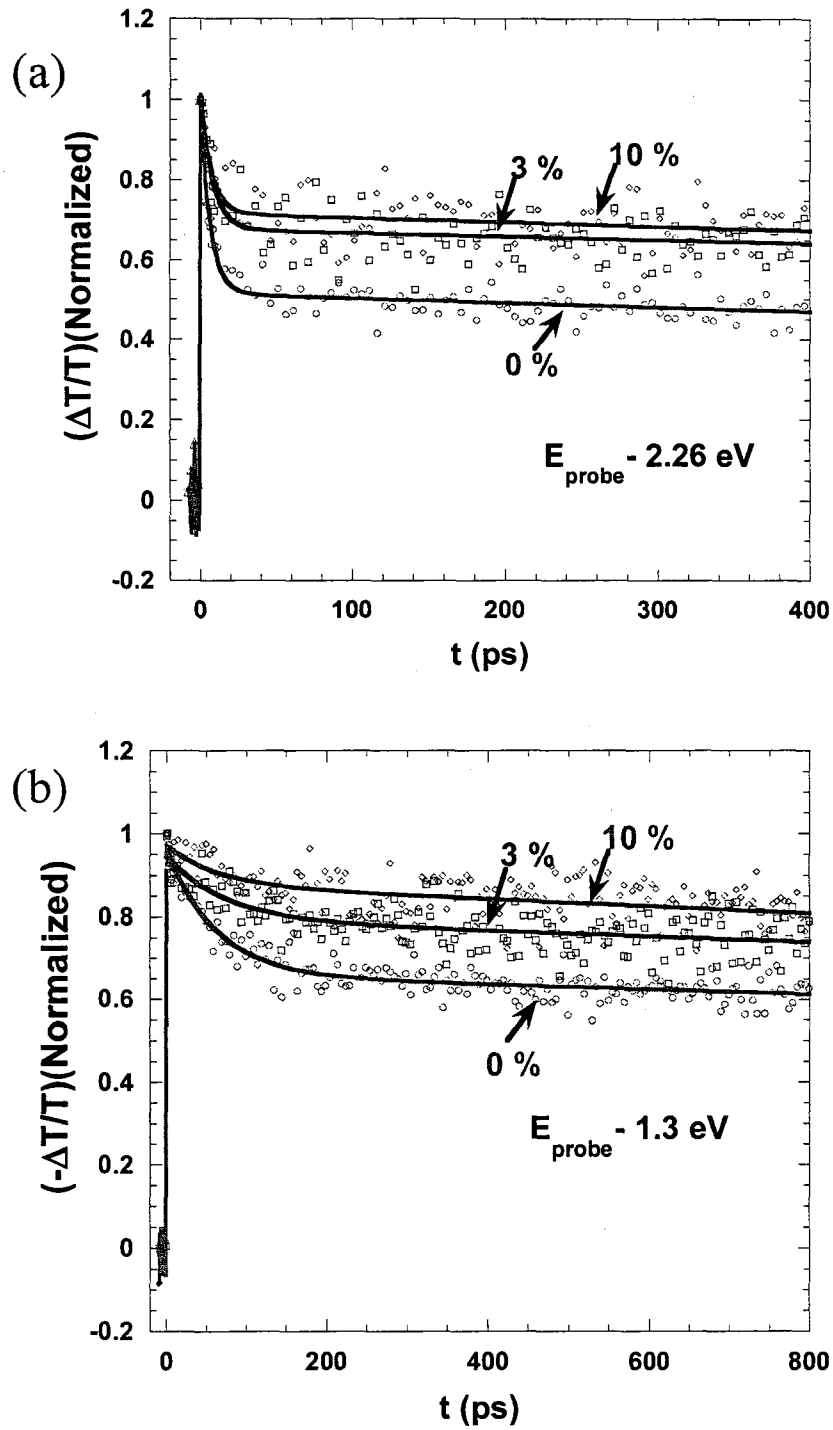

Figure 3.14: The transient decays in RR-P3HT / PCBM (1.2 : 1) films mixed with 0, 3 and 10% of Galvinoxyl impurities measured at (a) 2.26 eV (PB), and (b) 1.3 eV (P2). The inset to (a) shows the chemical structure of Galvinoxyl radical impurity.

P_2 decay also contains a short (~ 68 ps) and long (> 5 ns) lifetime components, and their contributions change with % of radical added. The important discovery here is that *the addition of radical impurities to the blend reduces the geminate (fast) recombination of hole polarons in the P3HT phase of the blend.*

The effect of Galvinoxyl radical on the rate of geminate recombination might be explained as follows. Galvinoxyl is a spin ½ radical, and this opens up the possibility of spin-spin interaction with the photogenerated species in the blend. In particular we speculate that the radical spin may interact with the electron and hole spins that are in the "singlet" configuration in the photogenerated PP species that exist at the interface of P3HT and PCBM as shown in Figure 3.15. This spin-spin interaction may cause a spin flip of one of the locked spins in the PP singlet configuration. Consequently the bound PP may undergo a fast intersystem crossing into the spin-triplet configuration that traditionally is longer-lived. The triplet PP species would therefore be more susceptible for efficient dissociation at later time into free electron- and hole-polarons in the PCBM and P3HT polymer phases, respectively, and this increases the photogenerated current density in the organic photovoltaic (OPV) devices made of these radical/blend mixtures.

To see the effect of reduction in geminate recombination rate of polarons due to the spin ½ radical impurities in OPV devices, we fabricated OPV devices based on radical/blend mixtures films, with various radical percentages as an active layer. The device characteristic parameters such as short-circuit current density, J_{sc}, fill-factor, open circuit voltage and power conversion efficiency are given in Table 3.3. As seen, the devices show increase in *all* typical parameters at ~3% addition of radical, especially in J_{sc}, which is consistent with the reduction in geminate recombination rate that we found

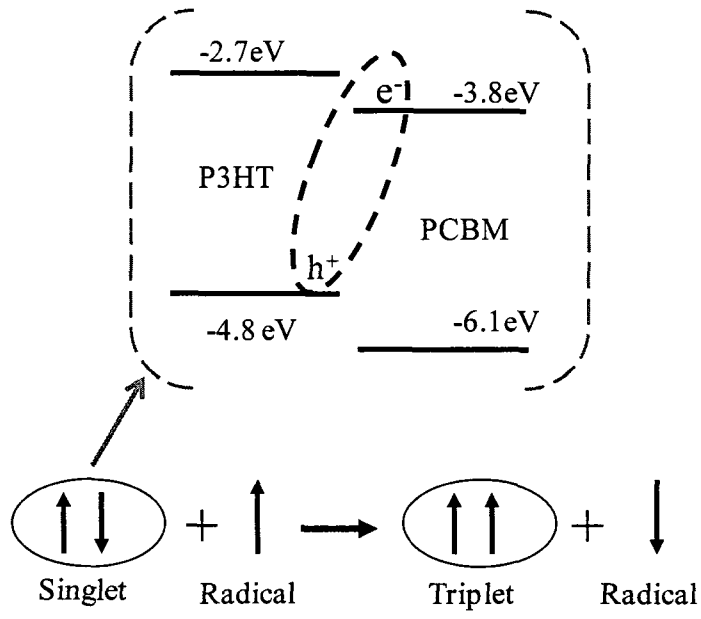

Figure 3.15: Schematic diagram of our assumed model for spin-spin scattering due to spin-1/2 radical, Galvinoxyl, with singlet exciton at the interface of P3HT/PCBM

here by the obtained ultrafast decays. The OPV parameters, however, start decreasing at 10% radicals, which might be due to change in morphology of the blend film at higher percentage of radicals that should decrease carrier mobility. The reduction in J_{sc} and FF of solar cells with 10% radicals supports this conclusion.

The photovoltaic devices based on RR-P3HT/ PCBM (1.2:1) have shown high power conversion efficiency (~6%), but on the other hand, devices based on RRa-P3HT/ PCBM (1.2:1) have poor power conversion efficiency (<0.5%). In order to resolve this huge change in power conversion efficiency in terms of photophysics, we studied pristine RRa-P3HT polymer and RRa-P3HT/ PCBM (1.2:1) blend system also.

3.3.8 Ultrafast photophysics of RRa-P3HT polymer

Unlike RR-P3HT, RRa-P3HT polymer does not form lamellae structure due to hindrance of side groups, and its photophysics is similar to other π-conjugated luminescent polymers. Figure 3.16(a) shows the ultrafast PM spectra of RRa-P3HT film at t = 0 ps and 200 ps in the 1.24–2.2 eV probe range. There are two main bands, namely stimulated emission, SE in the range of 1.75-2.1 eV, and PA1in the range (<1.3 eV). Figure 3.16(b) shows the normalized decay of SE and PA1 with the fitting decay constants in the inset; the decay dynamics are similar to each other. And since SE exists only for excitons, we conclude that these PA bands are due to singlet excitons. The PM spectrum in RRa-P3HT can be compared to that of RR-P3HT. It is interesting to note that there are no photogenerated polarons in the former; this shows the importance of lamella formation, and in general interchain interaction in charge carrier photogeneration process in polymer films.

3.3.9 Ultrafast photophysics of RRa-P3HT/PCBM (1.2:1)

3.3.9.1 Above-gap excitation

When RRa-P3HT is mixed with PCBM, it has been shown that it does not form donor/acceptor phase separation to such a degree as RR-P3HT/PCBM blend. In fact the polymer chains and PCBM molecules mix homogeneously throughout the film. In this case we do not expect the photogenerated excitons in the polymer chains of the RRa-P3HT blend to last very long. Figure 3.17(a) shows the ultrafast PM spectrum of RRa-P3HT/PCBM (1.2:1) film at t = 0 ps upon excitation at 3.1 eV, above the polymer band-gap. The PM spectrum contains two bands: CT1 at 0.7 eV and CT2 at 1.65 eV. There

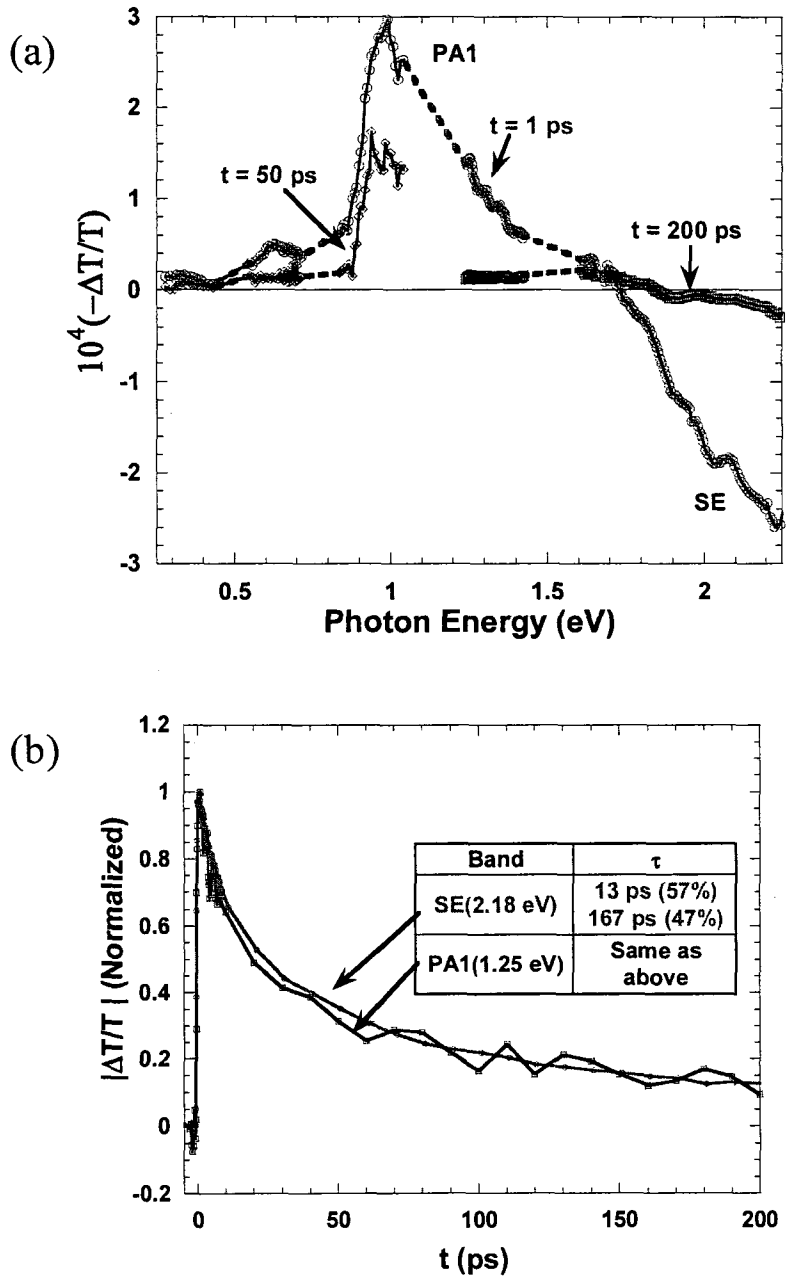

Figure 3.16: Transient PM measurement of RRa-P3HT film. (a) Transient spectra at t = 1 ps and 200 ps, showing two bands PA1 and SE (b) the decay dynamics of these bands. Inset of (b) shows the fitting parameters.

is also a small PA1 band due to singlet exciton at ~ 1eV, but is not clear in the PM spectrum due to its short life time (~0.4 ps). Figure 3.17(b) shows the decay dynamics of PA1, CT1 and CT2. PA1 decays very fast with lifetime of ~0.4 ps, and simultaneously CT1 and CT2 bands build-up. Since CT1 and CT2 are not due to excitons in the polymer, and they are created on the expense of singlet excitons, we interpret them as due to bound polaron pair transitions on the polymer and fullerene molecule, coming from a CT state. In order to understand the origin of these CT transitions, the active layer is also excited below-gap.

3.3.9.2 Below-gap excitation

Figure 3.18(a) shows the ultrafast PM spectrum of RRa-P3HT/PCBM (1.2:1) film at t = 10 ps in the range of 1.24-2.22 eV where the sample is excited below-gap at 1.55 eV; the above-gap spectrum is also shown for comparison. Both above-gap and below-gap excitation PM spectra are very similar to each other. In addition the normalized decay dynamics at 1.7 eV (CT2) and at 1.24 eV (close to PA1) are also the same, except the fast decay of singlet exciton in the above-gap excitation shown in Figure 3.18(b) and (c), respectively. These results indicate that the above gap and below-gap excitations yield the same kind of photoexcitation species in the RRa-P3HT/PCBM (1.2:1) film, following the dissociation of the singlet exciton (within ~ 0.4 ps in the former case).

Drori et al.[74] demonstrated that below-gap excitation creates only bound polarons in the donor/acceptor blends, and their contribution toward photocurrent is very small compared to above-gap excitation. Since in RRa-P3HT/PCBM (1.2:1) film the PM spectra of above- and below-gap excitations are the same, then they must be due to the

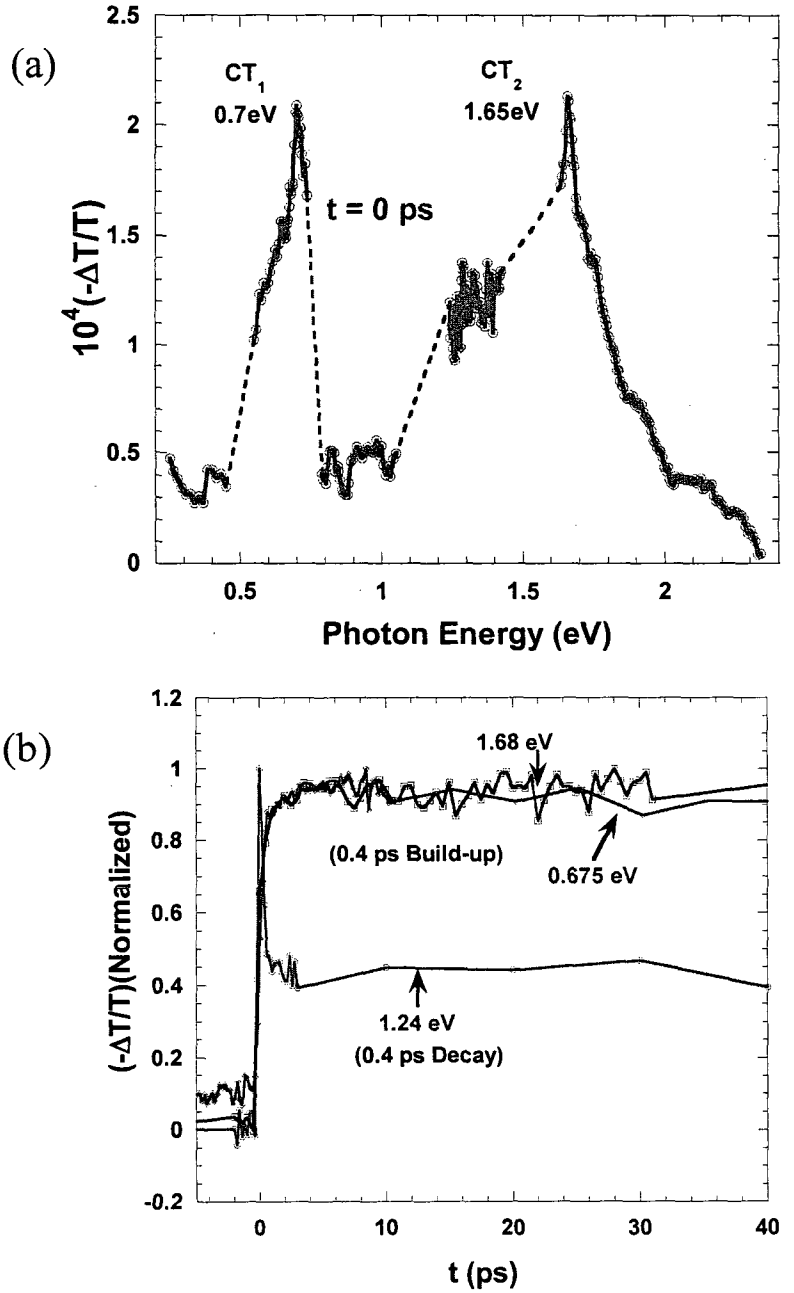

Figure 3.17: Transient PM measurement of RRa-P3HT/PCBM (1.2:1) film. (a) Transient spectrum at t = 0 ps showing different bands of CT1, CT2 and (b) the transient normalized decays of these bands.

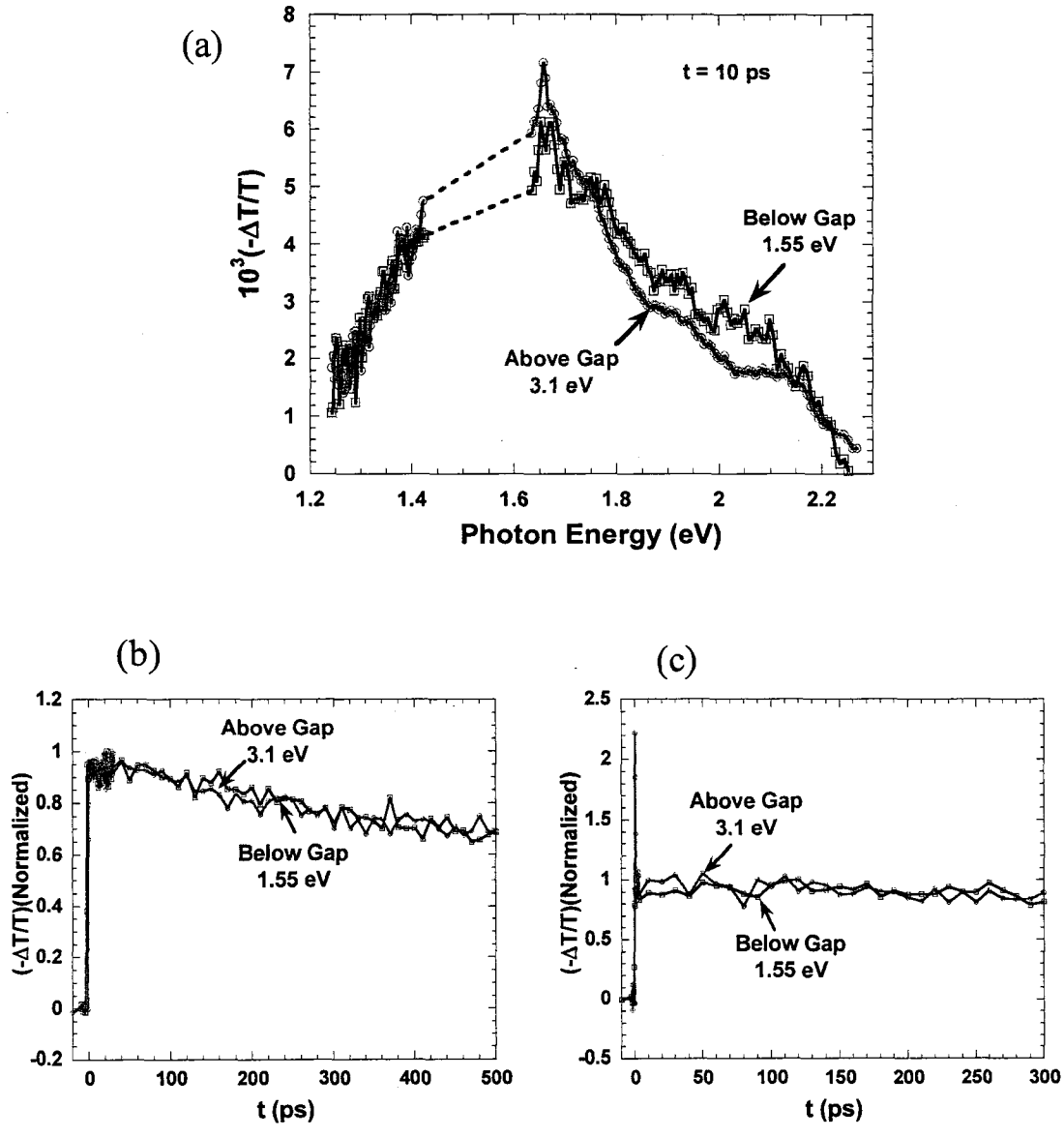

Figure 3.18: Comparison of above gap (3.1 eV) and below gap (1.55 eV) excitation of RRa-P3HT/PCBM (1.2:1) film (a) PM spectra at t = 10 ps; (b) transient decay dynamics at 1.7 eV; and (c) at 1.25 eV

CT excitons that do not separate into mobile polarons. This explains the poor photovoltaic performance of the RRa-P3HT/PCBM (1.2:1) active layer all across solar spectrum.

3.4 Conclusions

We have studied in detail the ultrafast photophysics of P3HT (both RR and RRa) and fullerenes (three derivatives: PCBM, JAL and HAB). JAL and HAB derivatives show a similar kind of photophysics as isolated molecules and film forms, with photogenerated intramolecular exciton in the former, and intramolecular excitons and CT excitons in the latter form. The only difference that appears is in their blend with P3HT polymer — geminate recombination is higher in the case of RR-P3HT/HAB blend compared to the PCBM and JAL blends, and this is reflected in the photovoltaic devices made of these blends, where RR-P3HT/HAB blend shows poor power conversion efficiency compared to PCBM and JAL blends.

The photophysics of RR-P3HT/PCBM blend is very different from that of RRa-P3HT/PCBM blend because of phase separation of polymer and PCBM in the former blend, namely the formation of RR-P3HT and PCBM nano-sized domains. The photophysics in the two blends is explained in Figure 3.19, which summarizes the effect of nano-sized domains on the photophysics of these blends. In case of RRa-P3HT/PCBM blend, there is no formation of nano-sized domains and the polymer and fullerenes are mixed uniformly. Therefore the polymer is excited either at the interface of D/A or very close to the interface. We found that the photogenerated excitons disappear in record time within 0.4 ps, and at the same time charge transfer state appears at the interface of D/A.

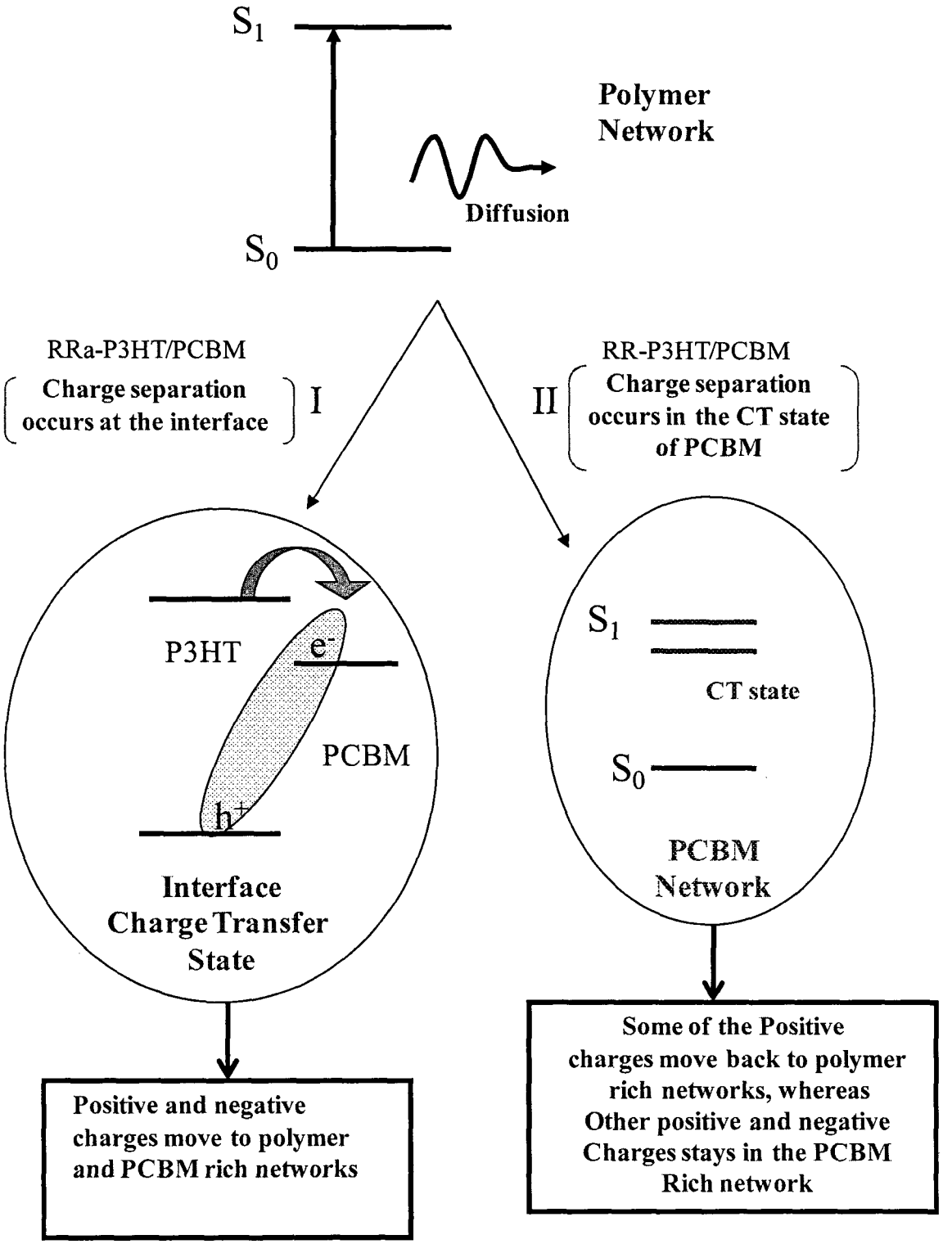

Figure 3.19: Schematic diagram of model for the photophysics of P3HT/Fullerenes

Moreover, the above-gap and below-gap excitations form the same PM spectrum and decay dynamics. These findings indicate that in case of RRa-P3HT/PCBM tightly bound polarons are created upon photon absorption irrespective of the excitation photon energy. This explains the poor photocurrent generation in the RRa-P3HT/PCBM blend. This mechanism is explained by path-I in Figure 3.19.

In contrast RR-P3HT/PCBM blend film follows path II in Figure 3.19. The excited singlet excitons on the polymer chains diffuse to the interface in longer time (~6 ps) compared to that in RRa-P3HT/PCBM blend because of the finite size of the nanodomain of the polymer. The majority of the excitons in this case enter into the PCBM domains in the form of charge transfer state (with characteristic PA band of PA' ~ 1.75 eV), where they dissociate at longer time. Since the presence of polaron band P1 is observed in CW PM measurement, it indicates that some of the positive polaron from the PCBM network ***come back*** to the RR-P3HT polymer domains. This finding has been confirmed by Light Induced Electron Spin Resonance (LESR) measurements, where Mrs. Golda Hucik found two unequal numbers of spins, with different g-factors.

The minority of excitons go through path I, namely they dissociate at the interface of D/A, and consequently positive and negative polarons are created in the polymer and PCBM domains, respectively, rather instantaneously. The existence of this mechanism is confirmed by the effect of spin-1/2 radical on the geminate recombination of polymer polarons.

CHAPTER 4

DECAY SPECTROSCOPY OF PHOTOEXCITATIONS IN PPV-DERIVATIVE POLYMERS AT AMBIENT AND HIGH HYDROSTATIC PRESSURE

This chapter is divided into two parts: (a) ultrafast transient polarized photomodulation (PM) in the visible/near-infrared range, and polarization memory decay (PMD) spectroscopy for studying the primary photoexcitations in films and solutions of two poly(phenylene-vinylene) [PPV] derivatives; namely 2-methoxy-5-(2'-ethylhexyloxy) PPV [MEH-PPV], and 2,5-dioctyloxy PPV [DOO-PPV] at ambient pressure. (b) Ultrafast transient PM of MEH-PPV films at high hydrostatic pressure (up to 100 kbar) in the visible/near-infrared spectral range.

4.1 Materials

The chemical structures of DOO-PPV and MEH-PPV polymers are shown in Figure 4.1(a) and 4.1(b), respectively. DOO-PPV was synthesized in-house [93], whereas MEH-PPV powder was bought from American Dye Corp. Both polymers were dissolved in toluene with concentration of 0.1 mg/ml for the solutions, and 5 mg/ml for the films. The polymer films were drop cast from the solution, and subsequently dried at 50 °C for

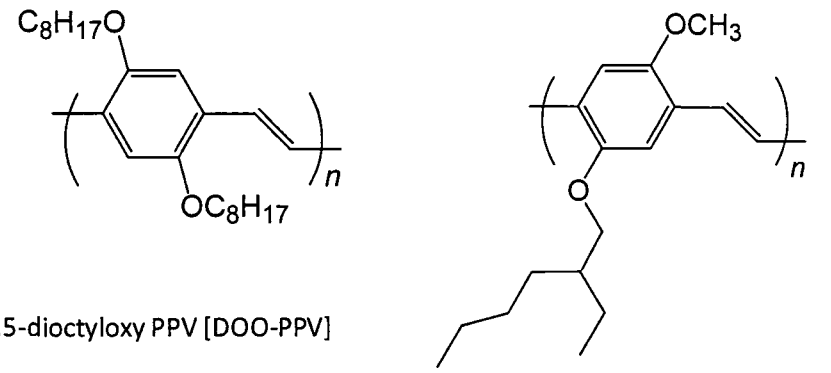

2,5-dioctyloxy PPV [DOO-PPV]

2-methoxy-5-(2'-ethylhexyloxy) PPV [MEH-PPV]

Figure 4.1: Chemical structures of DOO-PPV and MEH-PPV polymers.

1 hour in vacuum to remove any solvent left.

4.2 Polarization memory decay spectroscopy of photoexcitations in PPV-derivative polymers

In the last two decades π-conjugated polymers have been used as active layers in a variety of optoelectronic devices such as light emitting diodes, solar cells, photo-detectors, lasers, and light emitting field-effect transistors [1, 2, 94]. Among the variety of π-conjugated polymers, poly(phenylene-vinylene) [PPV] and its soluble derivatives have shown high photoluminescence (PL) quantum efficiency, and therefore these polymers have been excellent candidates to be utilized as active layers in electroluminescence devices. From the application point of view their photophysics is

crucial, and hence the PPV derivatives have been the subject matter of a large body of experimental and theoretical research studies [84, 95-98]. In spite of these efforts, there has still been an intense debate on the nature of the primary photoexcitations in these polymers. There is a consensus that the primary photoexcitations in PPV derivative polymers in *dilute solutions* are intrachain singlet excitons. However in *films* of PPV derivatives, due to the increased interchain coupling, species other than intrachain excitons may also be instantaneously photogenerated [84]. Some of these other species discussed in the literature are polaron pairs, excimers, and free polarons [84, 95-98]. These various photoexcitations have associated signature optical transitions, and thus their identification in the transient photomodulation (PM) spectra has been attempted based on their characteristic below-gap photoinduced absorption (PA) bands [1, 84]. Among the various instantaneously generated photoexcitations, however, only the intrachain exciton has been unambiguously identified due to the correlation of its characteristic PA bands with a stimulated emission (SE) band in the PM spectrum [1, 97]. But the other interchain species have always been hotly debated due to their intimate relation with the interchain interaction strength in the films, which varies substantially depending on the nature of side groups, solvent, and processing conditions used for the film fabrication, as well as different intensity of the pump laser excitation [99-101].

Recently an elegant theoretical investigation has been completed [102], in which the eigenstates of two coupled polymer chains having interchain interaction of various strengths were calculated. The basic Hamiltonian used in the calculation included both intrachain and interchain transfer integrals ($t_{\parallel}$ and $t_{\perp}$, respectively), as well as electron-electron and electron-hole interactions that were taken into account in a realistic way.

Based on these calculations it was concluded that when $t_{\perp}/t_{\parallel} > 0.1$, then the lowest excited state of the coupled chains is an *excimer*, where the charge ionicity, f on the two coupled chains varies between $0 < f < 1$. There are also states of polaron pair character with $f = 1$, and intrachain excitons with $f = 0$, but these states lie *above* the lowest excimer state. The excimer characteristic PA bands were also calculated [102]. Although the emphasis in that work was mainly on the excimer lowest energy PA band, PA', which actually red-shifts with respect to the PA band of the intrachain exciton, PA_1; a higher energy PA band is also anticipated for the excimer species at energy higher than that of PA_1. It thus remained experimentally unsettled whether excimers are indeed photogenerated in polymer films; a profound experimental verification is necessary to validate the theoretical calculation.

Due to the quasi one-dimensional nature of the π-conjugated polymer chains, most photoexcitation-related characteristic PA bands show anisotropic polarization behavior, which may be measured by the technique of polarization memory decay (PMD) kinetics, P(t) [103]. In our earlier work of ultrafast transient PM spectroscopy of various π-conjugated polymers [84], we found a relationship between the lifetime, τ_P of the photoexcitations PMD, and the interchain coupling strength of the polymer chains in the film, namely, the larger is the ratio $t_{\perp}/t_{\parallel}$, the smaller is τ_P. Furthermore the PMD kinetics technique may be an ideal tool to discern between the various photoexcitation species in polymer films. We expect fast PMD kinetics for intrachain excitons and free polarons, since these species are very mobile among the polymer chains in the film. However the excimers and polaron-pair species should be more localized in places along the chains

where the interchain distance between neighboring chains is the smallest, and consequently their binding energy (mainly Coulombic in nature) is the largest and this increases their stability. Of the two interchain photoexcitations, however, the excimer is the least mobile specie, since it is a quantum state based on the *interchain transfer integral* in addition to the Coulomb binding, and thus it is more sensitive to the interchain distance [104]. Therefore very slow PMD kinetics should characterize the excimer photoexcitations.

In this chapter we report the transient photomodulation (PM) spectra in the visible/near-infrared range from 1.25 to 2.55 eV, and PMD of various PA bands in the PM spectrum in films and solutions of two PPV derivatives, namely 2-methoxy-5-(2'-ethylhexyloxy) PPV [MEH-PPV], and 2,5-dioctyloxy PPV [DOO-PPV]. We found that DOO-PPV solutions and films and MEH-PPV solution mainly support *singlet excitons* as primary photoexcitations, since there is a *single* PA band in the PM spectrum that is well correlated with the SE band, and P(t) lifetime does not change across the PM spectrum. In contrast, MEH-PPV films support *two kinds of ultrafast photoexcitations*. These are (i) intrachain excitons with the same characteristic properties as excitons in DOO-PPV, and (ii) interchain species, that we identify as *excimers* with larger initial polarization memory, P(0) and *much slower PMD kinetics*. We also found that the relatively strong interchain coupling in MEH-PPV films influences the PL quantum efficiency and its decay, where most of the steady state PL comes from a long-lived component [105, 106].

4.2.1 Ultrafast measurement of DOO-PPV film

Figure 4.2(a) shows the transient PM spectrum of DOO-PPV film at t = 0 ps, along with the steady state cw PL and absorption spectra for comparison. The PL spectrum contains two bands with peaks at 2.1 eV (0-0) and 1.95 eV (0-1), respectively, where the lower energy band (0-1) is a phonon side-band of the main band (0-0). The transient PM spectrum shows a single PA band (PA_1) that peaks below 1.25 eV (at ~ 1.0 eV [84, 97]), and SE in the spectral range between 1.7-2.3 eV, which is in fact almost a mirror-image of the cw PL spectrum [1]. The transient PM spectrum also shows photobleaching (PB) in the absorption spectral range of the polymer that is generated in the ground state absorption due to the photoexcitations.

Figure 4.2(b) shows the PMD kinetics of DOO-PPV film at three probe frequencies that are related to various spectral features in the PM spectrum; these are 1.35 eV (PA_1), 1.6 eV (~ zero-crossing), and 2.0 eV (SE). The polarization memory initial value, P(0), and kinetics are roughly the same for all three probe frequencies, with short and long exponential components having lifetime τ_P ~7, and ~ 70 ps, respectively (Table 4.1). Moreover the PM decay kinetics shown in Figure 4.2(c), are also roughly the same at the three probe frequencies with a two-component decay lifetime τ_{PA} ~ 7 and ~ 90 ps (Table 4.1). This indicates that the PM spectrum results from a *single* excited species. Since the SE band decay is correlated with that of PA_1 band, we conclude that the primary photoexcitations in MEH-PPV films are *intrachain singlet excitons*. Also we obtained very similar results (except for τ) in DOO-PPV in solution (Table 4.1). From the PA decay dynamics and the known exciton radiative lifetime, τ_r ~ 1 ns in PPV derivatives [40], we calculate the PL QE efficiency, η (= τ_{SE}/τ_r) of DOO-PPV in film and solution to

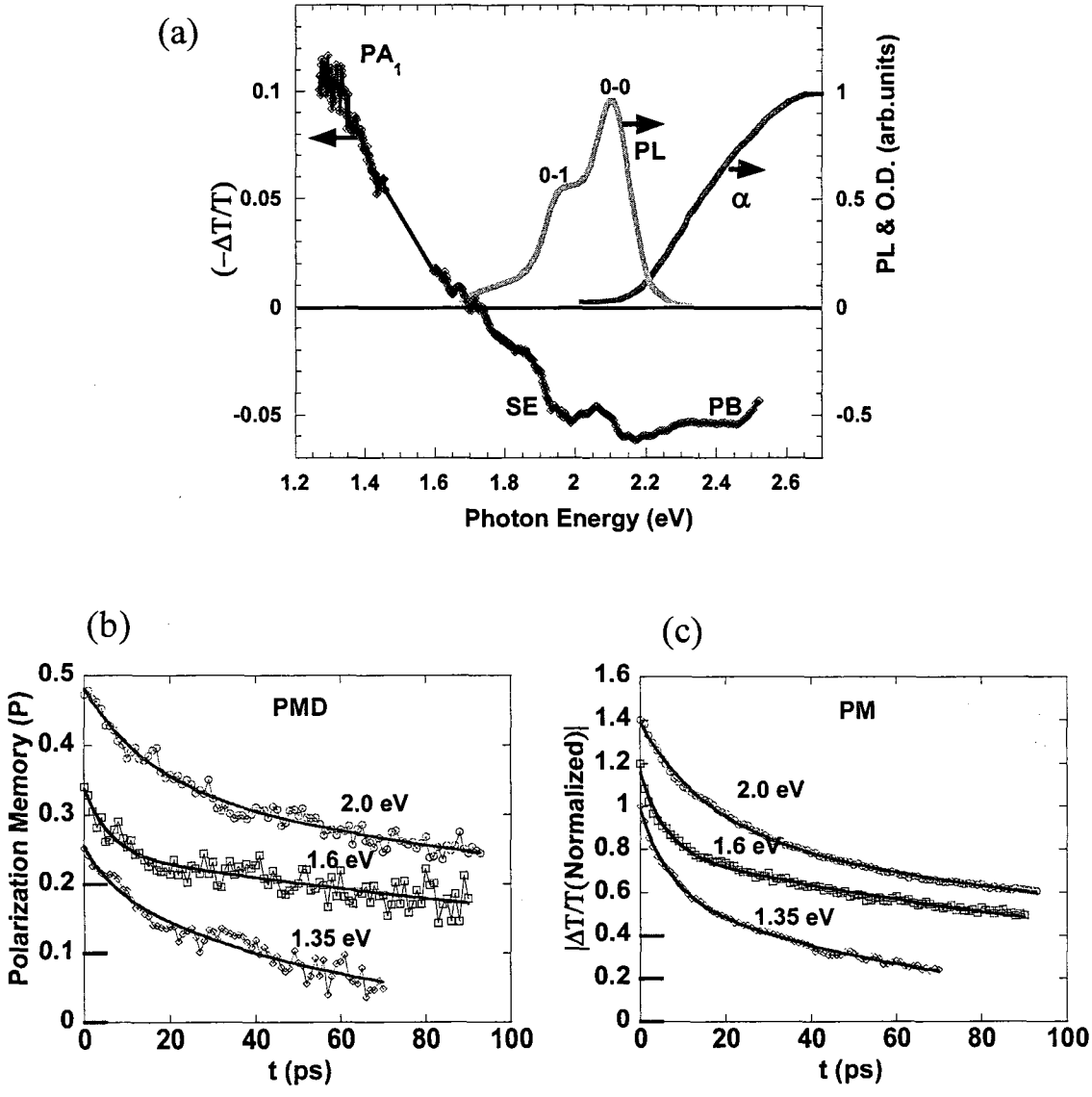

Figure 4.2: Transient PM measurement of DOO-PPV film. (a) Transient PM spectrum at t = 0 ps (right axis); various bands such as PA_1, SE and PB are assigned. The cw PL with 0-0 and 0-1 phonon replica, and absorption spectra are also shown (left axis). (b) PMD, and (c) PA kinetics at probe energies of 1.35 (PA_1) (diamonds), 1.6 (zero-crossing) (squares) and 2.0 eV (SE) (circles). The continuous lines are a guide to the eye, and for ease of comparison the various decays are shifted vertically along with their zero value. Adapted from Ref.[85]

Table 4.1: The photophysics parameters of DOO-PPV and MEH-PPV solutions and films. The measured and calculated steady state PL QE; and the PM and PMD lifetimes, τ at various probe frequencies in the transient PM spectra. P(0) is the PM value at t = 0. The short component lifetime is given as needed for a few samples and photon frequencies.

Sample	PL QE [meas.] (%)	PL QE [calcul.] (%)	Probe frequency (eV)	Initial PMD; P(0)	PM lifetime $\tau_{PA1};\tau_{PA2}$ (ps)	PMD lifetime $\tau_{P1};\tau_{P2}$ (ps)
DOO-PPV Solution	22	21	1.98	0.27	209	232
			1.66	0.25	221	373
			1.38	0.23	212	590
DOO-PPV Film	8	8	2.0	0.28	83	13; 67
			1.6	0.24	118	6; 130
			1.35	0.25	74	7; 56
MEH-PPV Solution	24	23	2.12	0.20	233	557
			1.66	0.24	213	344
			1.33	0.15	157	310
MEH-PPV Film	12	1	2.0	0.13	10	3
			1.66	0.16	3; 333	3; 540
			1.33	.09	15	2

be 22% and 8%, respectively (Table 4.1). The calculated QE is in fact verified by the actual PL QE obtained using an integrated sphere (Table 4.1). This shows that the same species are photogenerated in films and solutions, where the lower QE in the films is probably because of nonradiative channels such as impurities and defects into which the excitons may fall, which become operative due to the faster exciton diffusion among the polymer chains in the films.

4.2.2 Ultrafast measurement of MEH-PPV solution

Figure 4.3(a) shows the transient PM spectrum of MEH-PPV toluene *solution* at t = 0 ps, along with the cw PL and absorption spectra. The PL spectrum shows two peaks at 2.21 eV (0-0) and 2.09 eV (0-1), respectively. The transient PM spectrum is similar to that in DOO-PPV film and solution having a single PA band PA_1 that peaks below 1.24 eV and also SE that is similar, but slightly blue-shifted with respect to the cw PL spectrum. Figure 4.3(b) shows the PMD kinetics at three probe frequencies of 1.35, 1.66 and 2.12 eV; having the same P(0) value and lifetime, $\tau_P > 300$ ps (Table 4.1). τ_P value here is longer than that in DOO-PPV films, but close to that in DOO-PPV solution (Table 4.1). From the decay kinetics of the SE spectrum we obtained $\tau_{SE} \sim 230$ ps for the exciton lifetime, and calculate for the PL efficiency [40] $\eta \sim 23$ %, which is again in good agreement with the measured QE (Table 4.1). As in DOO-PPV film above, a similar conclusion can be drawn for the MEH-PPV solution, namely that intrachain *excitons* are the primary photoexcitations, with properties similar to the excitons in DOO-PPV.

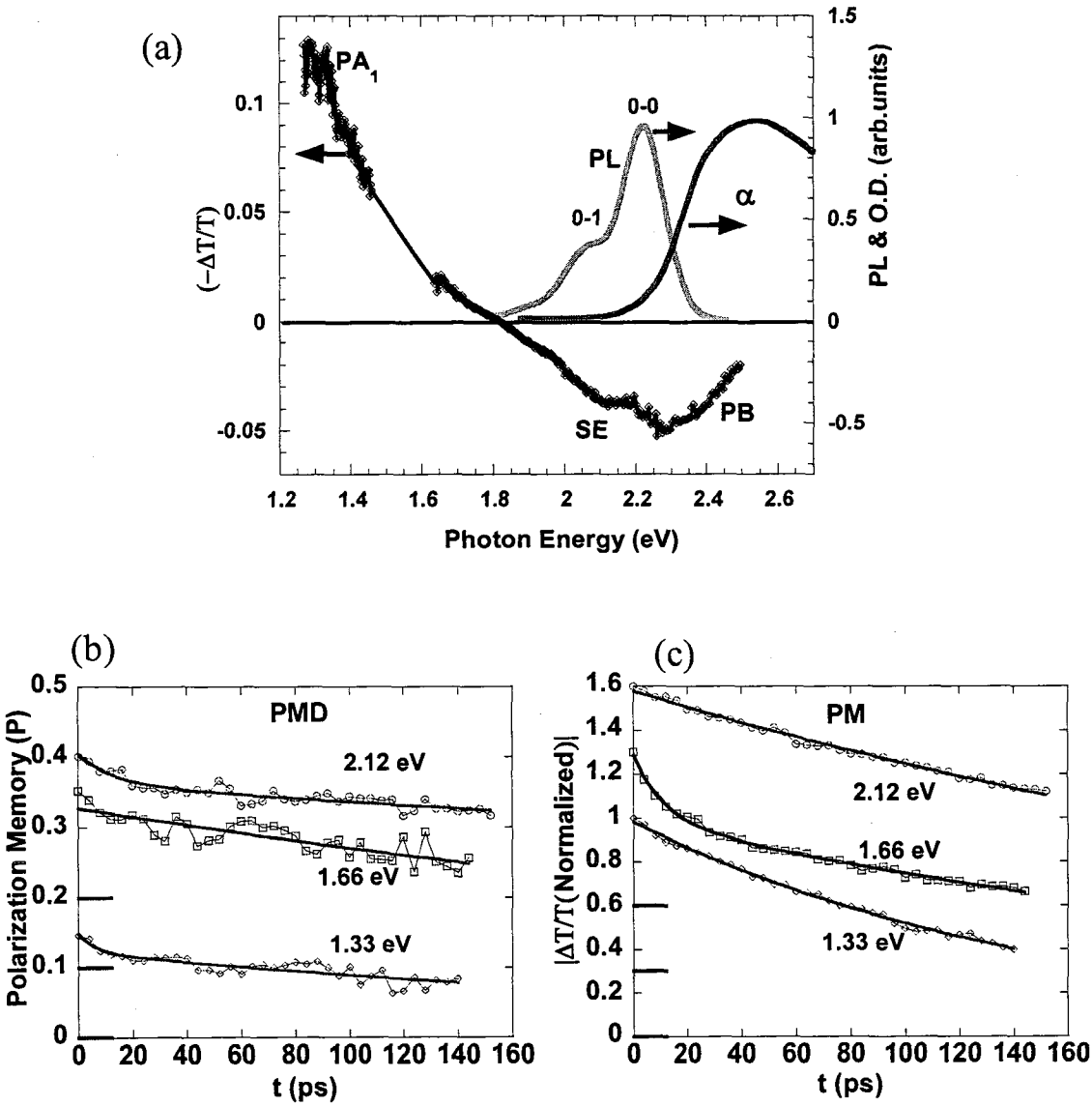

Figure 4.3: Same as in Figure 4.2, but for MEH-PPV solution.

4.2.3 Ultrafast measurement of MEH-PPV film

Figure 4.4(a) shows the transient PM spectrum of MEH-PPV *film* at t = 0, along with the steady state PL and absorption spectra. The cw PL spectrum here is *much broader* than the spectra in DOO-PPV and MEH-PPV solution, but still shows two emission bands at 2.13 eV and 2.0 eV, respectively. The enhanced PL width may be due to film inhomogeneity, but could be superposition of two types of PL emission, one from intrachain excitons similar to solution, whereas the other is red-shifted emission due to excimer formation, as originally suggested by Rothberg et al. [105, 107]. However the transient PM spectrum in this film shows very different characteristic properties compared to those in DOO-PPV film and MEH-PPV solution (Figures 4.2 and 4.3, respectively). **First**, the cw PL is substantially more red-shifted here relative to the two peaks in the t = 0 SE(0) spectrum (peaks at 2.25 and 2.05 eV, respectively). The larger cw PL red-shift with respect to SE(0) may originate from two different causes: (i) much faster exciton migration to lower energy sites exists in MEH-PPV films because the interchain coupling (that helps exciton diffusion among the polymer chains) here is stronger [97]. (ii) There is a lower state (excimer) that is formed for the most strongly coupled chains in the film, into which the original intrachain excitons fall [102]. This would substantially delay the PL emission from this sample; we indeed measured a rather long PL decay component in MEH-PPV films extending into the microsecond time domain [108]. We favor the latter scenario, because fast PMD kinetics is not always accompanied by a substantial PL red-shift with respect to SE(0), as is the case in DOO-PPV films discussed above. So the substantial mismatch between the cw PL and SE(0) obtained in MEH-PPV film is truly unique, and this requires a novel explanation.

Second, in addition to the PA_1 and SE bands, there is another PA band in the PM spectrum of MEH-PPV film, namely PA_{ex} at ~ 1.65 eV, which shows very different dynamics compared to that of PA_1 and SE. We directly compare the decay dynamics of PA_{ex}, SE and PA_1 by plotting the PM spectrum at t = 0 and 60 ps, respectively (Figure 4.4(a)). It is apparent that PA_{ex} kinetics is much slower than that of PA_1 and SE bands; this is shown more clearly in Figure 4.4(c), and summarized in Table 4.1. **Third**, the PMD kinetics is not the same across the PM spectrum in MEH-PPV film. Figure 4.4(b) shows the PMD kinetics at three probe photon energies that correspond to the various spectral features in the PM spectrum, namely 1.33 eV (PA_1), 1.66 eV (PA_{ex}), and 2.0 eV (SE). Whereas P(t) decays very fast within the PA_1 and SE bands, with τ_P ~ 3 ps (Table 4.1), it is *much slower* for the PA_{ex} band, where it hardly decays up to t = 80 ps.

Similar to the other polymer samples discussed above, we identify PA_1 and its correlated SE in MEH-PPV films as due to intrachain singlet excitons. Then from P(t) dynamics for PA_1 and SE, we conclude that excitons diffusion in MEH-PPV film is *very fast* (τ_P ~ 3 ps) relative to DOO-PPV film (τ_P ~ 60 ps), consistent with the increased interchain coupling in the former sample. In contrast, P(t) at 1.66 eV (Figure 4.4(b)) first shows a fast decay within 10 ps, which is probably due to P(t) decay of the excitons component at this probe frequency, which rides on a very slow component (τ_P > 100 ps). Also PA_{ex} decay is not correlated with that of SE, and thus does not have as strong a dipole coupling to the ground state. Taken together, these findings indicate that PA_{ex} *is not* related to the intrachain excitons; instead it belongs to a different photoexcitation species, which is not as mobile or as strongly coupled to the ground state. Yan et al. reported such a band with a peak at ~ 1.5 eV in another PPV derivative, and identified it

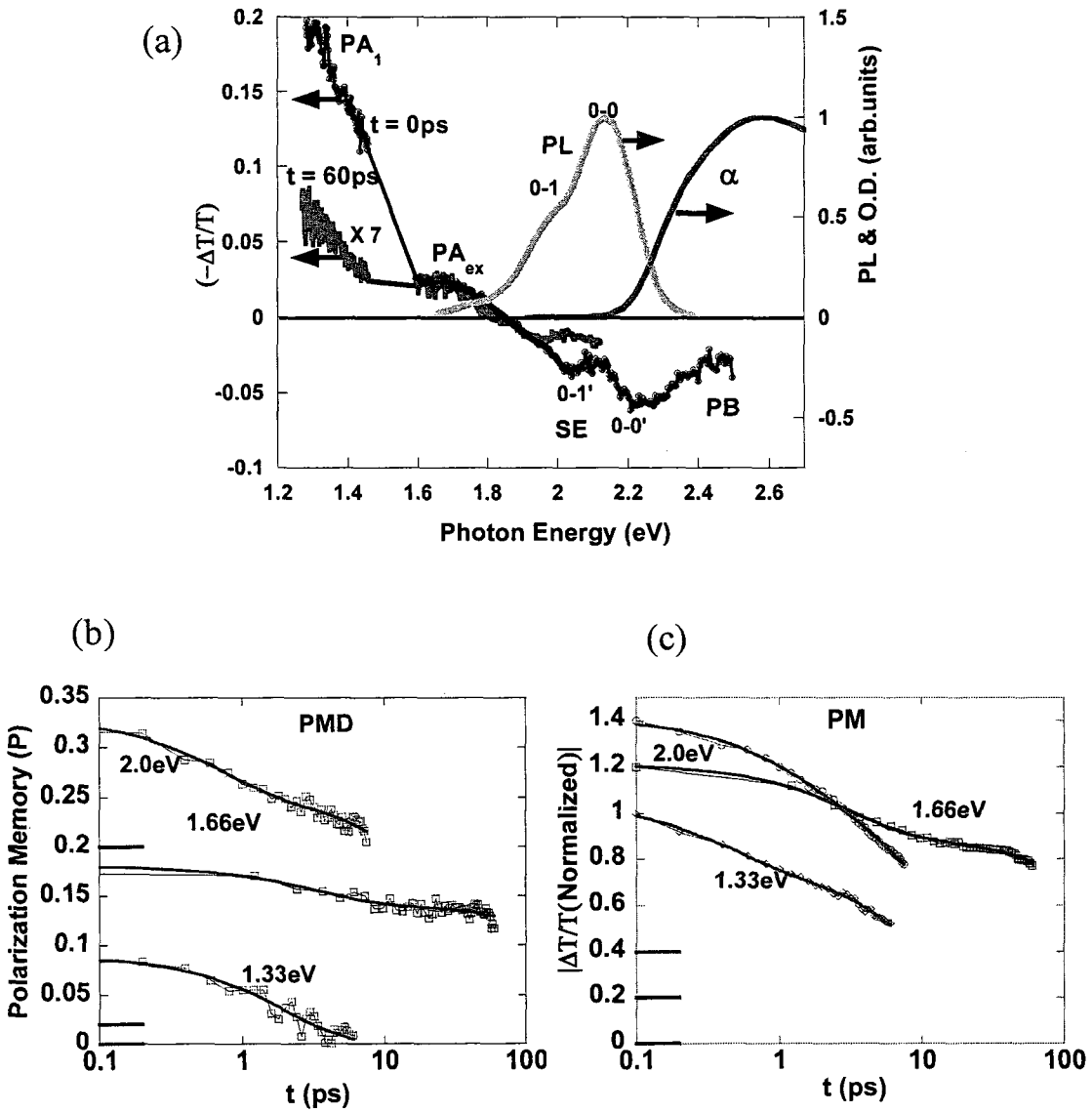

Figure 4.4: Same as in Figure 4.2 and 4.3, but for MEH-PPV film at t = 0 and 60 ps, respectively. In (a) the new PA_{ex} is assigned; and in (b) [(c)]the PMD [PA] kinetics is plotted in logarithmical time scale.

to be due to interchain polaron pairs [100]. This original interpretation, however, should be modified in favor of excimer, since it disagrees with the red-shifted cw PL band compared with SE(0) band, as discussed above and also explains the obtained slow PMD kinetics of these excitations.

Another indication that species other than intrachain excitons dominantly contribute to the cw PL in the MEH-PPV film is the PL QE. Assuming the same radiative lifetime as that of intrachain excitons (namely, $\tau_r \sim 1$ ns [93]), we calculate from PA_1 and SE lifetimes (~ 10 ps, Table 4.1) PL QE (= τ_{SE}/τ_r) of ~ 1% in MEH-PPV films. In contrast, we measured PL QE of ~ 12% for this film, and this relatively large QE cannot originate from intrachain excitons, which decay very fast. We thus conclude that the same long-lived species that is associated with PA_{ex} may also radiatively recombine at a later time, and thus also contribute to the PL, as indeed measured in our laboratory [108]. This interchain species has a *much longer radiative lifetime* compared with that of the intrachain exciton, which might be tracked back to its weaker dipole moment. We therefore identify this interchain species as *excimer* (or interchain charge transfer excitons), which is a quantum superposition state of the ionic polaron pair and covalent interchain exciton, and is also relatively immobile on the chains. The fact that these interchain species appear in ~ 150 fs, which is our time resolution, does not necessarily show that they are the 'primary photoexcitations' of the 'coupled chains', since they may be created by hot intrachain excitons that dissociate onto different chains during the excess energy relaxation process. However the recent theoretical work on 'coupled chains' shows [102] that the excimers are indeed the 'primary photoexcitations' of such a coupled chain system, and thus we doubt that measurements at time shorter than our time

resolution (say with 10 fs resolution [109] would reveal a build-up of the interchain species.

4.2.4 Conclusions

In summary, we investigated the photoexcited species that contribute to the ultrafast transient PM spectrum in the visible/near infrared range in both DOO-PPV and MEH-PPV film and solution using transient PM, and a new spectroscopic technique, namely the PMD kinetics spectroscopy. We show that the primary photoexcitations in MEH-PPV solution and DOO-PPV film and solution are exclusively singlet excitons with large SE band. However the ultrafast PM spectrum in MEH-PPV *film* contains another PA band at ~ 1.65 eV, which shows a much slower PA and PMD kinetics compared to those of the intrachain excitons. We identify the underlying species as *excimers*, (or *interchain charge transfer excitons*), which also explains the obtained cw PL red-shifted spectrum compared to SE(0) spectrum, and the relatively high PL QE in spite of the fast PA decay kinetics of the PA band associated with intrachain excitons in these films. Our results also show that PMD spectroscopy is a powerful tool for discerning various photoexcitations in the PM spectrum of π-conjugated polymers.

4.3 High pressure study of MEH-PPV films

The present section of this chapter deals with high hydrostatic pressure dependence (up to 100 kbar) of the photoluminescence (PL) and ultrafast photophysics of MEH-PPV film. Both of these studies show that there are two kinds of polymer chains in

the MEH-PPV film; one contains isolated polymer chains, and the other is composed of packed chains that are aggregated together. This conclusion is in agreement with the results from the previous section.

4.3.1 Introduction

The role of interchain interaction has always been a debatable issue in the photophysics of π-conjugated polymers over the last two decades [1]. In the previous section "*Polarization Memory Decay Spectroscopy of Photoexcitations in π-Conjugated Polymers*" [110] we found that the MEH-PPV polymer chains in the film form show more interchain interaction compared to DOO-PPV polymer, and hence interchain charge transfer exciton (or excimer) coexist with intrachain exciton as primary photoexcitations in MEH-PPV film. In another work, Sheng et al. showed that in films of substituted poly(phenylene-vinylene) [PPV] derivatives [84], a relatively weak transient photoinduced absorption (PA) band in the mid-IR spectral range (~0.4 eV) is instantaneously generated along with the PA band of the singlet excitons (PA_1 at ~0.9 eV). The 0.4 eV PA band was originally assigned to photogenerated polaron-pairs on neighboring chains based on the peak position, and correlation with weak photoinduced infrared active vibrational (IRAV) modes that appeared, however, only at low temperatures [111]. It was subsequently shown [84] that the polaron PG efficiency depends on the solvent used, which influences the film nanomorphology [112, 113], as well as on the PPV derivative side group. Thus it was concluded that carrier PG mechanism in PPV polymers depends on the chain packing in the solid state [84].

In the context of interchain interaction, there has been an elegant study on MEH-PPV solution in the research group of Prof. Lewis Rothberg, where MEH-PPV solution is made in different ratios of 'good' and 'bad' solvents to control the aggregation of chains in the solution [94, 105, 107, 113]. It has been found that there are two kinds of polymer phases, one phase that only contains isolated chains, and the other that contains packed (or aggregated) chains, depending on the contribution of bad/good solvent ratio in the solution from which the polymer films are cast. This study also indicates that upon increasing the ratio of bad/good solvent, the photophysics of MEH-PPV solution shows similarity with that of the solid film. Hence, it is clear that there would be two kinds of photoexcitation species in MEH-PPV film: one that belongs to the isolated chains, and the other that characterizes the packed chains. This model is dubbed here the 'two species model' for MEH-PPV [107].

In spite of these efforts, a more direct demonstration of intermolecular (interchain) interaction is still missing. Also, a clear description of the role of interchain interaction on the polymer photophysics in the solid state, such as aggregates formation, charge transport and exciton migration, all of which are critical for device applications, is still lacking.

In the majority of previous studies, variation of the intermolecular interaction in the material has often relied upon chemical modifications, or modified film processing conditions [112]. Applying hydrostatic pressure is a clean, simple method to probe intermolecular interactions of a material for a range of intermolecular distances *without such alterations*. Previous high pressure optical studies of π-conjugated polymers used optical absorption and reflection, photoluminescence (PL), Raman scattering, and

transient and continuous wave (cw) photomodulation [114-122]. Since pressure enhances intermolecular interactions, and simultaneously changes intramolecular conformation (which planarizes the chains [119-121]), it has been difficult to separate these two effects [117]. This is especially true since cw spectroscopies mainly probe the *lowest lying available states* in the polymer chains, thus missing the direct pressure effect on the *primary photoexcitations*, which might be more sensitive to high pressure.

4.3.2 Effect of pressure on the photoluminescence (PL) of MEH-PPV film

The PL emission of MEH-PPV film at ambient pressure has already been discussed in the previous section 4.2.3. Here, we focus on the effect of pressure on the PL of the MEH-PPV film. These measurements were done by Dr. Valentina Morandi in our group. Figure 4.5 shows the PL of MEH-PPV film at room-temperature under different applied pressures. There are two important changes observed in the PL spectra: (a) reduction in PL intensity, and (b) red-shift of PL peak position up to a certain pressure. The inset of Figure 4.5 shows the red-shift of PL peak position under high pressure. It can be seen that PL peak position red-shifts till 30 kbar, and then does not shift any more.

The pressure dependence on PL can be explained by the two-species model in MEH-PPV [107]. Upon application of high pressure, more isolated chains in the film are packed together, and their PL peak position is thus red-shifted due to excimer formation in the packed phase. This red-shift may be the result of longer conjugation length of the polymer backbone in the packed chains due to steric hindrance; or shows the formation of

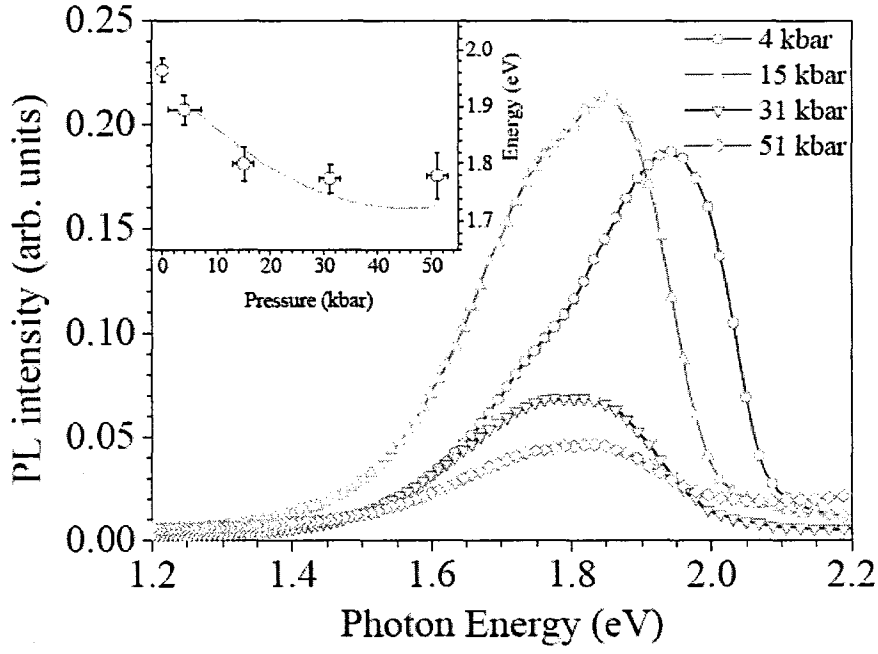

Figure 4.5: Photoluminescence (PL) spectra of MEH-PPV film at different pressures at 300K. Inset shows the pressure dependence of PL peak positions along with quadratic (E_{PL} = -10P + 0.11 P^2) and linear (E_{PL} = -2.76P) fits, where E_{PL} is in meV and P is in kbar. (Adapted from Ref. [123])

excimers that dominates the packed phase. After a certain pressure (~30 kbar) an optimum arrangement of polymer chains is reached, where further packing of isolated chains is not possible, and the shift in the PL peak position saturates with increase in pressure. The lower PL yield at higher pressure is the consequence of more weakly coupled emissive interchain species generated in the packed chains, in agreement with excimer formation.

4.3.3 Ultrafast transient photomodulation measurements

The ultrafast photomodulation (PM) spectroscopy at high pressure opens up the possibility of exploring the effect of interchain interaction on the primary photoexcitations of the polymer film, which is not possible by other steady state measurements like Raman scattering, absorption and cw photoluminescence measurements. Figure 4.6 shows the PM spectra of MEH-PPV film at t = 0 ps in the probe range of 0.25-2.1 eV at two different pressures of 0 kbar (ambient pressure) and 77 kbar. The 0 kbar spectrum shows four different bands: PA' at 0.35 eV, PA'' at 0.9 eV, PA_1 at 0.95 eV and SE at ~2.0 eV. The origin of bands PA', PA_1 and SE have already been reported [84, 85]. It was assumed that PA' originates from photogenerated polaron-pairs on neighboring chains, whereas PA1 and SE bands are due to intrachain exciton. The band PA'' was first predicted by Prof. Mazumdar [102, 124, 125], and is due to excimers that are formed because the rise of interchain interaction in the film. The same model predicted that there is a lower energy PA band from excimers; thus the original interpretation of PA' as due to polaron pairs needs be carefully scrutinized.

The second PM spectrum at 77 kbar looks very different from that at ambient pressure. The SE band at ~2.0 eV disappears, and a new band PA''' at ~1.85 eV appears in the PM spectrum at near-IR. In addition, PA' and PA'' are blue shifted to 0.65 and 1.3 eV, respectively. These transient absorption results can also be explained by the two species model for MEH-PPV [105, 107] similar to the photoluminescence measurements. The bands PA' and PA'' originate in the packed polymer chains, and they blue-shift upon the application of high pressure. The blue-shift of bands PA' and PA'' has been shown theoretically [102] to occur *only for excimers*, where the increase of interchain transfer

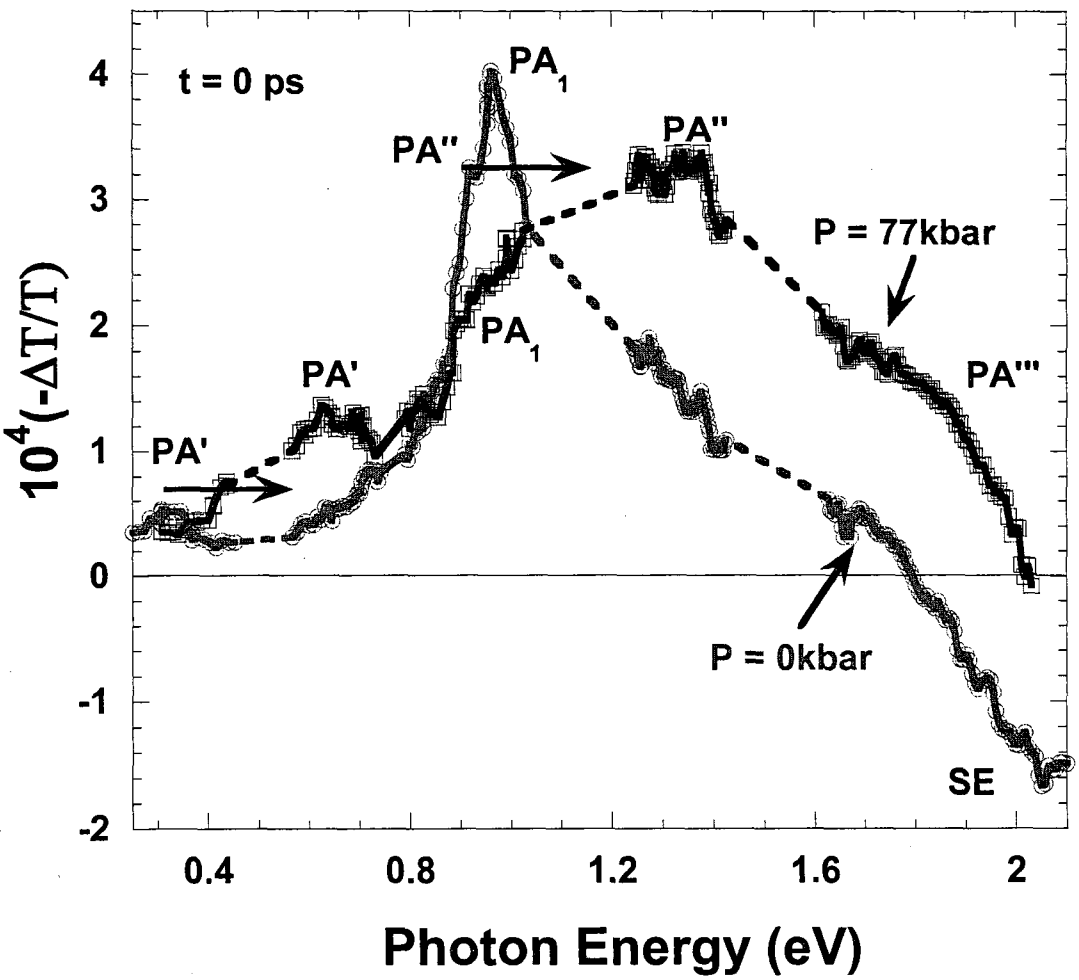

Figure 4.6: Transient photomodulation spectra of MEH-PPV film at two different pressures of 0 and 77 kbar at t = 0 ps. Various bands such as PA', PA'', PA_1, PA''' and SE are assigned. The blue-shifts of PA' and PA'' are shown by arrows.

integral, $t_{\perp}$, (equivalent to applying higher pressure in our measurement) results in substantial blue-shift of bands PA' and PA''. In contrast the band PA_1 remains at the same spectral position because it originates from isolated chains in the film. If the original explanation of PA' would be correct, then the theoretical work shows [13] that it would not blue shift upon the application of high pressure. We therefore conclude that the original explanation is incorrect; PA' is not due to polaron-pairs but it originates from photogenerated excimers in the packed –phase of the MEH-PPV film.

The near-IR/Vis part of the PM spectra have been plotted separately to emphasize bands lying in this range. Figure 4.7 shows three PM spectra of MEH-PPV film at t = 5 ps, at different pressures of 0, 67 and 103 kbar. The disappearance of SE band at higher pressure, namely 67 and 103 kbar, is either due to the red-shift of the absorption in MEH-PPV film at high pressure, or the appearance of band PA''' at 1.85 eV. The origin of band PA''' (clearly resolved in the 103 kbar PM spectrum) might be the result of blue-shift of band PA_{ex} at 1.65 eV (seen in the previous section at ambient pressure). PA''' has also been seen in CW PM spectrum of MEH-PPV film at the higher pressure. The CW PM spectrum was done by Ms. Ella Olejnik in our group. The inset of Figure 4.7 shows CW PM spectrum of MEH-PPV film at pressure of 77 kbar, where the band PA''' is clearly discerned, and this indicates its longer life time in agreement with excimer species.

The transient decay at different probe energies may give extra information about the temporal decay of the different species in the MEH-PPV. Figure 4.8 shows the effect of higher pressure on the transient decays at three different probe energies of 2.0, 1.29 and 1.63 eV. The decays at 1.29 and 1.63 eV have been fitted with tri-exponential

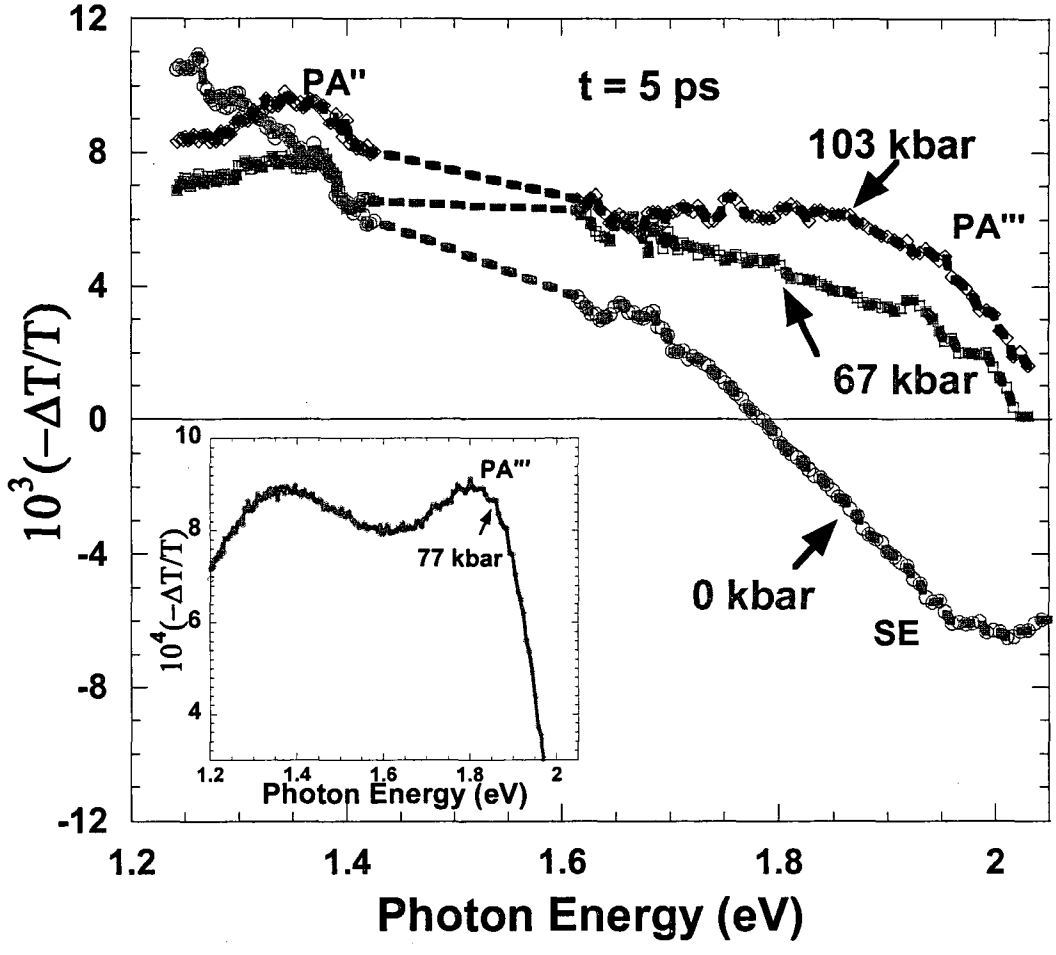

Figure 4.7: Transient photomodulation (PM) spectra of MEH-PPV film at three different pressures of 0 67 and 103 kbar at t = 5 ps. Various bands such as PA'', PA''' and SE are assigned. Inset shows the CW PM spectra of MEH-PPV film at the pressure of 77 kbar.

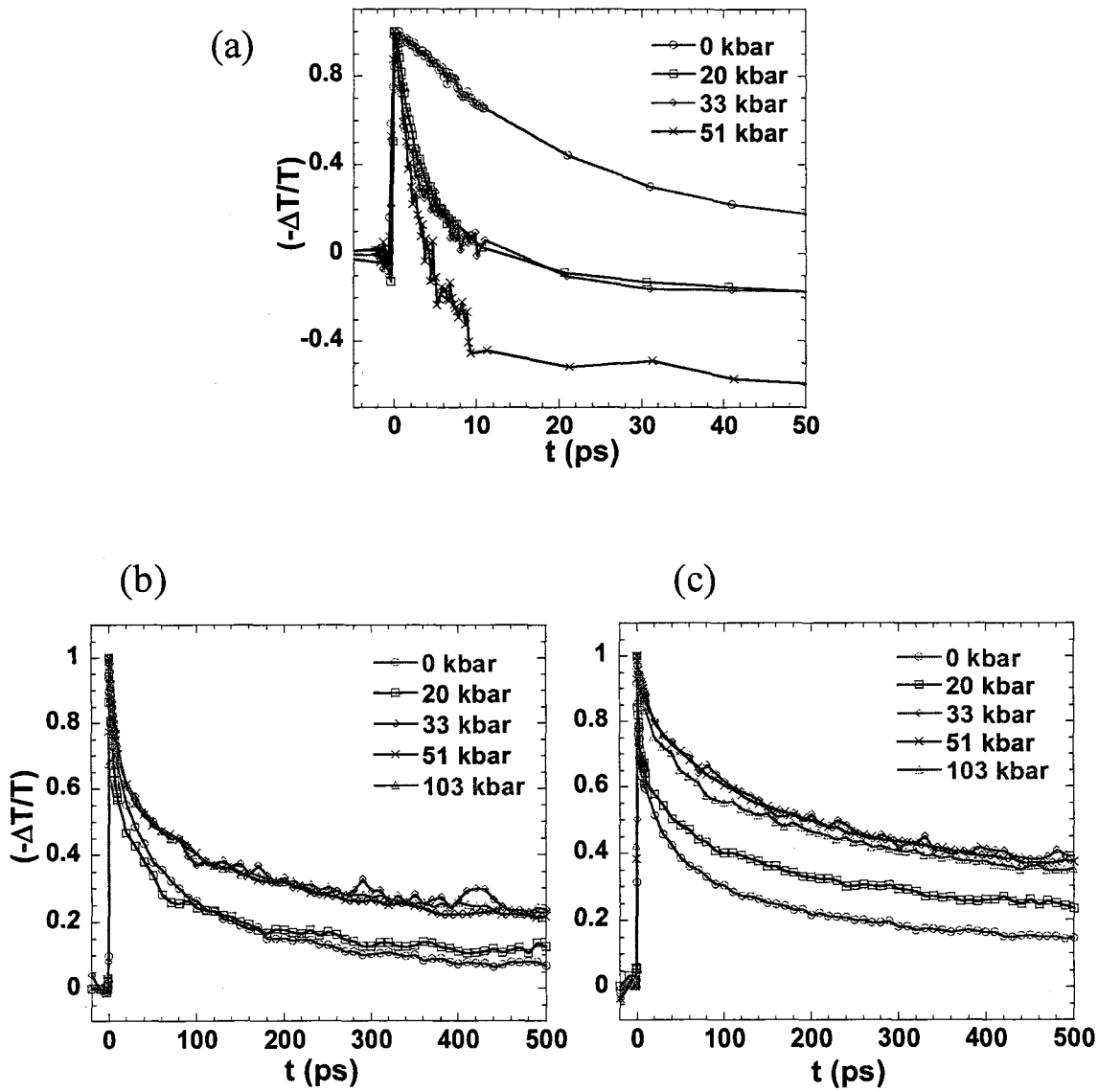

Figure 4.8: Photomodulation decay kinetics of MEH-PPV film at different indicated pressures and at different probe energies of (a) 2.0 eV, (b) 1.29 eV and (c) 1.63 eV.

dynamics and their fitting decay constants with relative contributions are summarized in Table 4.2. Figure 4.8(a) shows the SE band at ~2.0 eV, which disappears faster at higher pressure. As mentioned before, this disappearance might be the result of appearance of band PA''' at 1.85 eV. Figure 4.8(b) and (c) show the decay at 1.29 and 1.63 eV, respectively. Both decays are delayed at higher pressure due to the formation of more interchain species. Here, the interesting point to be noted is that, once a higher pressure (33 kbar in this case) is achieved, there is no further change in the transient decays at both probe energies with extra higher pressure (up to 100 kbar); similar to the PL red-shift that stops at about this pressure value. Hence, the pressure dependence of transient decays also supports the two species model in MEH-PPV film.

We have also studied the polarization of bands PA' and PA_1 of MEH-PPV film at ambient pressure in the mid-ir/near-ir spectral range. These measurements were done by Dr. ChuanXiang Sheng in our group. Figure 4.9((a) & (b)) show the polarized PM decay of MEH-PPV film at PA_1 (0.95 eV) and PA' (0.33 eV) bands, respectively. The faster depolarization of band PA_1 compared to PA' is consistent with our interpretation that PA' originates from excimer in the packed-chains, and therefore they are less mobile compared to intrachain exciton (PA_1).

4.3.4 Conclusions

We believe that the high pressure studies of MEH-PPV film can be explained using the *two species model* for MEH-PPV films. Firstly, with the increase in pressure (up to 30 kbar) some of the isolated chains become closely packed, and with further increase in pressure there is no change in the morphology. This behavior is confirmed by

Table 4.2: Photomodulation decay fitting parameters with their relative contributions of MEH-PPV film at different pressures and at the probe energies of 1.29 and 1.63 eV.

Pressure (kbar)	Transient decay at 1.29 eV (ps)	Transient decay at 1.63 eV (ps)
0	6 (33%)	2.7 (32%)
	60 (47%)	43 (37%)
	455 (21%)	615 (31%)
20	5 (40%)	1.2 (29%)
	50 (35%)	46 (30%)
	833 (25%)	835 (41%)
33	6 (31%)	2.6 (8%)
	65 (34%)	100 (41%)
	1250 (35%)	1920 (51%)
51	6 (34%)	9.2 (13%)
	81 (34%)	100 (34%)
	1060 (33%)	1350 (53%)
103	4 (28%)	7.8 (29%)
	57 (34%)	72 (18%)
	1000 (38%)	1110 (53%)

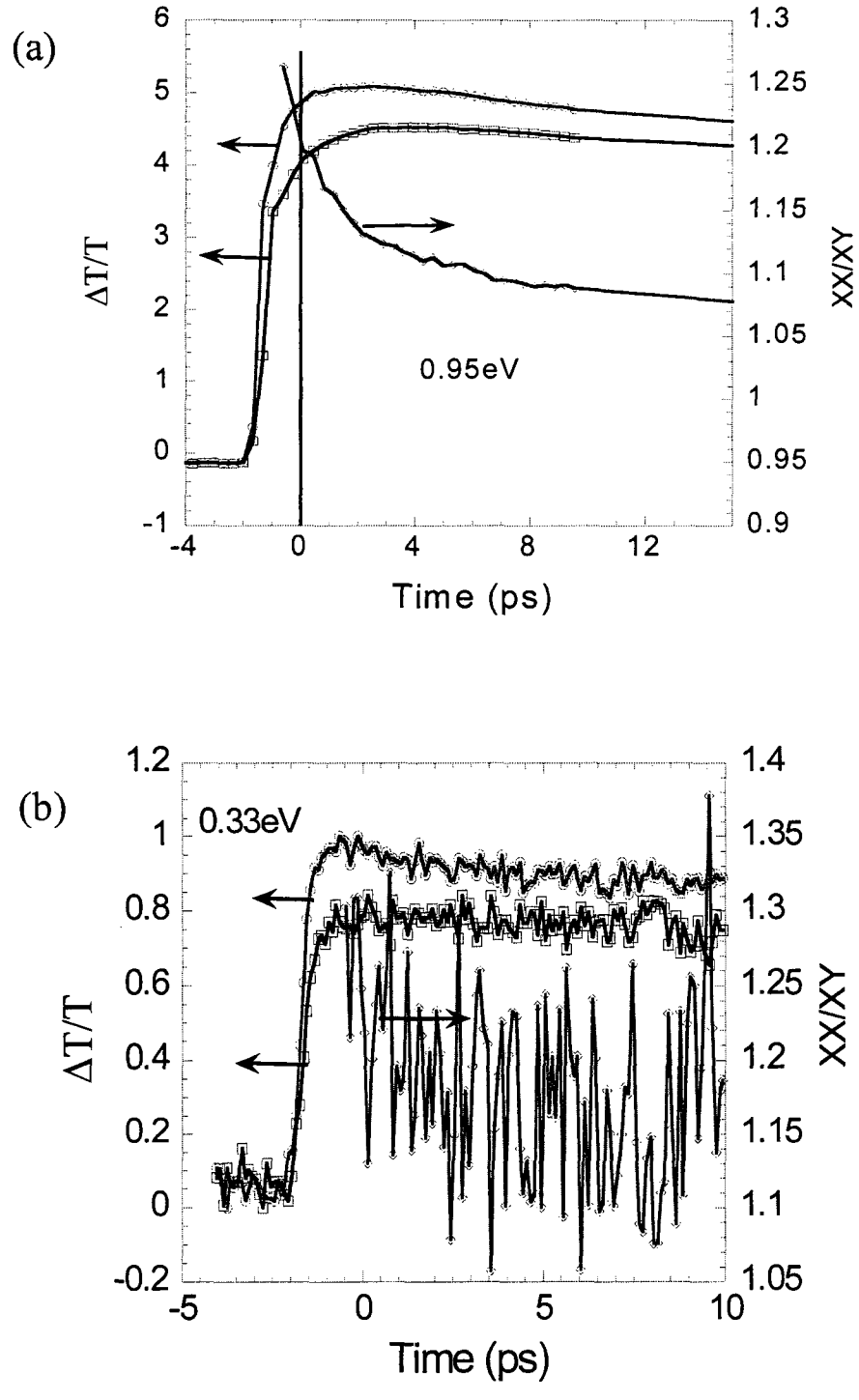

Figure 4.9: Polarized PM decay kinetics and their ratio (parallel/perpendicular) of MEH-PPV film at ambient pressure at the PM spectrum bands (a) PA1 (0.95 eV) and (b) PA' (0.33 eV)

the dependence of PL peak position and PM transient decay at high pressure (up to 30 kbar). Secondly, with further increase of pressure (>30 kbar) the packed chains get closer and the interchain transfer integral increases so that the blue-shift of bands PA', PA'' and PA''' indicates that these bands originate due to excimers in packed chains regions. In contrast, band PA_1 comes from isolated chains in the film, which does not shift at high pressure. Our results are in agreement with a model where intrachain excitons are the primary excitations in isolated MEH-PPV chains, but in contrast excimers, or interchain charge transfer excitons, dominate the photophysics in the packed chain phase of the MEH-PPV films. We therefore conclude that the evidence of excimer photoexcitations is strong in MEH-PPV; this paves the way to look at ordered chain phases in other polymers, such as RR-P3HT and PFO where ordered phases were identified.

CHAPTER 5

PHOTOEXCITED STUDIES OF PLATINUM CONTAINING π-CONJUGATED POLYMERS

π-conjugated polymers containing platinum (Pt) atoms in their backbone are novel polymer materials suitable for studying enhanced intersystem crossing rate of singlet to triplet excitons. The presence of Pt in the π-conjugated backbone will affect the excited states properties of these polymers. The present chapter mainly discusses the characterization of these excited states energy levels of two different Pt-containing polymers using electroabsorption (EA) and two-photon absorption (TPA) spectroscopies.

5.1 Introduction

5.1.1 Polymer materials

The Pt-containing polymers used in our measurements have been synthesized in-house at the Physics Department, University of Utah by Mr. Leonard Wojcik. The backbone structures of these polymers are shown in Figure 5.1(c), where a conjugated spacer unit is coupled to two Pt atoms. Two different types of Pt polymers with different spacer units were investigated, one that has only one spacer unit, dubbed Pt-1, and

another with three spacer units dubbed Pt-3. The main goal of synthesizing different polymers is to control the spin orbit interaction by modifying the spacer between Pt atoms. Figure 5.1(a) shows the backbone structure of the first spacer unit with single phenyl ring that separates the Pt atoms. Figure 5.1(b) shows the second spacer unit that consists of three phenyl rings. Hereafter, these polymers will be designated as Pt-1 and Pt-3 polymers based on the number of phenyl rings in their spacer unit.

5.1.2 Quantum chemistry calculation of the excited states in Pt-polymers

Quantum chemistry calculations have been done by Dr. Sergei Tretiak on Pt embedded polymers that differ in their spacer unit, similar to Pt-1 and Pt-3 polymers. It has been found that compared to Pt-2 (two phenyl rings spacer) and Pt-3, Pt-1 still has π–electron triplet states the lowest state in the triplet manifold. However, π–electron singlet state in Pt-1 is no longer the lowest S_1 singlet state. Rather, the lowest state in Pt-1 is Metal-to-Ligand Charge Transfer (MLCT) state, whereas in Pt-2 and Pt-3 polymers these states are well above the lowest π-electron singlet state. Figure 5.2 shows the schematic energy levels of the singlet and triplet manifolds in Pt-1 polymer showing that the MLCT state lie below the π-electron singlet state. The MLCT states are present in all Platinum compounds and correspond to electron transfer from carbon chain to platinum. They are somewhat mixed with π-electron states. Also the MLCT are localized states and thus their energy does not change much with oligomer length or type, and is calculated to be at about 3.5-3.6 eV.

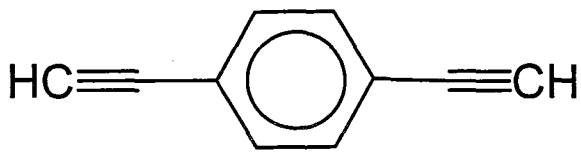

(a) Pt-1 spacer (1,4-diethynylbenzene)

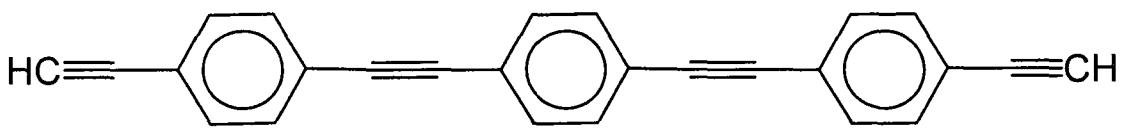

(b) Pt-3 spacer (1,1'-(1,4-phenylenediethyne-2,1-diyl)bis(4-ethynylbenzene))

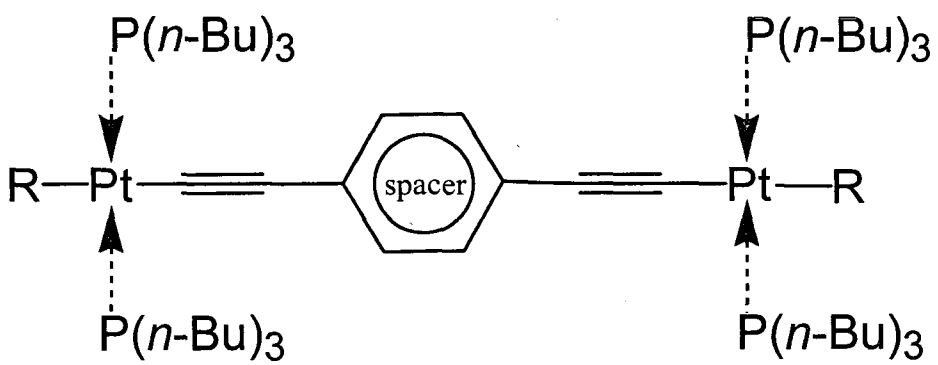

(c) Platinum polymer (generalized form)

Figure 5.1: Chemical structures of (a) Pt-1 spacer, (b) Pt-3 spacer, and (c) the generalized form of Pt-polymers.

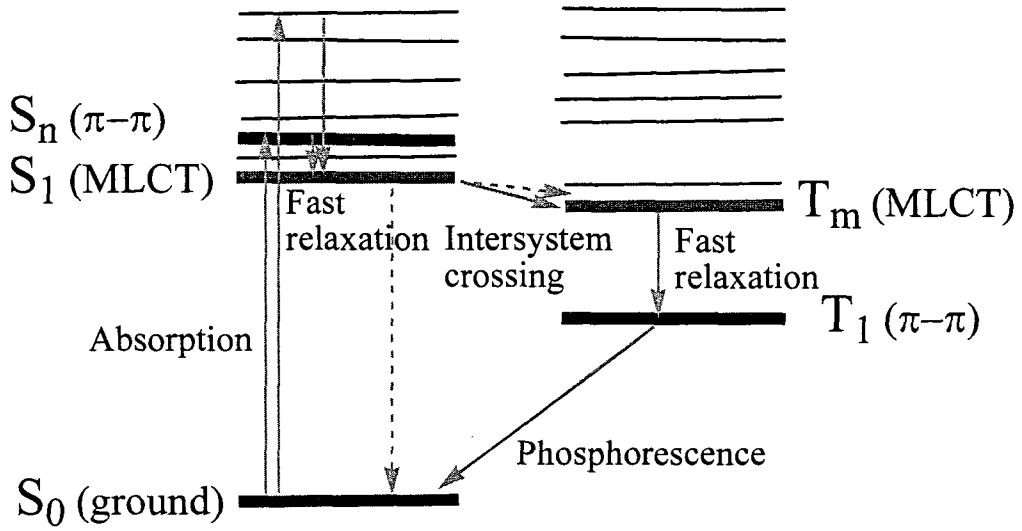

Figure 5.2: Schematic energy levels of the singlet and triplet manifolds in Pt-1 showing that the singlet MLCT lie below the π–electron state. Calculations were done by Dr. Tretiak at Los Alamos National Lab (2007).

5.2 Electroabsorption of Pt-3 polymer

Electroabsorption (EA) measurement is a unique method to probe both even and odd parity excited states in π-conjugated polymers, and thus it has been frequently used [51, 54, 71, 74, 75]. The EA spectroscopy is done at an electric field of ~$7x10^4$ V/cm and 80 K. Figure 5.3(a) shows the EA spectrum of Pt-3 polymer compared to the linear absorption spectrum. The linear absorption peaks at 3.1 eV with its onset at ~2.95 eV showing a singlet π-π^* exciton at ~ 3.05 eV. The EA spectrum contains many features: a first-derivative-like feature with zero-crossing at ~3.05 eV (assigned as $1B_u$), a modulation feature with zero-crossing at ~4.4 eV (assigned as nB_u), three well-resolved phonon side bands related to $1B_u$ at 3.1, 3.25 and 3.4 eV, and two induced absorption bands at 3.8 eV (assigned as mA_g) and 4.25 eV (assigned as $m'A_g$). The EA spectrum can

be interpreted as follows. The first-derivative-like feature at ~3.05 eV is due to stark-shift of the lowest-lying exciton, namely, the $1B_u$. The modulation feature centered at ~4.4 eV is due to the electric-field induced shift of the most strongly coupled exciton to the mA_g, namely, the nB_u. The derivative-like feature at energies just above $E(1B_u)$ is due to the stark shift of the $1B_u$-related phonon side-bands. These features are more easily observed in EA than in the linear absorption spectrum because of the strong dependence of the exciton polarizability on the conjugation length in the polymer chains, with preference to focus in EA on long oligomers. The EA-induced absorption feature at 3.8 eV does not have any corresponding spectral feature in the linear absorption spectrum. We therefore conclude that this feature in the EA spectrum involves a strongly coupled A_g state, namely mA_g. Such a state would not show up in the linear absorption spectrum, since the optical transition $1A_g \rightarrow mA_g$ is strictly forbidden. The presence of electric-field in the EA measurement breaks this symmetry resulting in the transfer of oscillator strength from the allowed $1A_g \rightarrow 1B_u$ transition to the forbidden $1A_g \rightarrow mA_g$ transition. The same applies for the EA feature at ~4.25 eV assigned as $m'A_g$. In general, the even parity state above mA_g is assigned as kA_g, which lies above the odd parity state nB_u in the π-conjugated polymers. However, in the present EA spectrum of Pt-3 polymer, the presence of an even parity state, namely $m'A_g$ below the nB_u indicates that $m'A_g$ belongs to a different exciton manifold, which might be MLCT states in case of Pt-polymer.

Figure 5.3(b) shows the polarized EA spectra of Pt-3 polymer film with light polarization parallel and perpendicular to the applied electric field direction, which is set by the direction of the electrodes on below the polymer film. The parallel and perpendicular spectra do not show an anisotropy of 2:1 [51], demonstrated in EA spectra

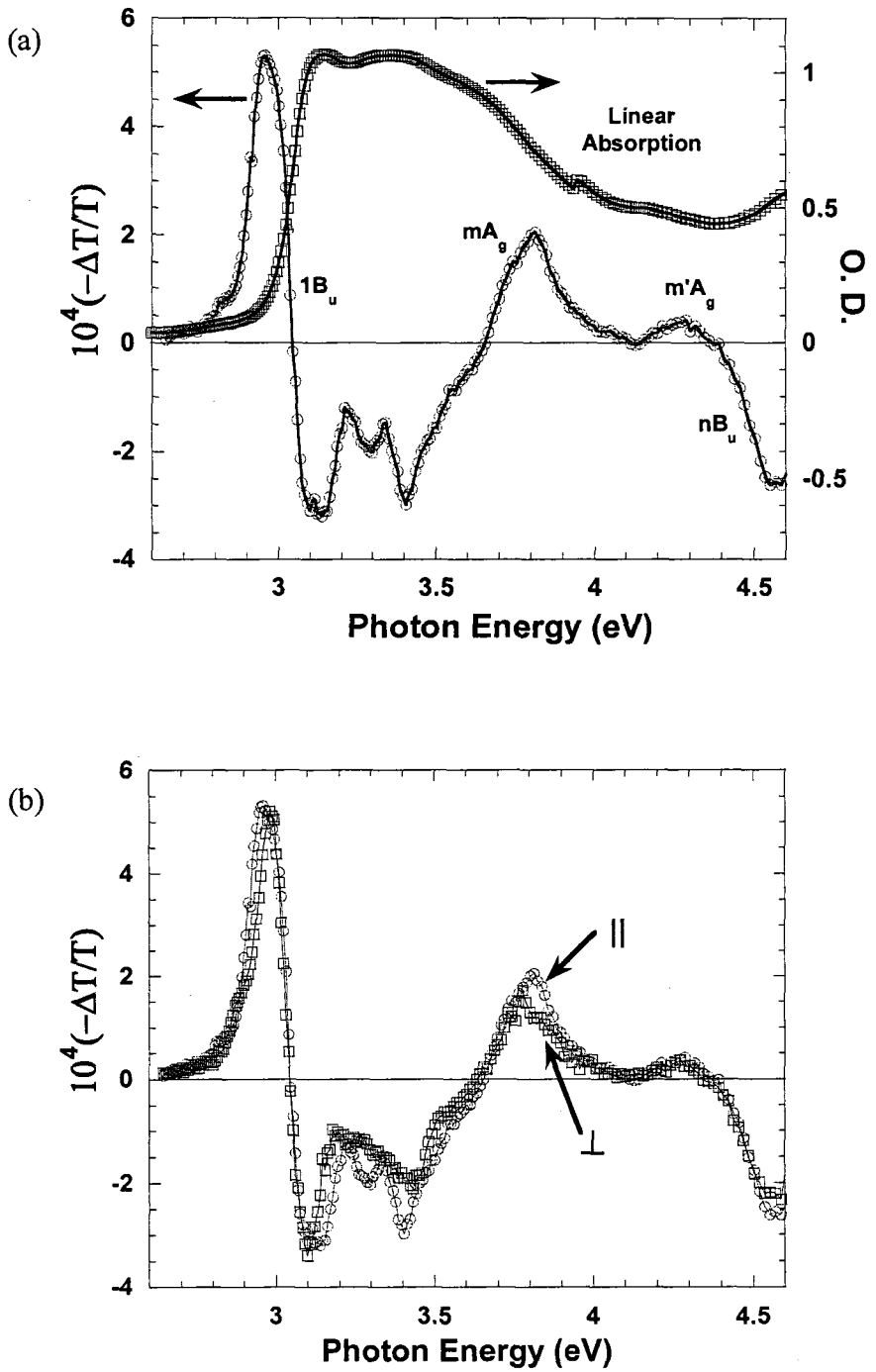

Figure 5.3: Electroabsorption (EA) measurement of Pt-3 film. (a) EA spectrum with linear absorption. The essential states $1B_u$, mA_g, $m'A_g$ and nB_u are assigned. (b) Polarized EA spectrum of Pt-3 film with light polarization parallel (empty circle) and perpendicular (empty square) to the applied electric field vector.

of most π-conjugated polymer films. On the contrary, the anisotropy is in between 1.3:1 and 1:1. The low anisotropy of Pt-3 film indicates that either there is relatively strong interchain interaction or some of the excited states do not lie along the polymer chain.

5.3 Two photon absorption of Pt-3 polymer film and solution

In π-conjugated polymers the optical transitions between the ground state $1A_g$ and the B_u excited states are allowed, and therefore the linear absorption spectrum contains mainly $1A_g \rightarrow 1B_u$ transition. On the contrary, the optical transitions between the ground state $1A_g$ and other state with A_g symmetry are forbidden. However, these transitions become allowed in two photon absorption (TPA). Figure 5.4(a) shows the TPA spectrum of Pt-3 film up to 4.1 eV compared with the linear absorption spectrum. The TPA spectrum peaks at 3.7 eV, with phonon side bands at 3.9 eV. These bands are due to mA_g state, as has been seen in the EA spectrum. The TPA spectrum goes to zero as it approaches the $1B_u$ state of the polymer. The TPA spectrum does not show other even parity state $m'A_g$ since it lies outside our spectral range.

Figure 5.4(b) shows the polarized TPA spectra of Pt-3 film. The polarization anisotropy between parallel and perpendicular spectra is 1.3:1 which is almost consistent with the polarization anisotropy in the EA spectra discussed above. The TPA spectrum diminishes close to the peak in the linear absorption spectrum. This indicates that there is a large energy separation between the 1Bu and mAg states in the Pt-3 polymer,

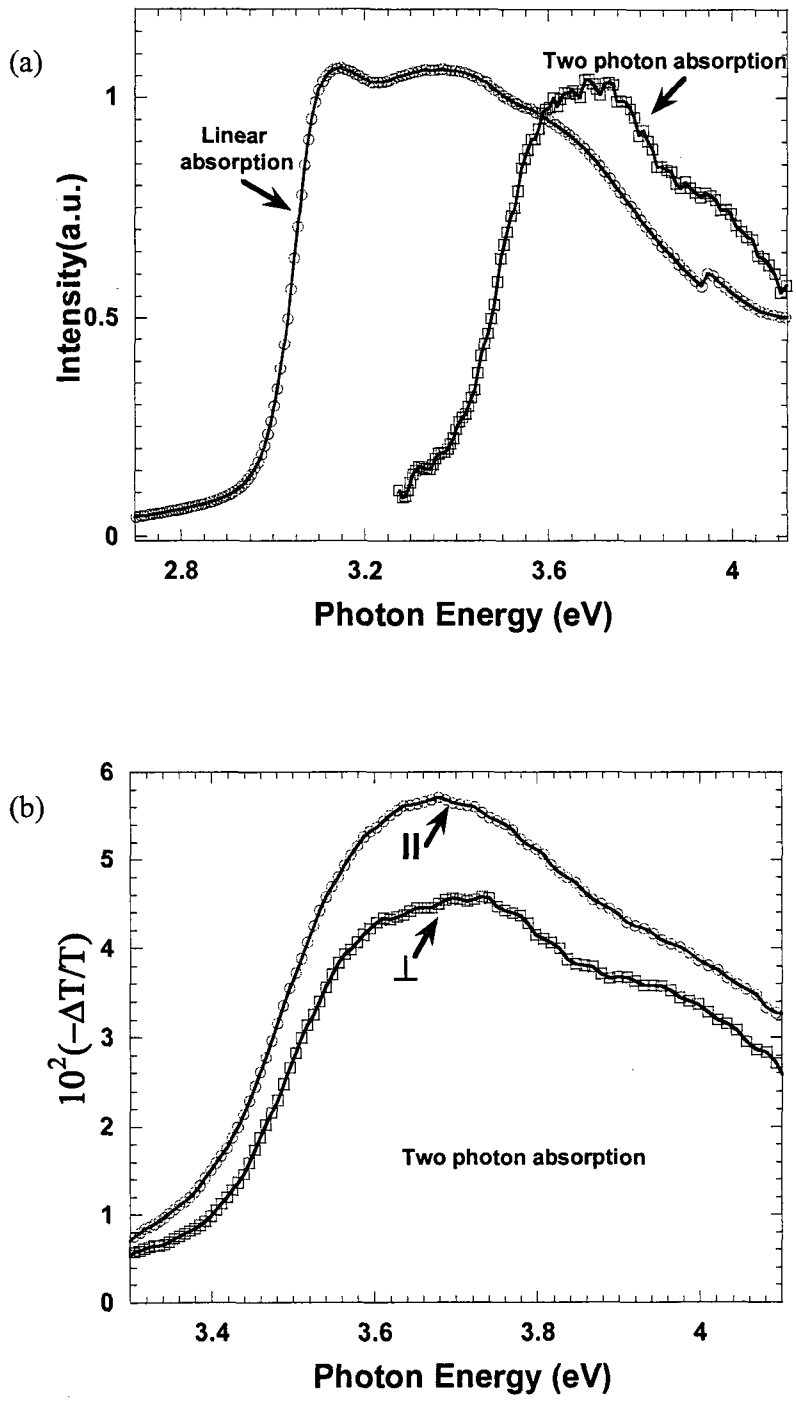

Figure 5.4: The two-photon absorption (TPA) measurement of Pt-3 polymer. (a) TPA spectrum compared to the linear absorption spectrum.(b) TPA spectra with pump and probe polarizations either parallel (empty circle) or perpendicular (empty square) to each other.

eliminating the explanation of single electron band model for this polymer, which would have shown the peaks in the absorption and TPA to be very close to each other.

TPA measurements were also done on the Pt-3 polymer solution to compare it with the film. Figure 5.5(a) shows the TPA spectrum of the Pt-3 solution compared with the linear absorption spectrum. Both of these spectra are blue-shifted by ~0.1 eV compared to the film, and this indicates that the polymer chains are isolated in the solution. Figure 5.5(b) shows the polarization anisotropy of the TPA spectra in the Pt-3 solution. A large anisotropy of 2.5:1 is observed for mA_g state in the solution, and this explains that the low anisotropy of film is due to interchain interaction. The enhanced interchain interaction in the Pt polymer may be due to the long extent of the Pt d-electrons that resemble long lobes extended outside the chain direction.

5.4 Electroabsorption of Pt-1 polymer

The model calculation of Pt-polymers has shown that the lowest lying singlet state in Pt-1 polymer is not π-electron singlet state, but rather is an MLCT state. Figure 5.6(a) shows the EA spectrum of Pt-1 polymer film compared with its linear absorption spectrum. The linear absorption spectrum peaks at ~3.05 eV with two humps at 3.8 and 4.15 eV, respectively. The EA spectrum shows many different features (similar to the EA spectrum of Pt-3 polymer film discussed above): a first-derivative-like feature with zero-crossing at ~3.17 eV (assigned as $1B_u$), a modulation feature with zero-crossing at ~4.1 eV (assigned as nB_u), two well-resolved phonon side bands related to $1B_u$ at 3.29 and 3.5 eV, respectively, and a single induced absorption band at 3.9 eV (assigned as mA_g). The position of $1B_u$ state is very different in Pt-1 polymer than in the Pt-3 polymer (or any

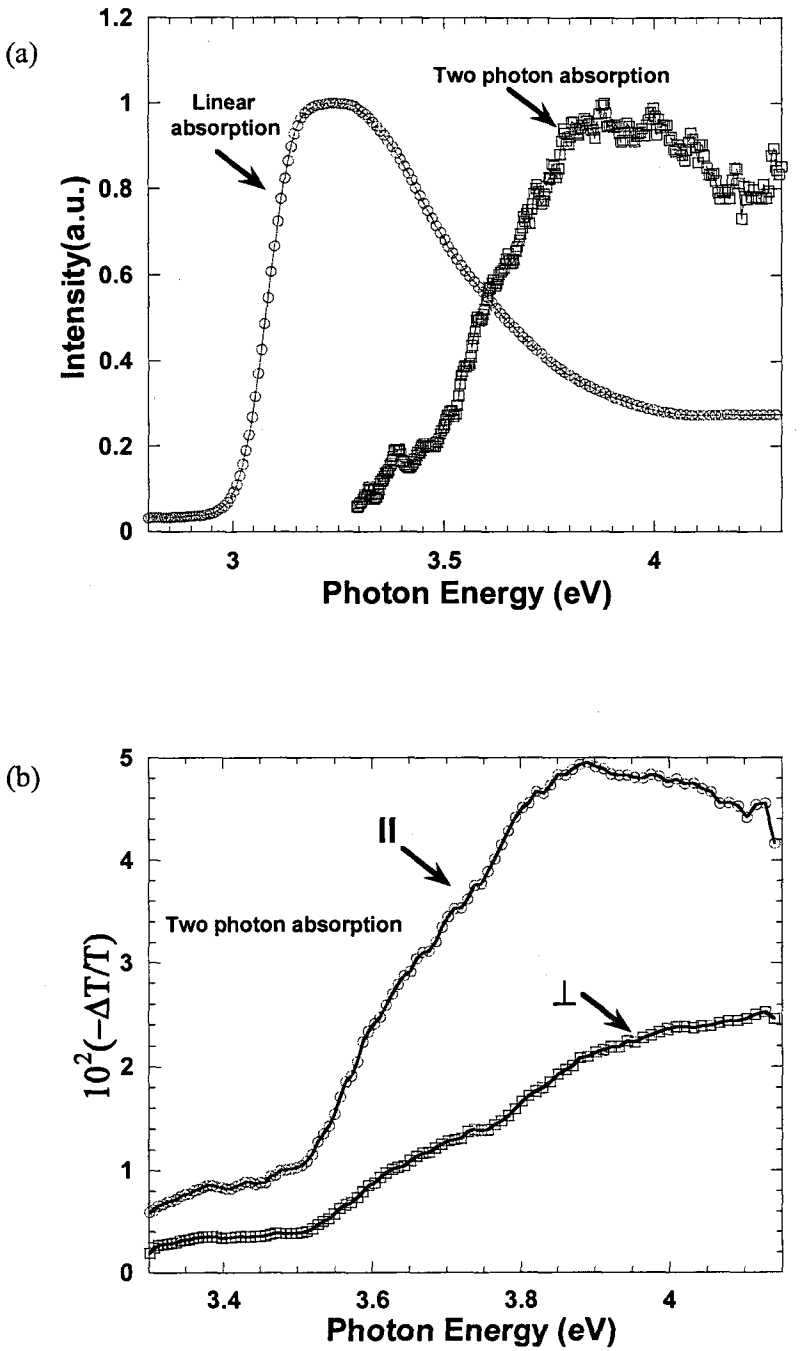

Figure 5.5: The two-photon absorption (TPA) measurement of Pt-3 polymer in solution. (a) TPA spectrum compared to the linear absorption spectrum.(b) TPA spectra with pump and probe polarizations either parallel (empty circle) or perpendicular (empty square) to each other.

π-conjugated polymers), and it lies **above** the linear absorption peak at ~3.05 eV. We speculate that linear absorption peak at ~3.05 eV is due to the lowest lying MLCT singlet state (shown by quantum chemistry calculation) whereas the EA derivative feature points to the $1B_u$ at ~3.17 eV, which is the π-electron singlet state. The explanations for other EA features are the same as in the Pt-3 polymer discussed above. We therefore conclude that the EA spectrum reveals a splitting of ~ 0.12 eV between the lowest lying MLCT state and that of the π-π* state, in good agreement with the theory.

Figure 5.6(b) shows the polarization anisotropy of the EA spectra of Pt-1 polymer, which varies from 1.8:1 to 2.0:1 in the entire spectral range. The large polarization anisotropy of Pt-1 film compared to Pt-3 polymer indicates that most excited states lie along the backbone chain of the Pt-1 polymer. This points to a larger hybridization of the Pt d-electron and the carbon π-electron on the polymer chains.

5.5 Two-photon absorption of Pt-1 solution

Figure 5.7(a) shows the two-photon absorption (TPA) of the Pt-1 solution along with linear absorption spectrum. We note that even in the solution, the linear absorption peak position is still at ~3.05 eV, the same as that of the film. This shows that the lower lying state in Pt-1, in contrast to Pt-3 is quite robust and does not depend on the chain conjugation length, in agreement with our conclusion that is due to the MLCT state. The TPA spectrum peaks at ~4.0 eV, and similar as in Pt-3 this band is assigned to mA_g state, which is also supported by the EA spectrum. Here, the important point to be noted is that the energy-gap between the linear absorption and TPA is ~0.95 eV whereas it is 0.6-0.7

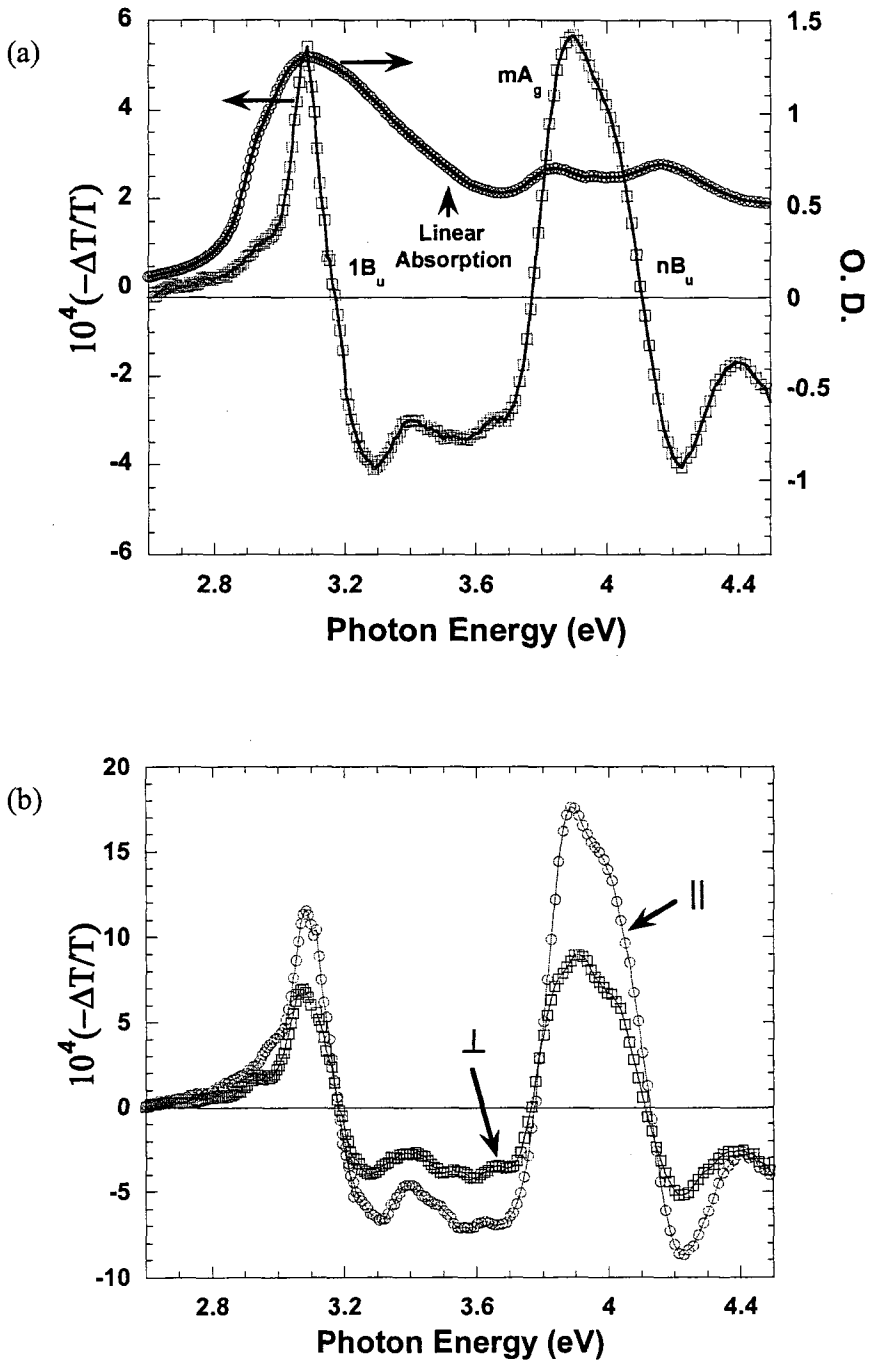

Figure 5.6: Electroabsorption (EA) measurement of Pt-1 polymer film. (a) EA spectrum with linear absorption. The essential states $1B_u$, mA_g, and nB_u are assigned. (b) Polarized EA spectrum with light polarization parallel (empty circle) and perpendicular (empty square) to the applied electric field vector.

eV in most π-conjugated polymers. This is the consequence of MLCT singlet state being the lowest excited state of Pt-1 polymer.

Figure 5.7(b) shows the polarized TPA spectra of Pt-1 solution. The polarization anisotropy between parallel and perpendicular spectra is 3.8:1, which is large compared to EA spectrum anisotropy of mA_g state (2.0:1) of Pt-1 film, and also higher than the TPA polarization anisotropy of Pt-3 solution. Thus, it is clear that the excited states of Pt-1 polymer are more aligned along the backbone chain compared to the excited states of Pt-3 polymer.

5.6 Ultrafast photomodulation of Pt-1 polymer

This measurement was done by Drs Tong and Gambetta in our group. Figure 5.8(a) shows the transient PM spectra of Pt-1 polymer at three different time scales of t = 0, 0.5 and 1 ps. The spectra reveal three different band structures: PA_1 at 0.8-0.9 eV, PA_2 at ~1.9 eV, and PA_3 at ~2.5 eV. Figure 5.8(b) shows the decay dynamics of these bands. PA_1 and PA_3 are strictly correlated with a decay time of about 2 ps deduced from pump-probe time traces, whereas PA_2 presents a much longer delay. The plateau in the PA_3 dynamics comes from the partial overlap with PA_2 band. Band PA1 and PA3 are seem to be related to singlet absorptions (respectively S_1-S_m and S_1-S_n transitions) because of the very fast decay time. We know that all the photoinduced transition originate from $1B_u$ (~3.1 eV), and they are between opposite parity states. Thus, PA_1 is in between $1B_u$ (~3.1 eV) and mA_g (~4.0 eV), and its spectral position (0.8-0.9 eV) in PM spectrum also supports that. All the other higher probe energy transitions, like PA_3, cannot be traced because our EA and TPA spectra are only up to 4.4 eV. Due to the similarity between

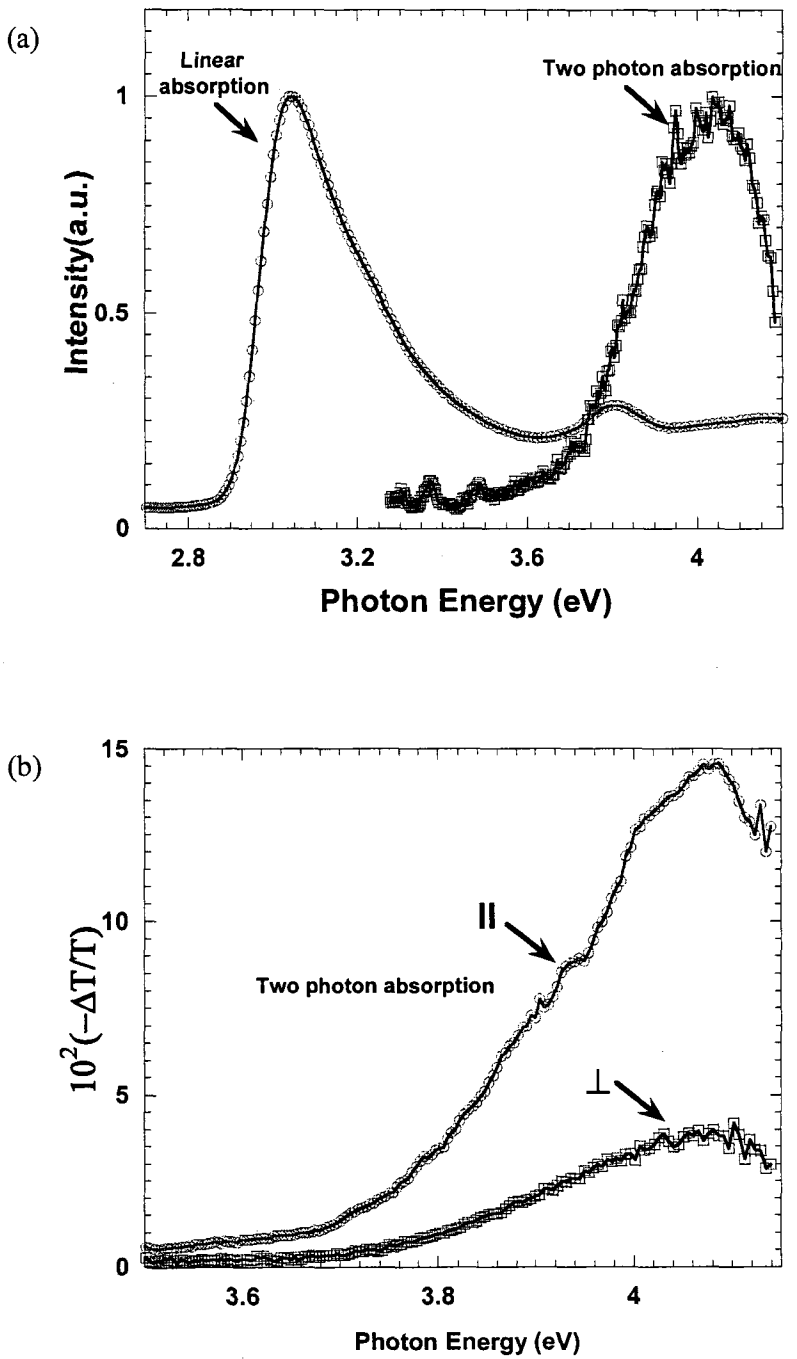

Figure 5.7: The two-photon absorption (TPA) measurement of Pt-1 polymer in solution. (a) TPA spectrum compared to the linear absorption spectrum.(b) TPA spectra with pump and probe polarizations either parallel (empty circle) or perpendicular (empty square) to each other.

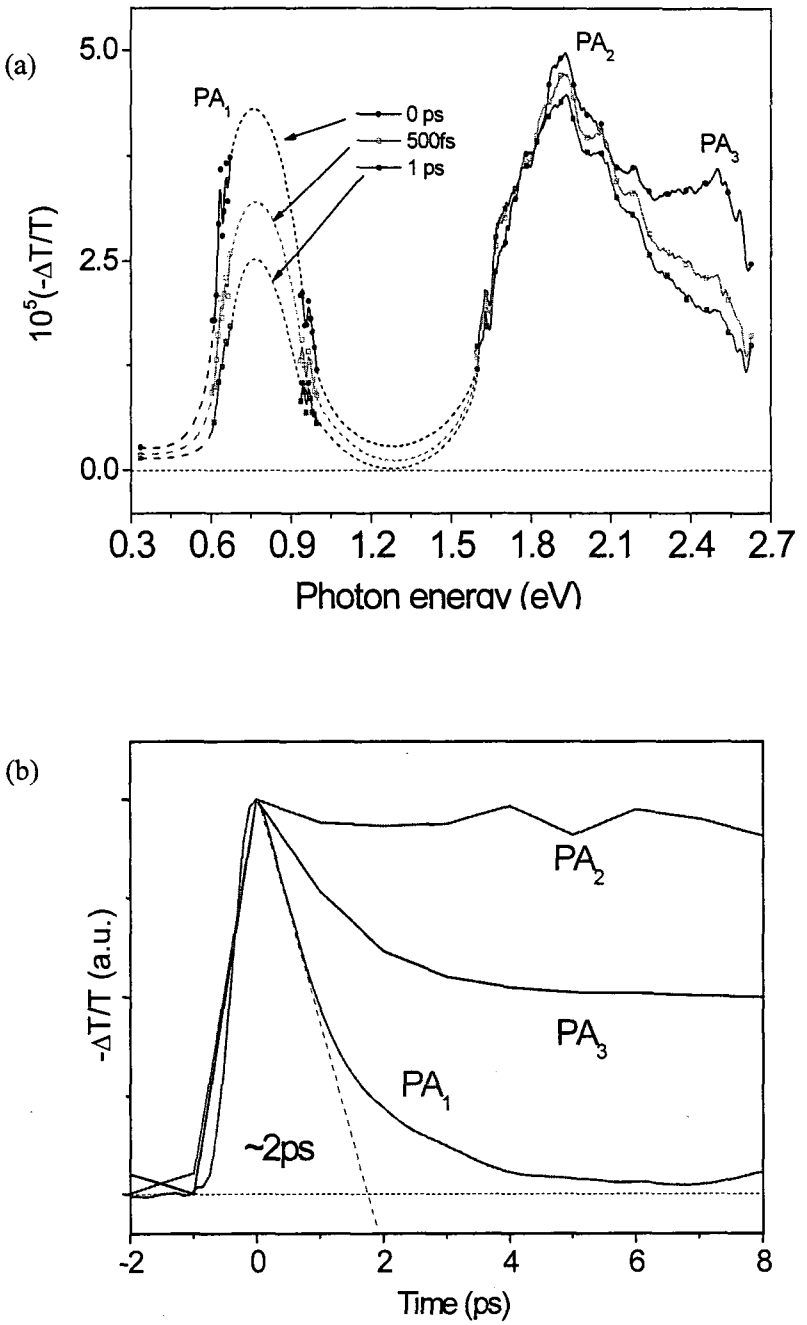

Figure 5.8: Transient photomodulation (PM) measurement of Pt-1 polymer. (a) The transient PM spectra using excitation of 3.1 eV at t = 0 ps, 0.5 ps and 1 ps, showing different bands PA_1, PA_2 and PA_3. (b) The decay dynamics of these bands in the spectrum. These measurements were done by Drs Tong and Gambetta in our group.

triplet absorption band in CW PM measurement and PA_2 band in transient measurement, we assign the origin of PA_2 band to triplet-triplet absorption in the triplet manifold.

5.7 Conclusions

The excited states properties of two Pt-polymers, namely, Pt-1 and Pt-3, using linear-absorption, EA and TPA spectroscopies have been studied. The presence of metal in the backbone of π-conjugated chains affects the location of $\pi-\pi^*$ excited states with respect to MLCT transitions, and their relative positions have been identified using EA and TPA spectroscopies. It has been found that the lowest lying singlet state in Pt-1 polymer is MLCT in nature whereas Pt-3 polymer has π-electron state as the lowest excited state like other π-conjugated polymers. The nonlinear spectra of these polymers show similar behavior as have been found in other regular π-conjugated polymers such as PPV derivatives, polythiophene etc.

CHAPTER 6

CONCLUSIONS

This dissertation explores the optical characterization of (a) compounds of polythiophene/fullerene blends; (b) various derivatives of poly(phenylene-vinylene) (PPV) polymers; and (c) Pt-containing π-conjugated polymers using ultrafast photomodulation measurements as well as electroabsorption and two-photon spectroscopies. The two laser systems used for these studies are a high-energy low-repetition rate laser system in the spectral range of 1.2 to 2.5 eV and a low-energy high repetition laser system in the range 0.25 to 1.1 eV. Using both systems we could study the transient PM spectrum in the time domain of ~100 fs to 1 ns.

In organic photovoltaics, bulk heterojunction polymer solar cells based on Regio-Regular-poly(3-hexylthiophene) (RR-P3HT)/fullerene have shown promising power conversion efficiency of up to 6%. To improve this value further, a deeper understanding of the ultrafast charge carrier photogeneration and recombination in the active layer of the polythiophene/PCBM blend is required. Two different donor polymers namely, Regio-Regular-poly(3-hexylthiophene) (RR-P3HT), which forms nano-morphological lamellae structure, and Regio-Random-poly(3-hexylthiophene) (RRa-P3HT), which forms lamellae with lesser extent, have been compared. In contrast to high efficiency photovoltaic devices based on RR-P3HT/PCBM, the devices based on RRa-P3HT/PCBM

blend have shown poor power conversion efficiency (< 0.1%). Therefore, these two polymers unravel the importance of phase separation of the material constituents in the active layer of donor/acceptor blend systems. These nano-morphologies have been studied by transmission electron microscopy (TEM). TEM images of (RR-P3HT)/PCBM blend show the nano-sized (~30 nm) domains of PCBM network, whereas for (RRa-P3HT)/PCBM blend, the polymer and PCBM are uniformly mixed, and TEM images do not show any phase-separation of polymer or PCBM.

The transient PM measurements of one of the most efficient RR-P3HT/fullerene blends (namely P3HT/PCBM) shows that the decay of exciton does not result in the generation of polarons in the donor and acceptor materials, as assumed by the present model of charge dissociation in photovoltaic devices. On the contrary, the decay of exciton fits very well the transient build-up of charge-transfer (CT) states in the fullerene phase. This indicates the migration of the photogenerated excitons in the polymer phase to the D-A interface, and then into the fullerene nano-domains. In contrast, the transient PM measurements of RRa-P3HT/fullerene blend, which does not form phase-separated nano-domains, show the formation of a CT state at the interface following by ultrafast geminate recombination.

The photophysics of 2-methoxy-5-(2'-ethylhexyloxy) poly(phenylene-vinylene) [MEH-PPV] polymer is, in general, one of the most debatable among π-conjugated polymers. MEH-PPV polymer and other PPV derivatives (such as DOO-PPV) have been studied by transient photomodulation (PM) and polarization memory decay spectroscopies. The transient PM measurements of MEH-PPV films show that there are two kinds of primary photoexcitations, namely, intrachain excitons and excimers, but

only intrachain excitons are photogenerated in other PPV derivative polymers and in MEH-PPV solutions. Subsequently, in order to study the interchain interaction, and its role in determining the excimer species, high-pressure (up to 100 kbar) study of MEH-PPV film was performed using a diamond anvil cell. The high-pressure study shows that there are two kinds of polymer chain orders in MEH-PPV film; in one of them the chains are isolated, whereas in the other order the chains are closely packed. The high pressure mainly affects the closely packed-chains. Related with this chain order we found three photoinduced absorption (PA) bands that blue-shift with pressure, namely PA' (~0.65 eV), PA'' (1.2 eV) and PA''' (1.85 eV) [the energies are given at 77 kbar], are observed, which are due to excimers in this polymer phase. In contrast, there is no substantive pressure effect on the PA_1 band at 0.9 eV that originates from photogenerated intrachain excitons in the isolated chains.

Platinum (Pt)-containing conjugated polymers are an interesting class of polymer materials due to existence of phosphorescence along with fluorescence emission, and this can increase the efficiency of light emitting diodes based on these materials. In addition, these polymers are important from fundamental aspects because, due to the large spin-orbit coupling of the intrachain Pt atoms triplet species can easily be detected, which is elusive in regular π-conjugated polymers,. The aim of our study here was to investigate the excited states properties of Pt-containing conjugated polymers, which may be very different than the excited states properties of known π-conjugated polymers such as PPV, polythiophene and polyfluorene, due to the incorporation of Pt atoms into the backbone of the π-conjugated chain.

The two Pt-containing π-conjugated polymers studied in this thesis are: (i) Pt-1, where the Pt atom is incorporated into the backbone of the polymer chain in each monomer unit; and (ii) Pt-3, where the Pt atom is incorporated into every three monomer units. The different parity of the excited states in these Pt-polymers are studied by electroabsorption and two-photon-absorption spectroscopies. These studies reveal that even after incorporation of Pt atoms, the excited state properties of these polymers are not very different from the regular π-conjugated polymers. The lowest lying singlet state in Pt-1 polymer is MLCT in nature, whereas Pt-3 polymer has a π-electron state as the lowest excited state, similar as in other π-conjugated polymers. These excited states are consistent with the transient PA bands seen in the PM spectrum.

REFERENCES

[1] T. A. Skotheim, R. L. Elsenbaumer, and J. R. Reynolds, *Handbook of Conducting Polymers*, 2nd ed., New York: M. Dekker, 1998.

[2] G. Malliaras and R. Friend, "An organic electronics primer," *Physics Today,* vol. 58, no. 5, pp. 53-58, May, 2005.

[3] J. H. Burroughes, D. D. C. Bradley, A. R. Brown, R. N. Marks, K. Mackay, R. H. Friend, P. L. Burns, and A. B. Holmes, "Light-emitting diodes based on conjugated polymers," *Nature,* vol. 347, no. 6293, pp. 539-541, 1990.

[4] D. Braun and A. J. Heeger, "Visible light emission from semiconducting polymer diodes," *Applied Physics Letters,* vol. 58, no. 18, pp. 1982-4, 1991.

[5] J. H. Burroughes, C. A. Jones, and R. H. Friend, "New semiconductor device physics in polymer diodes and transistors," *Nature,* vol. 335, no. 6186, pp. 137-41, 1988.

[6] B. Crone, A. Dodabalapur, Y. Y. Lin, R. W. Filas, Z. Bao, A. LaDuca, R. Sarpeshkar, H. E. Katz, and W. Li, "Large-scale complementary integrated circuits based on organic transistors," *Nature,* vol. 403, no. 6769, pp. 521-523, 2000.

[7] F. Garnier, R. Hajlaoui, A. Yassar, and P. Srivastava, "All-polymer field-effect transistor realized by printing techniques," *Science,* vol. 265, no. 5179, pp. 1684-1686, 1994.

[8] N. S. Sariciftci, L. Smilowitz, A. J. Heeger, and F. Wudl, "Photoinduced electron transfer from a conducting polymer to buckminsterfullerene," *Science,* vol. 258, no. 5087, pp. 1474-6, 1992.

[9] G. Yu, J. Gao, J. C. Hummelen, F. Wudl, and A. J. Heeger, "Polymer photovoltaic cells: Enhanced efficiencies via a network of internal donor-acceptor heterojunctions," *Science,* vol. 270, no. 5243, pp. 1789-91, 1995.

[10] R. E. Peierls, *Quantum Theory of Solids*, Oxford: Clarendon Press, 1955.

[11] L. Yu, *Solitons & Polarons in Conducting Polymers*, Singapore World Scientific, 1988.

[12] A. J. Heeger, S. Kivelson, J. R. Schrieffer, and W. P. Su, "Solitons in conducting polymers," *Reviews of Modern Physics,* vol. 60, no. 3, pp. 781, 1988.

[13] H. Shirakawa, T. Ito, and S. Ikeda, "Raman scattering and electronic spectra of poly(acetylene)," *Polymer Jour.,* vol. 4, pp. 460, 1973.

[14] C. K. Chiang, C. R. Fincher, Jr., Y. W. Park, A. J. Heeger, H. Shirakawa, E. J. Louis, S. C. Gau, and A. G. MacDiarmid, "Electrical conductivity in doped polyacetylene," *Physical Review Letters,* vol. 39, no. 17, pp. 1098-101, 1977.

[15] H. Shirakawa, E. J. Louis, A. G. MacDiarmid, C. K. Chiang, and A. J. Heeger, "Synthesis of electrically conducting organic polymers: Halogen derivatives of polyacetylene, (CH)x," *Journal of the Chemical Society, Chemical Communications*, no. 16, pp. 578, 1977.

[16] A. Tsumura, H. Koezuka, and T. Ando, "Macromolecular electronic device: Field-effect transistor with a polythiophene thin film," *Applied Physics Letters,* vol. 49, no. 18, pp. 1210-1212, 1986.

[17] Z. Bao, A. Dodabalapur, and A. J. Lovinger, "Soluble and processable regioregular poly(3-hexylthiophene) for thin film field-effect transistor applications with high mobility," *Applied Physics Letters,* vol. 69, no. 26, pp. 4108-4110, 1996.

[18] B. H. Hamadani and D. Natelson, "Temperature-dependent contact resistances in high-quality polymer field-effect transistors," *Applied Physics Letters,* vol. 84, no. 3, pp. 443-445, 2004.

[19] F. Hide, M. A. Diaz-Garcia, B. J. Schwartz, M. R. Andersson, Q. Pei, and A. J. Heeger, "Semiconducting polymers: A new class of solid-state laser materials," *Science,* vol. 273, no. 5283, pp. 1833-1836, 1996.

[20] N. Tessler, G. J. Denton, and R. H. Friend, "Lasing from conjugated-polymer microcavities," *Nature,* vol. 382, no. 6593, pp. 695-697, 1996.

[21] S. V. Frolov, M. Ozaki, W. Gellermann, Z. V. Vardeny, and K. Yoshino, "Mirrorless lasing in conducting polymer poly(2,5-dioctyloxy-p-phenylenevinylene) films," *Japanese Journal of Applied Physics, Part 2: Letters,* vol. 35, no. 10 B, pp. L1371-L1373, 1996.

[22] R. C. Polson and Z. V. Vardeny, "Organic random lasers in the weak-scattering regime," *Physical Review B (Condensed Matter and Materials Physics),* vol. 71, no. 4, pp. 45205-1, 2005.

[23] M. Pope and C. E. Swenberg, *Electronic Processes in Organic Crystals and Polymers*, 2nd ed., New York: Oxford University Press, 1999.

[24] N. W. Ashcroft and N. D. Mermin, *Solid State Physics*, New York: Holt, Rinehart and Winston, 1976.

[25] W. Barford, *Electronic and Optical Properties of Conjugated Polymers*, Oxford: Clarendon Press, 2005.

[26] W. P. Su, J. R. Schrieffer, and A. J. Heeger, "Soliton excitations in polyacetylene," *Physical Review B,* vol. 22, no. 4, pp. 2099, 1980.

[27] S. Mazumdar and S. N. Dixit, "Coulomb effects on one-dimensional peierls instability: The peierls-hubbard model," *Physical Review Letters,* vol. 51, no. 4, pp. 292, 1983.

[28] S. Mazumdar and S. N. Dixit, "Electronic excited states in conjugated polymers," *Synthetic Metals,* vol. 28, pp. 463-8, 1989.

[29] X. Wei, Z. V. Vardeny, N. S. Sariciftci, and A. J. Heeger, "Absorption-detected magnetic-resonance studies of photoexcitations in conjugated-polymer/c60 composites," *Physical Review B,* vol. 53, no. 5, pp. 2187, 1996.

[30] S. Mazumdar, D. Guo, and S. N. Dixit, "A four-level essential states model of third order optical nonlinearity in π-conjugated polymers," *Synthetic Metals,* vol. 57, pp. 3881-8, 1993.

[31] M. Kasha, "Characterization of electronic transitions in complex molecules," *Discussions of the Faraday Society,* vol. 9, pp. 14, 1950.

[32] T. Ogawa and T. Takagahara, "Interband absorption spectra and sommerfeld factors of a one-dimensional electron-hole system," *Physical Review B,* vol. 43, no. 17, pp. 14325, 1991.

[33] T. Ogawa and T. Takagahara, "Optical absorption and sommerfeld factors of one-dimensional semiconductors: An exact treatment of excitonic effects," *Physical Review B,* vol. 44, no. 15, pp. 8138, 1991.

[34] L. Sebastian and G. Weiser, "One-dimensional wide energy bands in a polydiacetylene revealed by electroreflectance," *Physical Review Letters,* vol. 46, no. 17, pp. 1156, 1981.

[35] R. Loudon, "One-dimensional hydrogen atom," *American Journal of Physics,* vol. 27, no. 9, pp. 649-655, 1959.

[36] J. S. Wilson, A. Kohler, R. H. Friend, M. K. Al-Suti, M. R. A. Al-Mandhary, M. S. Khan, and P. R. Raithby, "Triplet states in a series of pt-containing ethynylenes," *Journal of Chemical Physics,* vol. 113, no. 17, pp. 7627-34, 2000.

[37] S. A. Jenekhe and J. A. Osaheni, "Excimers and exciplexes of conjugated polymers," *Science,* vol. 265, no. 5173, pp. 765-768, 1994.

[38] R. Farchioni and G. Grosso, *Organic Electronic Materials : Conjugated Polymers and Low Molecular Weight Organic Solids*, Berlin ; New York: Springer, 2001.

[39] D. D. Gebler, Y. Z. Wang, D. K. Fu, T. M. Swager, and A. J. Epstein, "Exciplex emission from bilayers of poly(vinyl carbazole) and pyridine based conjugated copolymers," *The Journal of Chemical Physics,* vol. 108, no. 18, pp. 7842-7848, 1998.

[40] I. D. W. Samuel, G. Rumbles, and C. J. Collison, "Efficient interchain photoluminescence in a high-electron-affinity conjugated polymer," *Physical Review B,* vol. 52, no. 16, pp. R11573, 1995.

[41] J. W. Blatchford, S. W. Jessen, L. B. Lin, J. J. Lih, T. L. Gustafson, A. J. Epstein, D. K. Fu, M. J. Marsella, T. M. Swager, A. G. MacDiarmid, S. Yamaguchi, and H. Hamaguchi, "Exciton dynamics in poly(p-pyridyl vinylene)," *Physical Review Letters,* vol. 76, no. 9, pp. 1513, 1996.

[42] J. M. Lupton, "On-chain defect emission in conjugated polymers - comment on 'exciton dissociation dynamics in a conjugated polymer containing aggregate states'," *Chemical Physics Letters,* vol. 365, no. 3-4, pp. 366-368, 2002.

[43] U. Lemmer, S. Heun, R. F. Mahrt, U. Scherf, M. Hopmeier, U. Siegner, E. O. Go¨bel, K. Mu¨llen, and H. Ba¨ssler, "Aggregate fluorescence in conjugated polymers," *Chemical Physics Letters,* vol. 240, no. 4, pp. 373-378, 1995.

[44] M. Asaki, "Generation of 11-fs pulses from a self-mode-locked ti:Sapphire laser," *Optics letters,* vol. 18, no. 12, pp. 977-979, 1993.

[45] Positive light incorporation, Los Gatos, California.

[46] AC-1 Interferometric Autocorrelator Kit, Clark Instrumentation.

[47] J.-C. Diels and W. Rudolph, *Ultrashort Laser Pulse Phenomena: Fundamentals, Techniques and Applications on a Femtosecond Time Scale*, 2nd ed., San Diego: Academic Press, 2006.

[48] *The Supercontinuum Laser Source*, New-York: Springer-Verlag, 1989.

[49] A. Chakrabarti and S. Mazumdar, "Theory of even-parity states in polyphenylenes," *Physical Review B (Condensed Matter),* vol. 59, no. 7, pp. 4839-48, 1999.

[50] S. N. Dixit, D. Guo, and S. Mazumdar, "Essential-states mechanism of optical nonlinearity in π-conjugated polymers," *Physical Review B (Condensed Matter),* vol. 43, no. 8, pp. 6781-4, 1991.

[51] M. Tong, C. X. Sheng, and Z. V. Vardeny, "Nonlinear optical spectroscopy of excited states in polyfluorene," *Physical Review B,* vol. 75, 2007.

[52] R. W. Boyd, *Nonlinear Optics*, San Diego: Academic Press, 1992.

[53] Y. R. Shen, *The Principles of Nonlinear Optics*, New York: J. Wiley, 1984.

[54] S. A. Jeglinski, "Electroabsorption spectroscopy of conjugated polymers and carbon fullerenes and conjugated-polymer light-emitting-devices," Thesis (Ph D), Department of Physics, University of Utah, Salt Lake City, 1996.

[55] A. Jayaraman, "Diamond anvil cell and high-pressure physical investigations," *Reviews of Modern Physics,* vol. 55, no. 1, pp. 65, 1983.

[56] L. Merrill and W. A. Bassett, "Miniature diamond anvil pressure cell for single crystal x-ray diffraction studies," *Review of Scientific Instruments,* vol. 45, no. 2, pp. 290-294, 1974.

[57] "High pressure diamond optics, inc.," http://www.hpdo.com/.

[58] R. A. Forman, G. J. Piermarini, J. D. Barnett, and S. Block, "Pressure measurement made by the utilization of ruby sharp-line luminescence," *Science,* vol. 176, no. 4032, pp. 284-5, 1972.

[59] G. J. Piermarini, S. Block, J. D. Barnett, and R. A. Forman, "Calibration of the pressure dependence of the r1 ruby fluorescence line to 195 kbar," *Journal of Applied Physics,* vol. 46, no. 6, pp. 2774-80, 1975.

[60] G. J. Piermarini and S. Block, "Ultrahigh pressure diamond-anvil cell and several semiconductor phase transition pressures in relation to the fixed point pressure scale," *Review of Scientific Instruments,* vol. 46, no. 8, pp. 973-9, 1975.

[61] J. Peet, J. Y. Kim, N. E. Coates, W. L. Ma, D. Moses, A. J. Heeger, and G. C. Bazan, "Efficiency enhancement in low-bandgap polymer solar cells by processing with alkane dithiols," *Nature Materials,* vol. 6, no. 7, pp. 497-500, Jul, 2007.

[62] K. Kim, J. Liu, M. A. G. Namboothiry, and D. L. Carroll, "Roles of donor and acceptor nanodomains in 6% efficient thermally annealed polymer photovoltaics," *Applied Physics Letters,* vol. 90, no. 16, pp. 3, Apr, 2007.

[63] M. A. Green, K. Emery, Y. Hishikawa, and W. Warta, "Solar cell efficiency tables (version 31)," *Progress in Photovoltaics: Research and Applications,* vol. 16, no. 1, pp. 6-12, 2008.

[64] G. Dennler, M. C. Scharber, and C. J. Brabec, "Polymer-fullerene bulk-heterojunction solar cells," *Advanced Materials,* vol. 21, no. 13, pp. 1323-1338, 2009.

[65] O. J. Korovyanko, R. Osterbacka, X. M. Jiang, Z. V. Vardeny, and R. A. J. Janssen, "Photoexcitation dynamics in regioregular and regiorandom polythiophene films," *Physical Review B (Condensed Matter and Materials Physics),* vol. 64, no. 23, pp. 235122-1, 2001.

[66] R. Osterbacka, C. P. An, X. M. Jiang, and Z. V. Vardeny, "Two-dimensional electronic excitations in self-assembled conjugated polymer nanocrystals," *Science,* vol. 287, no. 5454, pp. 839-842, 2000.

[67] J. XiaoMei, R. Osterbacka, O. Korovyanko, C. P. An, B. Horovitz, R. A. J. Janssen, and Z. V. Vardeny, "Spectroscopic studies of photoexcitations in regioregular and regiorandom polythiophene films," *Advanced Functional Materials,* vol. 12, no. 9, pp. 587-97, 2002.

[68] K. Youngkyoo, S. Cook, S. M. Tuladhar, S. A. Choulis, J. Nelson, J. R. Durrant, D. D. C. Bradley, M. Giles, I. McCulloch, H. Chang-sik, and M. Ree, "A strong regioregularity effect in self-organizing conjugated polymer films and high-efficiency polythiophene:Fullerene solar cells," *Nature Materials,* vol. 5, no. 3, pp. 197-203, 2006.

[69] Y. Kim, S. Cook, S. M. Tuladhar, S. A. Choulis, J. Nelson, J. R. Durrant, D. D. C. Bradley, M. Giles, I. McCulloch, C.-S. Ha, and M. Ree, "A strong regioregularity effect in self-organizing conjugated polymer films and high-efficiency polythiophene:Fullerene solar cells," *Nat Mater,* vol. 5, no. 3, pp. 197-203, 2006.

[70] S. Cook, "A photophysical study of pcbm thin films," *Chemical Physics Letters,* vol. 445, no. 4, pp. 276-80, 2007.

[71] D. Dick, X. Wei, S. Jeglinski, R. E. Benner, Z. V. Vardeny, D. Moses, V. I. Srdanov, and F. Wudl, "Transient spectroscopy of excitons and polarons in c60 films from femtoseconds to milliseconds," *Physical Review Letters,* vol. 73, no. 20, pp. 2760-3, 1994.

[72] S. Morita, A. A. Zakhidov, and K. Yoshino, "Doping effect of buckminsterfullerene in conducting polymer: Change of absorption spectrum and quenching of luminescence," *Solid State Communications,* vol. 82, no. 4, pp. 249-52, 1992.

[73] J. J. Benson-Smith, L. Goris, K. Vandewal, K. Haenen, J. V. Manca, D. Vanderzande, D. D. C. Bradley, and J. Nelson, "Formation of a ground-state charge-transfer complex in polyfluorene/[6,6]-phenyl-c61 butyric acid methyl ester (pcbm) blend films and its role in the function of polymer/pcbm solar cells," *Advanced Functional Materials,* vol. 17, no. 3, pp. 451-7, 2007.

[74] T. Drori, C. X. Sheng, A. Ndobe, S. Singh, J. Holt, and Z. V. Vardeny, "Below-gap excitation of π-conjugated polymer-fullerene blends: Implications for bulk organic heterojunction solar cells," *Physical Review Letters,* vol. 101, no. 3, pp. 037401 (4 pp.), 2008.

[75] J. Holt, S. Singh, T. Drori, Y. Zheng, and Z. V. Vardeny, "Optical probes of π-conjugated polymer blends with strong acceptor molecules," *Physical Review B (Condensed Matter and Materials Physics),* vol. 79, no. 19, pp. 195210 (8 pp.), 2009.

[76] L. Goris, A. Poruba, L. Hod'akova, M. Vanecek, K. Haenen, M. Nesladek, P. Wagner, D. Vanderzande, L. D. Schepper, and J. V. Manca, "Observation of the subgap optical absorption in polymer-fullerene blend solar cells," *Applied Physics Letters,* vol. 88, no. 5, pp. 052113, 2006.

[77] P. Panda, D. Veldman, J. Sweelssen, J. J. A. M. Bastiaansen, B. M. W. Langeveld-Voss, and S. C. J. Meskers, "Charge transfer absorption for π-conjugated polymers and oligomers mixed with electron acceptors," *The Journal of Physical Chemistry B,* vol. 111, no. 19, pp. 5076-5081, 2007.

[78] W. Ma, A. Gopinathan, and A. J. Heeger, "Nanostructure of the interpenetrating networks in poly(3-hexylthiophene)/ fullerene bulk heterojunction materials: Implications for charge transport," *Advanced Materials,* vol. 19, no. 21, pp. 3656-3659, 2007.

[79] W. Ma, C. Yang, and A. J. Heeger, "Spatial fourier-transform analysis of the morphology of bulk heterojunction materials used in 'plastic' solar cells," *Advanced Materials,* vol. 19, no. 10, pp. 1387-1390, 2007.

[80] J. S. Moon, J. K. Lee, S. Cho, J. Byun, and A. J. Heeger, "Columnlike Structure of the cross-sectional morphology of bulk heterojunction materials," *Nano Letters,* vol. 9, no. 1, pp. 230-234, 2009.

[81] M. Hallermann, I. Kriegel, E. Da Como, J. M. Berger, E. von Hauff, and J. Feldmann, "Charge transfer excitons in polymer/fullerene blends: The role of morphology and polymer chain conformation," *Advanced Functional Materials,* vol. 19, no. 22, pp. 3662-3668, Nov, 2009.

[82] T. Drori, "Optical study of π-conjugated polymers and π-conjugated polymers/fullerene blends," Thesis (Ph D), Department of Physics, University of Utah, Salt Lake City, 2008.

[83] M. Hallermann, S. Haneder, and E. Da Como, "Charge-transfer states in conjugated polymer/fullerene blends: Below-gap weakly bound excitons for polymer photovoltaics," *Applied Physics Letters,* vol. 93, no. 5, 2008.

[84] C. X. Sheng, M. Tong, S. Singh, and Z. V. Vardeny, "Experimental determination of the charge/neutral branching ratio η in the photoexcitation of π-conjugated polymers by broadband ultrafast spectroscopy," *Physical Review B (Condensed Matter and Materials Physics),* vol. 75, no. 8, pp. 85206-1, 2007.

[85] S. Singh, T. Drori, and Z. V. Vardeny, "Polarization memory decay spectroscopy of photoexcitations in π-conjugated polymers: Evidence for excimers," *Physical Review B,* vol. 77, no. 19, 2008.

[86] D. D. C. Bradley, O. M. Gelsen, S. Ducharme, J. C. Scott, R. J. Twieg, and W. E. Moerner, "Comment on 'observation of the photorefractive effect in a polymer'," *Physical Review Letters,* vol. 67, no. 18, pp. 2589-90, 1991.

[87] I. W. Hwang, D. Moses, and A. J. Heeger, "Photoinduced carrier generation in p3ht/pcbm bulk heterojunction materials," *Journal of Physical Chemistry C,* vol. 112, no. 11, pp. 4350-4354, Mar, 2008.

[88] S. De, T. Pascher, M. Maiti, K. G. Jespersen, T. Kesti, F. L. Zhang, O. Inganas, A. Yartsev, and V. Sundstrom, "Geminate charge recombination in alternating polyfluorene copolymer/fullerene blends," *Journal of the American Chemical Society,* vol. 129, no. 27, pp. 8466-8472, Jul, 2007.

[89] J. G. Müller, J. M. Lupton, J. Feldmann, U. Lemmer, M. C. Scharber, N. S. Sariciftci, C. J. Brabec, and U. Scherf, "Ultrafast dynamics of charge carrier photogeneration and geminate recombination in conjugated polymer:Fullerene solar cells," *Physical Review B,* vol. 72, no. 19, pp. 195208, 2005.

[90] C. G. Shuttle, B. O'Regan, A. M. Ballantyne, J. Nelson, D. D. C. Bradley, and J. R. Durrant, "Bimolecular recombination losses in polythiophene: Fullerene solar cells," *Physical Review B,* vol. 78, no. 11, pp. 4, Sep, 2008.

[91] N. Natascha, D. Tesfaye Hailu, W. Lorenz, Z. Vitali, S. Heinz-Jurgen, O. Jens, and S. Sylvia, "Galvinoxyl monolayers on au(111) studied by stm, epr, and cyclic voltammetry," *Physical Review B (Condensed Matter and Materials Physics),* vol. 74, no. 23, pp. 235424, 2006.

[92] I. Novak and B. Kovac, "Electronic structure of galvinoxyl radical," *Chemical Physics Letters,* vol. 413, no. 4-6, pp. 351-5, 2005.

[93] R. C. Polson, G. Levina, and Z. V. Vardeny, "Spectral analysis of polymer microring lasers," *Applied Physics Letters,* vol. 76, no. 26, pp. 3858-3860, Jun, 2000.

[94] G. Hadziioannou, *Semiconducting Polymers: Chemistry, Physics, and Engineering*, Weinheim: Wiley-VCH-Verl., 2007.

[95] M. Chandross, S. Mazumdar, S. Jeglinski, X. Wei, Z. V. Vardeny, E. W. Kwock, and T. M. Miller, "Excitons in poly(para-phenylenevinylene)," *Physical Review B,* vol. 50, no. 19, pp. 14702, 1994.

[96] M. Chandross, S. Mazumdar, M. Liess, P. A. Lane, Z. V. Vardeny, M. Hamaguchi, and K. Yoshino, "Optical absorption in the substituted phenylene-based conjugated polymers: Theory and experiment," *Physical Review B,* vol. 55, no. 3, pp. 1486-1496, 1997.

[97] S. V. Frolov, Z. Bao, M. Wohlgenannt, and Z. V. Vardeny, "Excited-state relaxation in π-conjugated polymers," *Physical Review B,* vol. 65, no. 20, pp. 12, May, 2002.

[98] S. V. Frolov, M. Shkunov, Z. V. Vardeny, and K. Yoshino, "Ring microlasers from conducting polymers," *Physical Review B,* vol. 56, no. 8, pp. R4363-R4366, Aug, 1997.

[99] J. W. P. Hsu, M. Yan, T. M. Jedju, L. J. Rothberg, and B. R. Hsieh, "Assignment of the picosecond photoinduced absorption in phenylene vinylene polymers," *Physical Review B,* vol. 49, no. 1, pp. 712, 1994.

[100] M. Yan, L. J. Rothberg, E. W. Kwock, and T. M. Miller, "Interchain excitations in conjugated polymers," *Physical Review Letters,* vol. 75, no. 10, pp. 1992, 1995.

[101] B. Kraabel, V. I. Klimov, R. Kohlman, S. Xu, H. L. Wang, and D. W. McBranch, "Unified picture of the photoexcitations in phenylene-based conjugated polymers: Universal spectral and dynamical features in subpicosecond transient absorption," *Physical Review B,* vol. 61, no. 12, pp. 8501-8515, Mar, 2000.

[102] Z. D. Wang, S. Mazumdar, and A. Shukla, "Photophysics of charge-transfer excitons in thin films of π-conjugated polymers," *Physical Review B,* vol. 78, no. 23, 2008.

[103] Z. Vardeny, J. Strait, D. Moses, T. C. Chung, and A. J. Heeger, "Picosecond photoinduced dichroism in trans-(CH)x: Direct measurement of soliton diffusion," *Physical Review Letters,* vol. 49, no. 22, pp. 1657, 1982.

[104] S. Mazumdar, *Private communication*, 2007.

[105] P. Wang, C. J. Collison, and L. J. Rothberg, "Origins of aggregation quenching in luminescent phenylenevinylene polymers," *Journal of Photochemistry and Photobiology a-Chemistry,* vol. 144, no. 1, pp. 63-68, Oct, 2001.

[106] I. B. Martini, A. D. Smith, and B. J. Schwartz, "Exciton-exciton annihilation and the production of interchain species in conjugated polymer films: Comparing the ultrafast stimulated emission and photoluminescence dynamics of meh-ppv," *Physical Review B,* vol. 69, no. 3, pp. 12, Jan, 2004.

[107] C. J. Collison, L. J. Rothberg, V. Treemaneekarn, and Y. Li, "Conformational effects on the photophysics of conjugated polymers: A two species model for meh-ppv spectroscopy and dynamics," *Macromolecules,* vol. 34, no. 7, pp. 2346-2352, 2001.

[108] C. Yang, "Spectroscopic study of excitations in π-conjugated polymers," Thesis (Ph D), Department of Physics, University of Utah, Salt Lake City, 2006.

[109] L. Lüer, C. Manzoni, G. Cerullo, G. Lanzani, and Z. V. Vardeny, "Intra-chain exciton generation by charge recombination in substituted polyacetylenes," *Chemical Physics Letters,* vol. 444, no. 1-3, pp. 61-65, 2007.

[110] S. Singh, T. Drori, and Z. V. Vardeny, "Polarization memory decay spectroscopy of photoexcitations in π-conjugated polymers: Evidence for excimers," *Physical Review B,* vol. 77, no. 19, pp. 6, May, 2008.

[111] R. Österbacka, X. M. Jiang, C. P. An, B. Horovitz, and Z. V. Vardeny, "Photoinduced quantum interference antiresonances in π-conjugated polymers," *Physical Review Letters,* vol. 88, no. 22, pp. 226401, 2002.

[112] B. J. Schwartz, "Conjugated polymers as molecular materials: How chain conformation and film morphology influence energy transfer and interchain interactions," *Annual Review of Physical Chemistry,* vol. 54, no. 1, pp. 141-172, 2003.

[113] V. M. Agranovich and G. C. La Rocca, *Organic nanostructures : Science and applications* Amsterdam ; New York: IOS Press, 2002.

[114] B. C. Hess, G. S. Kanner, and Z. Vardeny, "Photoexcitations in polythiophene at high pressure," *Physical Review B,* vol. 47, no. 3, pp. 1407, 1993.

[115] B. C. Hess, G. S. Kanner, Z. V. Vardeny, and G. L. Baker, "High-pressure effects on ultrafast-relaxation kinetics of excitons in polydiacetylene 4bcmu," *Physical Review Letters,* vol. 66, no. 18, pp. 2364, 1991.

[116] J. P. Schmidtke, R. H. Friend, and C. Silva, "Tuning interfacial charge-transfer excitons at polymer-polymer heterojunctions under hydrostatic pressure," *Physical Review Letters,* vol. 100, no. 15, pp. 157401, 2008.

[117] J. P. Schmidtke, K. Ji-Seon, J. Gierschner, C. Silva, and R. H. Friend, "Optical spectroscopy of a polyfluorene copolymer at high pressure: Intra- and intermolecular interactions," *Physical Review Letters,* vol. 99, no. 16, pp. 167401-1, 2007.

[118] C. M. Martin, S. Guha, M. Chandrasekhar, H. R. Chandrasekhar, R. Guentner, P. Scanduicci de Freitas, and U. Scherf, "Hydrostatic pressure dependence of the luminescence and raman frequencies in polyfluorene," *Physical Review B (Condensed Matter and Materials Physics),* vol. 68, no. 11, pp. 115203-1, 2003.

[119] S. Guha, W. Graupner, R. Resel, M. Chandrasekhar, H. R. Chandrasekhar, R. Glaser, and G. Leising, "Planarity of para hexaphenyl," *Physical Review Letters,* vol. 82, no. 18, pp. 3625, 1999.

[120] M. A. Loi, A. Mura, G. Bongiovanni, Q. Cai, C. Martin, H. R. Chandrasekhar, M. Chandrasekhar, W. Graupner, and F. Garnier, "Ultrafast formation of nonemissive species via intermolecular interaction in single crystals of conjugated molecules," *Physical Review Letters,* vol. 86, no. 4, pp. 732, 2001.

[121] S.-C. Yang, W. Graupner, S. Guha, P. Puschnig, C. Martin, H. R. Chandrasekhar, M. Chandrasekhar, G. Leising, C. Ambrosch-Draxl, and U. Scherf, "Geometry-dependent electronic properties of highly fluorescent conjugated molecules," *Physical Review Letters,* vol. 85, no. 11, pp. 2388, 2000.

[122] S. Webster and D. N. Batchelder, "Absorption, luminescence and raman spectroscopy of poly(p-phenylene vinylene) at high pressure," *Polymer,* vol. 37, no. 22, pp. 4961-4968, 1996.

[123] J. M. Holt, "Ultrafast opitcal measurements of charge generation and transfer mechanisms of π-conjugated polymers for solar cell applications," Thesis (Ph D), Department of Physics, University of Utah, Salt Lake City, 2009.

[124] D. Psiachos and S. Mazumdar, "Correlated-electron description of the photophysics of thin films of π-conjugated polymers," *Physical Review B,* vol. 79, no. 15, 2009.

[125] K. Aryanpour, D. Psiachos, and S. Mazumdar, "Theory of exciplex photophysics in π-conjugated polymer-fullerene blends," *http://aps.arxiv.org/abs/0908.0366v1*, 2010.